EPR and NMR Spectroscopy of Spin-Labeled Proteins

Proefschrift

ter verkrijging van
de graad van Doctor aan de Universiteit Leiden,
op gezag van Rector Magnificus prof. mr. P.F. van der Heijden,
volgens besluit van het College voor Promoties
te verdedigen op
op woensdag 28 september 2011
klokke 13:45 uur

door

Michelina Giuseppina Finiguerra

geboren te Foggia, Italië
in 1967

Promotiecommissie

Promotores:	Prof. dr. E. J. J. Groenen
	Prof. dr. M. Ubbink
Co-promotor:	Dr. M. Huber
Overige leden:	Prof. dr. J. Brouwer
	Prof. dr. G. W. Canters
	Prof. dr. J. M. van Ruitenbeek
	Prof. dr. H.-J. Steinhoff (Universität Osnabrück)

A mia madre e mio padre

Table of Contents

Abbreviations

Amp	ampicillin
cam	chloamphenicol
CSPs	chemical shift perturbations
Cyt f	soluble part of the transmembrane cytochrome f
CW	continuous wave
DEER	double electron-electron resonance
DDT	dithiothreitol
EDTA	N,N,N',N'-ethylenediaminetetraacetic acid disodium salt
EPR	electron paramagnetic resonance
FPLC	fast protein liquid chromatography
FRET	Förster resonance energy transfer
HSQC	heteronuclear single-quantum coherence
IPTG	isopropyl-β-D-thiogalactopyranoside
LB	Luria – Bertani medium
MTS	(1-acetyl-2,2,5,5-tetramethyl-3-pyrroline-3-methyl)-methanethiosulfonate
MTSL	(1-oxyl-2,2,5,5-tetramethyl-3-pyrroline-3-methyl)-methanethiosulfonate
NMR	nuclear magnetic resonance
Pc	Plastocyanin
PCSs	pseudocontact shifts
PRE	paramagnetic relaxation enhancement
rmsd	root-mean-square deviation
RT	room temperature
SDSL	site-directed spin labelling
SL	spin label
Tris-HCl	tris(hydroxymethyl)aminomethane hydrochloride
wt	wild type
Zn-Pc	Zinc Pc
τ_c	rotational correlation time
^{15}N-Pc	^{15}N-labeled Pc

Chapter I

Introduction

This thesis explores novel routes of structure determination for dynamic and flexible protein systems, such as transient protein-protein complexes. To do so, a magnetic resonance approach is chosen in which specifically introduced spin probes play the main role. Such spin probes make the approach general, as systems devoid of natural paramagnetic centres can be investigated as well. Electron paramagnetic resonance (EPR) and nuclear magnetic resonance (NMR) are employed. For the EPR part of the investigation, biologically relevant models have been made and new high-field EPR methods were applied. In the NMR part, transient protein complexes have been studied with paramagnetic NMR. In the following, the background of both approaches is explained and an overview of the contents of this thesis is provided.

Proteins and protein interactions

Proteins are an important class of biological macromolecules present in all forms of life. These large and complex molecules show excellent functional flexibility, allowing them to play key roles in a great number of activities essential for the living world. No other type of biological macromolecule could perform all of the functions that proteins have gathered over billions of years. The characteristics of proteins permit to arrange their spatial structure so that specific chemical groups may be placed in definite positions. This mechanism allows them to act as catalysts in a number of reactions, and to carry out important structural, transport, and regulatory functions. Proteins normally perform these functions together with other biomolecules, rather than in isolation; indeed, a change in their quaternary state is often coupled with some particular function, or activity. Proteins bind frequently other proteins, as well as copies of the same protein, with which they form dimers or higher-order oligomers. The interaction with the biomolecular partner may occur either in relative isolation or within protein interaction networks and chains[1,2]. Therefore, it can be claimed that the study of proteins and in particular of how they interact is essential to understand countless biological processes.

Lifetime and strength of the protein complex are tightly coupled to the function performed by the complex. The affinity between the proteins that constitute the complex is a thermodynamic property expressed by the dissociation constant K_d, equal to the ratio between the dissociation rate constant k_{off} and the association rate constant k_{on}; it is therefore linked to the lifetime of the complex. The values for K_d may vary between 10^{-2} and 10^{-16} M and with it the nature of the protein complexes also gradually varies between the two extremes, of static complexes on the one hand, and of transient complexes on the other[3]. Static complexes are those where proteins are bound tightly to each other in a single, well-defined orientation. The value for K_d in this type of

complexes[3] is in the order of $10^{-15} – 10^{-16}$ M; examples are complexes formed between antigens and antibodies or between enzymes and inhibitors (e.g. the barnase-barstar complex[4]).

Opposite characteristics are found for transient complexes; these are typical of processes where a rapid rate of reaction is requested, which permits chained reactions to happen in an efficient way. Binding specificity, i.e. binding in a well-defined orientation, is needed; for instance, in the case of electron transfer processes, in which a minimal distance between the redox centres is necessary[5,6], since the reaction efficiency decreases exponentially with this distance. At the same time, affinity must be low so that, once the reaction has happened, the proteins can rapidly dissociate and a new partner can be found. For this to happen, the binding surfaces must have characteristics such that an efficient reaction is possible, without them being perfectly complementary as is observed for the interaction surfaces of static complexes.

A compromise between good specificity and low affinity is therefore necessary in transient complexes. A high dissociation rate constant is usually combined with a high association rate constant resulting in K_d values[7] in the order of $10^{-3} – 10^{-6}$ M. Studies on electron transfer systems provided evidence for the existence of the encounter complex. This is the initial complex formed between proteins (or between proteins and other macromolecules like DNA), which precedes the formation of the specific complex. In the encounter complex, the partners sample each others surface through a series of micro-movements, until the more stable active complex is formed. The current work provides a contribution to the investigation of the nature and characteristics of encounter complexes. The structure and dynamics of protein complexes are explored using proteins to which spin labels have been attached; these complexes are analyzed using both EPR and NMR techniques.

Spin labels for structural and dynamic protein-protein studies

A spin label is a stable radical, in which the unpaired electron is shared almost equally between the nitrogen and the oxygen atoms. Such a spin label can be attached covalently and specifically to a native or engineered cysteine in a protein. Introducing a spin label as a probe permits to explore structural and dynamic aspects of the protein by measuring the EPR observables of the spin label.

A spin label is commonly attached to a protein through the site-directed spin labelling technique. In site-directed spin labelling, a nitroxide side chain is introduced *via* cysteine substitution mutagenesis, followed by
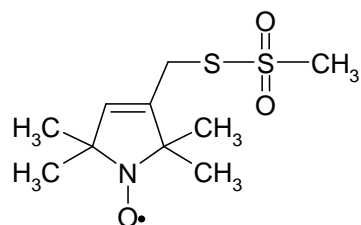

Figure 1.1 MTSL: the paramagnetic label used in this study.

modification of the unique sulfhydryl group with a specific nitroxide reagent[8]. Measurements of the spectral properties of the paramagnetic nitroxide probe with EPR spectroscopy provide a wealth of information on the environment of the spin label in the protein.
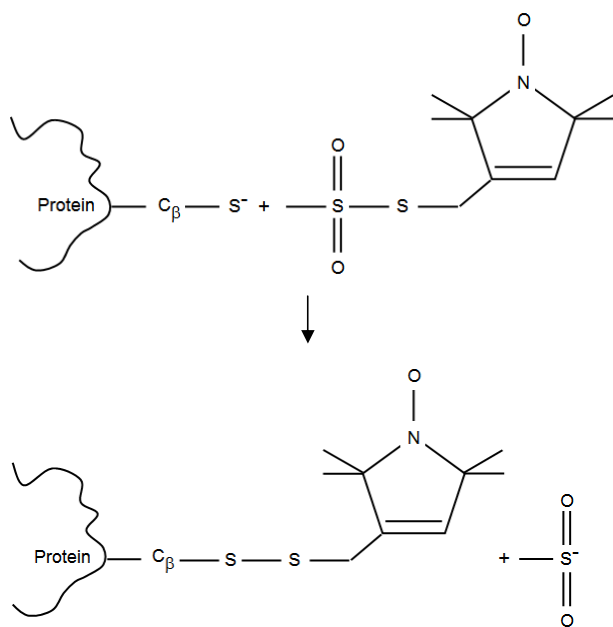
Figure 1.1 shows the (1-oxyl-2,2,5,5-tetramethyl-3-pyrroline-3-methyl)-methanethiosulfonate spin label (MTSL), which is the nitroxide spin label used in the present work.

Figure 1.2 shows the reaction scheme of MTSL with a thiolate group of a protein.

The site-directed spin labelling technique has been successfully employed for the characterisation of protein structure[9-11] and was shown to work even for membrane proteins[10,12]. For surface-exposed spin labels, perturbation of the protein structure should be minimal, giving reliable

Figure 1.2 Reaction scheme of MTSL with a thiolate group of a cysteine residue of a protein.

information on the structure and dynamics at the site of the spin label [13-15]. Such information can be relevant for the study of protein-protein interactions, because these are determined by the surface properties of the interacting surfaces. Two EPR observables of the spin label reflect the polarity and proticity of the environment of the spin label, where proticity refers to the propensity of the protein environment to donate hydrogen bonds. The influence of solvent polarity and hydrogen bonding on the EPR parameters of a nitroxide spin label can therefore be used to extract information on the microenvironment[16].

The EPR techniques are also helpful for determination of the distance between two spin labels attached to the protein, permitting to solve structural problems that are not easily accessible by standard structural techniques. Usually, two spin labels are introduced so that their distance reflects the structural property of interest. The distance distributions that are obtained contain information about the structure of the molecule and the flexibility of the spin label linker. These parameters can help to understand dynamics of the macromolecules, which is particularly important in a biological context.

Basic aspects of the EPR technique

Important parameters obtained in EPR experiments are the g-tensor (**G**) and the hyperfine coupling tensor (**A**). To explain how they can be read from an EPR spectrum a brief introduction is given. In an EPR experiment, the sample, a spin labeled-protein in the present work, is placed in a strong magnetic field and exposed to electromagnetic radiation in the microwave range. The EPR permits to measure the energy separation between the spin states of an unpaired electron in the environment of other magnetic species which perturb the external magnetic field, B.

Resonance condition: g- tensor and electron-nuclear hyperfine interaction

In the simple case of a free electron, the spin, and the magnetic moment associated with it, is quantized to be parallel or antiparallel to the external field. The energy separation ΔE between the two states is:

$$\Delta E = g_e \mu_B B = h\nu \qquad \text{(Eq. 1.1)}$$

where g_e is the free electron g-factor (≈ 2.0023) and β is the Bohr magneton ($\approx 9.3*10^{-27}$ J/mT). The populations of the energy levels are determined by Boltzmann statistics. Irradiation with electromagnetic radiation of frequency ν, satisfying the resonance condition, can induce transitions between the two levels (Figure 1.3). The population difference caused by the energy separation can then be detected as absorption[17].

Field on

$$m_s = +\tfrac{1}{2}$$

Field off

α

$g_e \mu_B B$

β
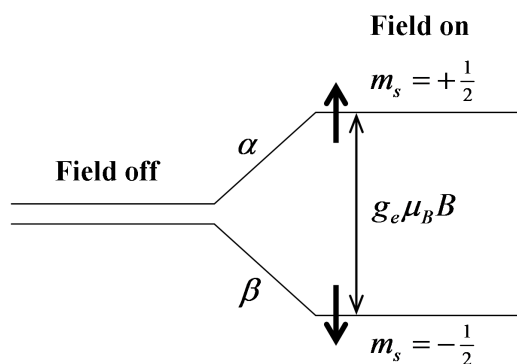
$$m_s = -\tfrac{1}{2}$$

Figure 1.3 Free electron energy levels separation and transitions in presence of a magnetic field.

The interaction of the electronic spin S with an external magnetic field B (or **B**) (Zeeman term) and a magnetic nucleus having nuclear spin I can be described by the spin Hamiltonian H_s:

$$H_s = \mu_B S \cdot \mathbf{g} \cdot \mathbf{B} + S \cdot \mathbf{A} \cdot I \qquad \text{(Eq. 1.2)}$$

The orbital angular momentum of the electron in a molecule gives a contribution to the total magnetic moment, which produces a shift in the g-factor from the free electron value and can also be the cause for g to become anisotropic. The resonance is then described by the g-tensor (**G**), with the principal components g_{xx}, g_{yy} and g_{zz}. The isotropic g-value is defined as $g_{iso}=(g_{xx}+g_{yy}+g_{zz})/3$.

The principal directions of the g tensor of a nitroxide are shown in Figure 1.4. In nitroxides the magnitude of g_{xx} is particularly sensitive to hydrogen bonding to the oxygen atom.
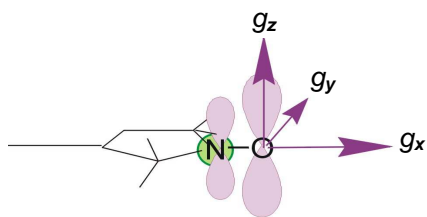

Figure 1.4 The principal directions of the g tensor of a nitroxide.

The second term in Eq. 1.2 describes the hyperfine interaction between the electronic spin S and the nuclear spin I through the hyperfine coupling tensor **A**, with the principal components A_{xx}, A_{yy} and A_{zz}. The isotropic hyperfine coupling constant is defined as: $A_{iso}=(A_{xx}+A_{yy}+A_{zz})/3$.

The magnitude of A_{zz} gives an indication about the polarity of the environment[16]. The isotropic hyperfine coupling is due to the Fermi contact term. It is caused by the spin density in the s-orbitals of the atom and reflects the distribution of the unpaired electron spin over the molecule. The anisotropy of A derives from the classical dipolar interaction between nuclear and electronic magnetic spin moments[17]. It is a measure for the distance between the electron spin and the nuclei[17] (dipolar interaction).

The internal magnetic fields derived from the nuclei can shift and/or split the basic resonance line into several components. The specific number, separation and relative intensities of these lines give information on the number of magnetic nuclei, their spin and the strength of the hyperfine interactions in the radical.
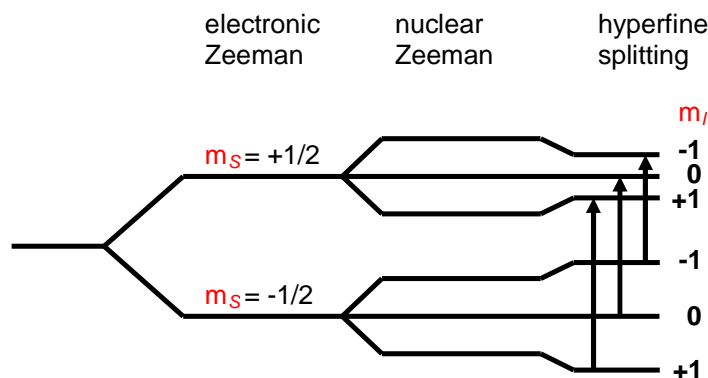
Figure 1.5 Energy level scheme and allowed transitions for S=1/2 and I=1.

In the MTSL molecule, the interaction between the nitrogen nucleus (^{14}N (I=1) in MTSL) and the electronic spin (S=1/2) results in the energy level scheme shown in Figure 1.5. The resonance is split into three lines.

To improve the spectral resolution, EPR spectroscopy can be performed at high magnetic fields using superconducting magnets, which enhance t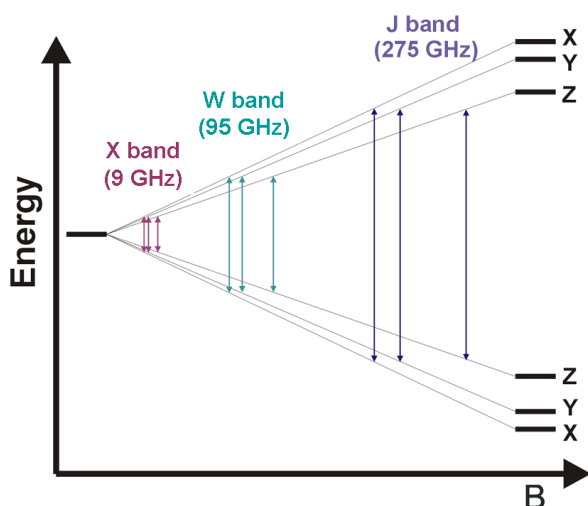he Zeeman resolution[18]. Figure 1.6 shows how the separation between the energy levels increases with increasing magnetic field strength, as it occurs moving from conventional X-band (9 GHz) EPR to W- and J-band (95 and 275 GHz, respectively). At these high fields, the spectra of a nitroxide in frozen solution are clearly resolved into three separate regions corresponding to the g-tensor components g_{xx}, g_{yy} and g_{zz} (Figure 1.7). For molecules with **B** parallel to g_x, a resonance, g_{xx}, at the low field side of the spectra (Figure 1.7) is observed and

Figure 1.6 Energy levels separation at different magnetic field strength.

analogously resonances at g_{yy} and g_{zz} for molecules with **B** parallel to g_y and g_z. At the high field side of the spectrum three resonances, split by A_{zz}, are observed.
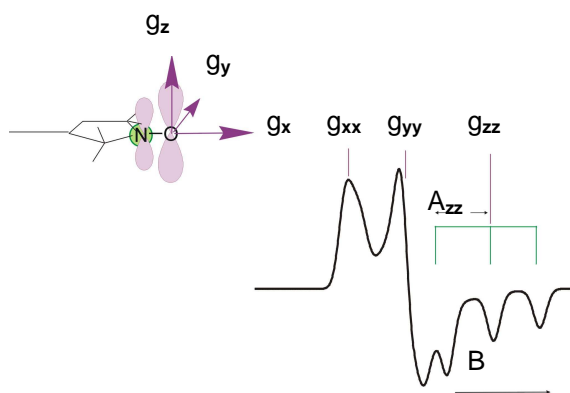
Figure 1.7 High field spectrum of MTSL at low temperature (powder spectrum).

The g-tensor component g_{xx} is particularly affected by hydrogen bonding whereas the A-tensor component A_{zz} is mostly influenced by the polarity of the environment. This is particularly interesting for proteins, for which it is often difficult to determine the local polarity.

In the present thesis, EPR spectroscopy at frequencies up to 275 GHz was performed, using a 275 GHz EPR spectrometer engineered and constructed at Leiden University[19].

Polarity and proticity from High Field EPR on nitroxide spin label

High-field EPR techniques allow to determine properties of the spin label environment such as polarity and proticity. Increasing the field above 95 GHz makes it possible to discriminate

between positions of similar polarity[18], such as those expected for positions at the surface of the protein. The principal g-tensor components and their variation due to solute-solvent interactions can be determined with high precision. The enhanced sensitivity to local structural influences on spin labels has been used to determine changes in the g-tensor as a function of solvent polarity and chemical structure of nitroxides[18,20-23].

The g- and A-tensor values are determined from the experimental spectra. The variation of g_{xx} for different samples is revealed by the shift of the position of the low-field maximum. Generally a protic environment shifts g_{xx} to smaller values, i.e. higher fields. The A_{zz} component of the A-tensor is read off as shown in Figure 1.7. The other components of A, A_{xx} and A_{yy} are too small to be resolved in the spectra.

Recent high-field EPR studies on polarity and proticity

Most studies investigating the properties of the protein environment with spin label EPR so far employ 95 GHz EPR. The polarity differences between different regions of a membrane protein were determined for a transducer protein[24]. Conformational changes of a membrane binding protein and the advantage of EPR at even higher field-frequency combinations are reviewed in Möbius *et al.*[25] The potential of these techniques to improve pH sensing has been explored also in the work of Möbius[25] and Voinov[26].

These are just a few of the examples of employing high-field EPR to learn about protein structure. The incentive to do such experiments at even higher fields than 95 GHz EPR derives from the presence of multiple components[16,24,25,27] in these spectra. Often the full interpretation of polarity and proticity trends is impeded by overlapping signals in the g_{xx} region of the spectra, which, as shown in Chapter II, can be resolved by EPR at 275 GHz and above[28].

Distance determination by EPR

Distance measurements are used in biological systems for which traditional methods of structure determination do not work well, such as certain peptides, proteins, RNA/DNA complexes or, as in the present thesis, protein-protein complexes. The EPR spectroscopic methods can be used when the biomolecule contains either stable or transient paramagnetic centers, like metal ions or clusters, amino acid radicals, or organic cofactor radicals. If the biomolecule is diamagnetic, it can be spin-labelled with nitroxides.

Both intra- and intermolecular distances between two spin labels may be measured through site-directed spin labelling combined with EPR spectroscopy[9,10,29]. Two types of techniques are normally used: a CW experiment in which, through the analysis of the line broadening caused by the dipolar interaction between two nitroxides, distances in the range of 8-20 Å can be

measured[30,31]. Larger distances (in the 20-70 Å range) can be determined using a pulsed EPR method, double electron-electron resonance (DEER)[15,32-35]as recently reviewed[36,37]. The pulsed techniques allow to measure distance information by producing a spin echo that is modulated at the frequency of the dipolar interaction[38]. The amplitude of the generated spin-echo is analysed and a distance distribution is obtained[34,39].

Model systems that serve as a reference for distance determination are essential for the comparison and the evaluation of the experimental data. Often, rigid molecules possessing two nitroxide groups are used[40]. For structure determination in protein-based systems, the disadvantage of such models is that they do not take into account the flexibility at the spin-label linker. One of the aspects that must be considered is that the linker may have multiple conformations when it is bound to the protein, because rotations over five torsion angles are possible (see spin labeled protein in Figure 1.2). Such mobility affects the distances obtained.

As a model for distance measurements we use azurin, a small protein for which the structure is known from X-ray crystallography[41], with two spin labels introduced by site-directed spin labelling[42].

Paramagnetic NMR for transient protein-protein complexes studies

Weak or transient interactions between proteins occur when the affinity between the proteins is low. Electron-transfer protein complexes are an example of transient complexes and are the result of a compromise between a tight binding, required for the reaction between the two partner proteins to occur, and the need for a fast dissociation, to ensure a high turnover of the complex and rapid electron shuttling. For these reasons, electron-transfer protein complexes are on the border of specific and nonspecific complexes. Several studies provided information on the dynamic nature of transient complexes, offering evidence that differently populated states may contribute to the complex structure. Paramagnetic NMR techniques are effective methods to study the structure of protein complexes and the dynamics of the proteins. Molecules naturally containing a paramagnetic centre (like a metal in metalloproteins), or containing paramagnetic labels specifically attached to them, can affect NMR signals, highlighting dynamics in protein complexes, and providing structural information, even of lowly populated states. The application of paramagnetic NMR, to obtain information about protein structure started already about 40 years ago[43], but has shown rapid progress and increasing popularity in the last ten years. Using paramagnetic tags, different types of NMR methods are employed to investigate structure and dynamics of protein complexes. One of them is the paramagnetic relaxation enhancement technique (PRE), which arises from the large magnetic dipolar interaction that exists between unpaired electrons and nearby nuclear spins. The

PRE effect results in an increase of the relaxation rate of the nucleus, which is manifested as a linewidth change. The rate increase can be used to calculate the distance between the paramagnetic centre and the affected nucleus.

In solution, the correlation time of the dipolar electron-nucleus interaction depends on two factors; the flipping of the electron spin, caused by longitudinal relaxation of the unpaired electrons, and the rotation of the molecule in the magnetic field. The first contribution to the correlation time is characterized by the electronic relaxation time, τ_s, and the second by the rotational correlation time τ_r of the molecule. The effective correlation time, τ_c, is given by $\tau_c^{-1} = \tau_s^{-1} + \tau_r^{-1}$. For metals with a fast electronic relaxation τ_c is dominated by τ_s. For some other metals (Cu^{2+}, Gd^{3+}) as well as nitroxide spin labels, τ_c is determined largely by τ_r. The enhancement of the nuclear relaxation rates is correlated with the distance between the paramagnetic centre and the nucleus, and specifically depends on the inverse of the sixth power of this distance. The relaxation enhancement can be very strong at short range but falls off quickly, yielding distances up to 25-35 Å, depending on the type of paramagnetic tag that is used[44]. This technique, PRE, is used in this thesis to investigate the structure of a transient complex. In a previous work[45] the same protein complex investigated within this thesis has been studied using pseudocontact shifts (PCSs) and chemical shift perturbations (CSPs).

The PCS is a consequence of the time-averaged anisotropic component of the unpaired electron spin. The pseudocontact effect is described by the magnetic susceptibility tensor $\Delta\chi$, and can provide long-range restraints for structure determination, with an r^{-3} dependence, where r is the distance between the metal and the nucleus. The PCS also provides angular information, because the size of the PCS contribution depends both on the orientation of the protein nuclei relative to the magnetic susceptibility tensor and on the distance from the paramagnetic centre. When intermolecular PCS are measured, from the metal in one protein to the nuclei of another, information about the orientation of one protein relative to the other can be obtained. Figure 1.8 shows the geometric parameters that are used in PRE and PCS technique.
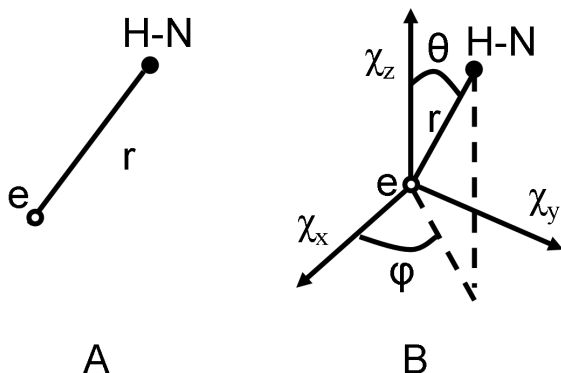

Figure 1.8 Schematic representations of the geometric dependence of the paramagnetic effects in paramagnetic relaxation enhancement (PRE) (A) and pseudocontact shifts (PCSs) (B)[46]. The unpaired electron is represented by 'e' and the observed nuclei, in this case an amide group, by 'H-N'. The axes labeled with 'χ' represent the orientation of the magnetic susceptibility tensor. The idea and the layout of the figure were taken from ref. 47 in modified form.

The CSP analysis is generally used to define a binding site and to calculate the dissociation constant of the protein complexes. In practice, CSP are found by comparison of the spectra during the titration of one protein with another protein with which it forms a complex. Well-defined complexes yield large and localized CSP. Conversely, if CSP arises from a time average of the relative orientation between the proteins due to the dynamic nature of the complex, as it happens in transient complexes, the changes are small and spread over a large area of the protein.

Thesis outline

This thesis is organised as follows. In chapters II and III the EPR experiments are described. Chapter II focuses on the polarity/proticity of the environment of the spin labels.
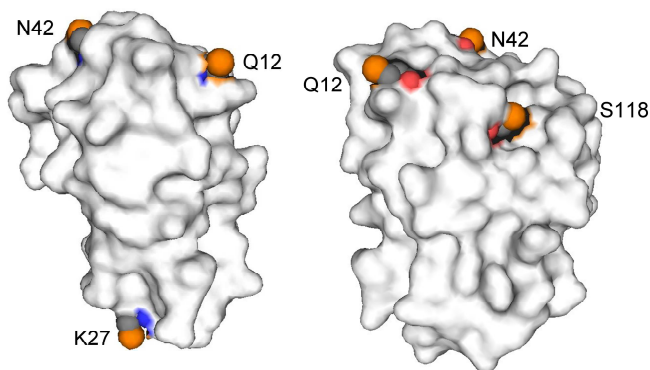

Figure 1.9 Azurin is depicted in surface representation (grey), while the Cys residues are shown with the sulphur in orange. The right view is rotated by 90° around the vertical axis relative to the left one.

Four single mutants of azurin were prepared by site directed mutagenesis. Figure 1.9 shows the location of the mutated residues. The properties of these sites are investigated by EPR at 95 GHz and 275 GHz.

Chapter III illustrates distance measurements by a pulsed, two frequencies EPR technique (DEER). Two double mutants are described: the first one, in which Q12 and K27 have each been replaced by a cysteine (Cys) (Q12C/K27C); and the second one in which K27 and N42 were replaced by Cys (K27C/N42C). The singly labeled mutant protein K27C was used as reference. It was shown that distances in the 4 nm region can be measured with high accuracy.

In Chapter IV the dynamics in the complex of *Nostoc* sp. PCC 7119 cytochrome *f* – plastocyanin (Cyt *f*-Pc) investigated by NMR is described. The PREs from five spin labels on Cyt *f* were used as distance restraints in docking calculations. A previous study on the same complex indicated that the proteins spend most of the time in a well-defined, single-orientation structure. Here we suggest instead that the complex is more dynamic. These two apparently contrasting results can actually coexist in an encounter complex model.

Reference List

1. Alm,E. & Arkin,A.P. Biological networks. *Current Opinion in Structural Biology* **13**, 193-202 (2003).

2. Nooren,I.M.A. & Thornton,J.M. Diversity of protein-protein interactions. *Embo Journal* **22**, 3486-3492 (2003).

3. Janin,J. Kinetics and thermodynamics of protein-protein interactions in *Protein-protein recognition*, Klaenthous,C. (ed.) pp. 1-32 (Oxford University Press, New York,2000).

4. Schreiber,G. & Fersht,A.R. Rapid, electrostatically assisted association of proteins. *Nature Structural Biology* **3**, 427-431 (1996).

5. Marcus,R.A. On the theory of oxidation-reduction reactions involving electron transfer. *Journal of Chemical Physics* **24**, 966-978 (1956).

6. Marcus,R.A. & Sutin,N. Electron transfers in Chemistry and Biology. *Biochimica et Biophysica Acta* **811**, 265-322 (1985).

7. Crowley,P.B. & Ubbink,M. Close encounters of the transient kind: Protein interactions in the photosynthetic redox chain investigated by NMR spectroscopy. *Accounts of Chemical Research* **36**, 723-730 (2003).

8. Bulaj,G., Kortemme,T. & Goldenberg,D.P. Ionization-reactivity relationships for cysteine thiols in polypeptides. *Biochemistry* **37**, 8965-8972 (1998).

9. Hubbell,W.L., Gross,A., Langen,R. & Lietzow,M.A. Recent advances in site-directed spin labeling of proteins. *Current Opinion in Structural Biology* **8**, 649-656 (1998).

10. Altenbach,C., Marti,T., Khorana,H.G. & Hubbell,W.L. Transmembrane Protein-Structure - Spin Labeling of Bacteriorhodopsin Mutants. *Science* **248**, 1088-1092 (1990).

11. Sen,K.I., Wu,H.Y., Backer,J.M. & Gerfen,G.J. The structure of p85ni in class IA phosphoinositide 3-kinase exhibits interdomain disorder. *Biochemistry* **49**, 2159-2166 (2010).

12. Oh,K.J., Singh,P., Lee,K., Foss,K., Lee,S., Park,M., Lee,S., Aluvila,S., Park,M., Singh,P., Kim,R.S., Symersky,J. & Walters,D.E. Conformational changes in BAK, a pore-forming proapoptotic Bcl-2 family member, upon membrane insertion and direct evidence for the existence of BH3-BH3 contact interface in BAK homo-oligomers. *Journal of Biological Chemistry* **285**, 28924-28937 (2010).

13. Hustedt,E.J. Nitroxide spin-spin interactions: Applications to protein structure and dynamics. *Annual Review of Biophysics and Biomolecular Structure* **28**, 129-153 (1999).

14. Hubbell,W.L., Cafiso,D.S. & Altenbach,C. Identifying conformational changes with site-directed spin labeling. *Nature Structural Biology* **7**, 735-739 (2000).

15. Columbus,L. & Hubbell,W.L. A new spin on protein dynamics. *Trends in Biochemical Sciences* **27**, 288-295 (2002).

16. Owenius,R., Engstrom,M., Lindgren,M. & Huber,M. Influence of solvent polarity and hydrogen bonding on the EPR parameters of a nitroxide spin label studied by 9-GHz and 95-GHz EPR spectroscopy and DFT calculations. *Journal of Physical Chemistry A* **105**, 10967-10977 (2001).

17. Wertz,J.E. & Bolton,J.R. Electron Spin Resonance. (1972).

18. Steinhoff,H.J., Savitsky,A., Wegener,C., Pfeiffer,M. & Plato,M. High-field EPR studies of the structure and conformational changes of site-directed spin labeled bacteriorhodopsin. *Biochimica Et Biophysica Acta-Bioenergetics* **1457**, 253-262 (2000).

19. Blok,H., Disselhorst,J.A.J.M. & Orlinskii,S.B. A continuous-wave and pulsed electron spin resonance spectrometer operating at 275 GHz. *Journal of Magnetic Resonance* **166**, 92-99 (2004).

20. Burghaus,O., Rohrer,M., Gotzinger,T., Plato,M. & Möbius,K. A Novel High-Field High-Frequency Epr and Endor Spectrometer Operating at 3 Mm Wavelength. *Measurement Science & Technology* **3**, 765-774 (1992).

21. Prisner,T.F., Vanderest,A., Bittl,R., Lubitz,W., Stehlik,D. & Möbius,K. Time-Resolved W-Band (95 Ghz) Epr Spectroscopy of Zn-Substituted Reaction Centers of Rhodobacter-Sphaeroides R-26. *Chemical Physics* **194**, 361-370 (1995).

22. Huber,M. & Torring,J.T. High-Field Epr on the Primary Electron-Donor Cation-Radical in Single-Crystals of Heterodimer Mutant Reaction Centers of Photosynthetic Bacteria - First Characterization of the G-Tensor. *Chemical Physics* **194**, 379-385 (1995).

23. Earle,K.A., Moscicki,J.K., Ge,M.T., Budil,D.E. & Freed,J.H. 250-Ghz electron spin resonance studies of polarity gradients along the aliphatic chains in phospholipid membranes. *Biophysical Journal* **66**, 1213-1221 (1994).

24. Brutlach,H., Bordignon,E., Urban,L., Klare,J.P., Reyher,H.J., Engelhard,M. & Steinhoff,H.J. High-field EPR and site-directed spin labeling reveal a periodical polarity profile: The sequence 88 to 94 of the phototransducer NpHtrII in complex with sensory rhodopsin, NpSRII. *Applied Magnetic Resonance* **30**, 359-372 (2006).

25. Möbius,K., Savitsky,A., Wegener,C., Rato,M., Fuchs,M., Schnegg,A., Dubinskii,A.A., Grishin,Y.A., Grigor'ev,I.A., Kuhn,M., Duche,D., Zimmermann,H. & Steinhoff,H.J. Combining high-field EPR with site-directed spin labeling reveals unique information on proteins in action. *Magnetic Resonance in Chemistry* **43**, S4-S19 (2005).

26. Voinov,M.A., Ruuge,A., Reznikov,V.A., Grigor'ev,I.A. & Smirnov,A.I. Mapping local protein electrostatics by EPR of pH-Sensitive thiol-specific nitroxide. *Biochemistry* **47**, 5626-5637 (2008).

27. Savitsky,A., Dubinskii,A.A., Plato,M., Grishin,Y.A., Zimmermann,H. & Möbius,K. High-field EPR and ESEEM investigation of the nitrogen quadrupole interaction of nitroxide spin labels in disordered solids: Toward differentiation between polarity and proticity matrix effects on protein function. *Journal of Physical Chemistry B* **112**, 9079-9090 (2008).

28. Bordignon,E., Brutlach,H., Urban,L., Hideg,K., Savitsky,A., Schnegg,A., Gast,P., Engelhard,M., Groenen,E.J.J., Möbius,K. & Steinhoff,H.J. Heterogeneity in the nitroxide

micro-environment: polarity and proticity effects in spin-labeled proteins studied by multi-frequency EPR. *Applied Magnetic Resonance* **37**, 391-403 (2010).

29. Eaton,G.R., Eaton,S.S. & Berliner,L.J. Distance measurements in biological systems by EPR. New York, USA: Kluwer, (2000).

30. Rabenstein,M.D. & Shin,Y.K. Determination of the distance between 2 spin labels attached to a macromolecule. *Proceedings of the National Academy of Sciences of the United States of America* **92**, 8239-8243 (1995).

31. Altenbach,C., Oh,K.J., Trabanino,R.J., Hideg,K. & Hubbell,W.L. Estimation of inter-residue distances in spin labeled proteins at physiological temperatures: Experimental strategies and practical limitations. *Biochemistry* **40**, 15471-15482 (2001).

32. Cai,Q., Kusnetzow,A.K., Hideg,K., Price,E.A., Haworth,I.S. & Qin,P.Z. Nanometer distance measurements in RNA using site-directed spin labeling. *Biophysical Journal* **93**, 2110-2117 (2007).

33. Kurshev,V.V., Raitsimring,A.M. & Tsvetkov,Y.D. Selection of dipolar interaction by the 2+1 pulse train ESE. *Journal of Magnetic Resonance* **81**, 441-454 (1989).

34. Jeschke,G. Distance measurements in the nanometer range by pulse EPR. *Chemphyschem* **3**, 927-932 (2002).

35. Larsen,R.G. & Singel,D.J. Double electron-electron resonance spin-echo modulation: Spectroscopic measurement of electron-spin pair separations in orientationally disordered solids. *Journal of Chemical Physics* **98**, 5134-5146 (1993).

36. Borbat,P.P. & Freed,J.H. Measuring distances by pulsed dipolar ESR spectroscopy: Spin-labeled histidine kinases. (2007).

37. Schiemann,O. & Prisner,T.F. Long-range distance determinations in biomacromolecules by EPR spectroscopy. *Quarterly Reviews of Biophysics* **40**, 1-53 (2007).

38. Milov,A.D., Ponomarev,A.B. & Tsvetkov,Y.D. Electron electron double-resonance in electron-spin echo: Model biradical systems and the sensitized photolysis of decalin. *Chemical Physics Letters* **110**, 67-72 (1984).

39. Fanucci,G.E. & Cafiso,D.S. Recent advances and applications of site-directed spin labeling. *Current Opinion in Structural Biology* **16**, 644-653 (2006).

40. Sartori,E., Corvaja,C., Oancea,S., Formaggio,F., Crisma,M. & Toniolo,C. Linear configuration of the spins of a stable trinitroxide radical based on a ternary helical peptide. *Chemphyschem* **6**, 1472-1475 (2005).

41. Nar,H., Messerschmidt,A., Huber,R., Vandekamp,M. & Canters,G.W. Crystal structure analysis of oxidized *Pseudomonas Aeruginosa* azurin at pH 5.5 and pH 9.0 - A pH-induced conformational transition involves a peptide bond flip. *Journal of Molecular Biology* **221**, 765-772 (1991).

42. Hubbell,W.L. Investigation of structure and dynamics in membrane proteins using site-directed spin labeling. *Current Opinion in Structural Biology* **4**, 566-573 (1994).

43. Keizers,P.H.J. & Ubbink,M. Paramagnetic tagging for protein structure and dynamics analysis. *Progress in Nuclear Magnetic Resonance Spectroscopy* **58**, 88-96 (2011).

44. O'Connell,M.R., Gamsjaeger,R. & Mackay,J.P. The structural analysis of protein-protein interactions by NMR spectroscopy. *Proteomics* **9**, 5224-5232 (2009).

45. Diaz-Moreno,I., Diaz-Quintana,A. & De la Rosa,M.A. Structure of the complex between plastocyanin and cytochrome *f* from the cyanobacterium *Nostoc* sp PCC 7119 as determined by paramagnetic NMR - The balance between electrostatic and hydrophobic interactions within the transient complex determines the relative orientation of the two proteins. *Journal of Biological Chemistry* **280**, 18908-18915 (2005).

46. Pintacuda,G., Keniry,M.A., Huber,T., Park,A.Y., Dixon,N.E. & Otting,G. Fast structure-based assignment of N-15 HSQC spectra of selectively N-15-labeled paramagnetic proteins. *Journal of the American Chemical Society* **126**, 2963-2970 (2004).

Chapter II

High-field (275 GHz) spin-label EPR for high-resolution polarity determination in proteins

Abstract

The polarity of protein surfaces is one of the factors driving protein-protein interactions. High-field, spin-label EPR at 95 GHz, i.e., a frequency 10 times higher than for conventional EPR, is an upcoming technique to determine polarity parameters of the inside of proteins. Here we show that by 275 GHz EPR even the small polarity differences of sites at the protein surface can be discriminated. To do so, four single cysteine mutations were introduced at surface sites (positions 12, 27, 42 and 118) of azurin and spin labeled. By 275 GHz EPR in frozen solution, polarity/proticity differences between all four sites have been resolved, which is impossible by 95 GHz EPR. In addition, by 275 GHz EPR, two spectral components are observed for all mutants. The difference between them corresponds to one additional hydrogen bond.

Introduction

Protein-protein interactions are driven by the properties of the respective protein surfaces, for example, the polarity of the surface. Therefore, methods to determine the polarity of protein surfaces experimentally are sought. Spin-label, high-field EPR has proven useful to determine polarity parameters of the interior of proteins. To do so, a spin label is placed at the position of interest in the protein. The EPR parameters of the spin label reflect the polarity and proticity of the environment of the spin label, where proticity refers to the propensity of the protein environment to donate hydrogen bonds. Placing the spin label at different positions in the protein enables determination of the protein polarity locally. To obtain sufficient spectral resolution, EPR spectroscopy performed at high magnetic fields and microwave frequencies is advantageous. As an example, by EPR performed at 3 T and 95 GHz (W-band), i.e., at 10 times higher fields and frequencies than conventional 9 GHz (X-band) EPR, polarity profiles of membrane proteins have been determined[1]. In order to discriminate between positions of similar polarity, such as expected for positions at the surface of the protein, it is important to be able to perform EPR at even higher magnetic fields and frequencies. Several 250 GHz EPR studies have been reported for model systems of biological membranes using spin-labeled lipids with the focus on dynamics rather than polarity[2]. Experiments to determine polarity by EPR at fields higher than 95 GHz on spin-labeled proteins have only recently been performed, namely by EPR at 360 GHz (K. Möbius *et al.*, private communication).
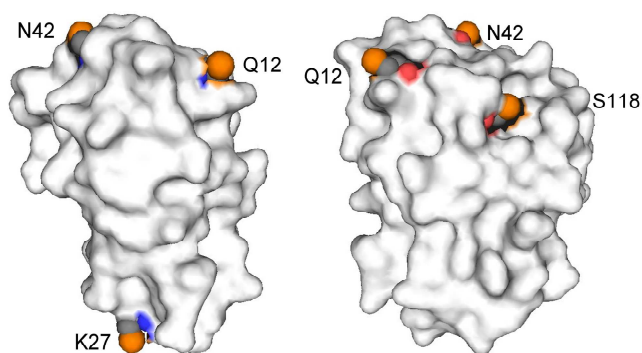
Figure 2.1 Location of the mutated residues. Azurin is depicted in surface representation (grey). The residues mutated in this study are shown as Cys residues, with the sulfur in orange. The right view is rotated by 90° around the vertical axis relative to the left one.

In the present study, spin labels were introduced at positions close to the surface of the protein by spin label mutagenesis[3]. Four single mutants of a protein of known structure, azurin (Figure 2.1), were prepared. To avoid interference from the paramagnetic Cu(II) of azurin, the metal ion was replaced by Zn(II), Zn-azurin. To obtain sufficient resolution for the small differences in polarity and proticity expected, we employed an EPR spectrometer operating at 9 T and 275 GHz (J-band)[4] which is designed to provide the high sensitivity needed for the study of biological samples. The data were compared with those obtained using a commercial W-band EPR spectrometer.

The EPR experiments reveal that even the small differences in polarity of these mutants become detectable at 275 GHz. The most striking result is that in the spectra of all mutants two spectral components are observed that can not be resolved by W-band EPR.

Materials and methods

Four mutants of Zn-azurin (azurin with Cu(II) replaced by Zn(II)) containing a surface exposed cysteine residue have been prepared. The N42C mutant[5] and the K27C and S118C mutants were prepared as described in ref. 9, the preparation of the Q12C mutant will be described elsewhere (S. Alagaratnam, unpublished results). The procedure for spin labeling these mutants is also described in ref. 9.

Sample preparation and measurements

The concentration of the samples used was between 0.8 and 1.2 mM. The volume used for W-band EPR measurement was about 0.8 μl including 30% glycerol, and the sample was introduced into a Wilmad suprasil quartz tube with an inner diameter (i.d.) of 0.60 mm and an outer diameter (o.d.) of 0.84 mm, from Wilmad-Labglass (Buena, NJ, USA) sealed at one end. The W-band measurements were performed at 40 K and the sample was frozen directly by introduction into the cryostat.

The volume used for J-band EPR measurement was about 17 nl including 50% glycerol. The sample was measured in a locally made quartz capillary with i.d. of 0.15 mm and o.d. of 0.3 mm. Measurements were performed at 100 K. The modulation frequencies were 100 kHz (W-band) and 2 kHz (J-band); modulation amplitude: 0.5 mT (W-band) and 1 mT (J-band); microwave (mw) power: 8 nW (W-band) and 10 μW (J-band); total measurement time: 20 min (W-band) and 9 min (K27 and Q12), respectively, 17 min (S118 and N42) (J-band).

Instrumentation

For W-band EPR experiments a Bruker Elexsys 680 (Bruker Biospin GmbH Rheinstetten, Germany) spectrometer and for J-band EPR experiments a laboratory-designed spectrometer[4] was used.

Spectral simulations

The program used for simulations was SimFonia (Bruker-Biospin, Rheinstetten). Errors of parameters have been determined by changing each parameter by the smallest possible amount that produced a visible deterioration of the quality of the simulation with respect to the spectrum. For

the unresolved hyperfine couplings A_{xx} and A_{yy}, in the simulation of the W- and J-band EPR spectra the following values were used. The A_{xx} values were: Q12C 0.50 mT, K27C 0.50 mT, N42C 0.48 mT and S118 0.43 mT. The A_{yy} values were: Q12C 0.50 mT, K27C and N42C 0.48 mT, and S118 0.45 mT. The error in A_{xx} and A_{yy} is ±0.03 mT, except for A_{xx} of Q12C in J-band EPR, where it is ±0.05 mT. The simulation parameters A_{xx} and A_{yy} depend on the component linewidth used in the simulation, which was fixed at 0.82 mT for W-band simulations and at 1.6 mT for J-band simulations.

The EPR parameters obtained from the J-band and the W-band EPR spectra should be identical. Nevertheless, the A_{zz} values obtained from J-band EPR were systematically lower (by 0.05 to 0.08 mT) than those from W-band EPR. With a Mn(II) standard sample we observed a deviation in the same direction, suggesting that the calibration of the slope of the field sweep (dB/dI, with B the static magnetic field, and I, the magnet current) of the J-band EPR magnet differs from that of the W-band magnet. The difference in the slope calibration observed on the standard sample corresponds to a correction of +0.024 mT for the A_{zz} values from J-band EPR. The same re-calibration applied to the field separation between the g_{zz} and the g_{xx} (and the g_{yy}) component results in a correction by +4 x 10^{-5} for g_{xx} and by +3 x 10^{-5} for g_{yy} for the values from J-band EPR. The parameters from J-band EPR in Table 2.1 are corrected accordingly. Remaining differences in the W-band and the J-band EPR parameters can be attributed to the differences in temperature, which was 100 K in the J-band EPR and 40 K in the W-band EPR experiments, and in glycerol content, i.e., 50% in J-band EPR and 30% in W-band EPR experiments. We measured for two of the mutants (K27C and S118C), that A_{zz} at 100 K is smaller by ca. 0.03 mT than at 40 K. At 50% glycerol content, A_{zz} is larger by ca. 0.06 mT than at 30%. Combining both effect, for the measurement conditions in the J-band EPR experiments, a differences of +0.03 mT is expected for A_{zz} compared to A_{zz} from W-band EPR. The differences in temperature also seems to affect the g_{xx} values, since, at 100 K, the Q12C sample (50% glycerol content, measured by J-band EPR) had a g_{xx} (av) value that was larger by 3 x 10^{-5} than g_{xx} (av) at 40 K.

Results

Mutants of azurin with spin labels at positions 12, 27, 42, and 118 (Q12C, K27C, N42C, and S118C) have been investigated. The EPR measurements were performed on frozen solutions of the spin-labeled mutants using W-band and J-band EPR.

In Figure 2.2, the EPR spectra at J-band of the spin label in all four mutants of the Zn-azurin are
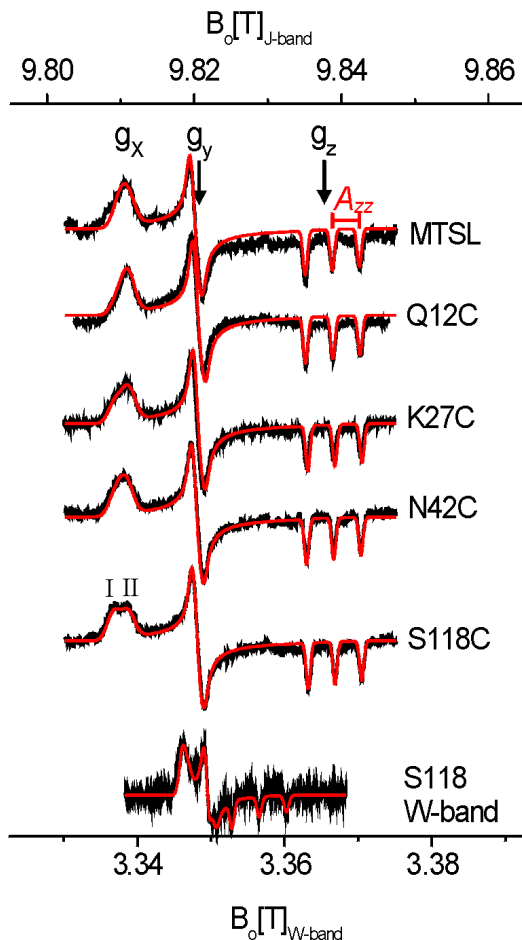

shown. The resonance field positions for B_0 along the nitroxide x-, y- and z-axes of the g tensor are indicated. The W-band EPR spectra of frozen solutions of all mutants were measured, and in Figure 2.2 one of these, the spectrum of S118C is shown. Compared with the W-band spectra, the J-band spectra have a higher resolution. This can be seen by the larger separation of the group of three lines that are centered at g_{zz} and separated by A_{zz}, and the peak at g_{yy}. The overlap of the lower field A_{zz} line with the g_{yy} feature in the W-band spectra causes an additional peak at the high field side of the g_{yy} band (see S118 W-band EPR spectrum, Figure 2.2). That feature is difficult to simulate as it depends on a combination of simulation parameters. Moreover, in the J-band spectra, a splitting of the EPR signal at g_{xx} into two components, g_{xx} (I) (the larger g_{xx}-value that appears at lower field) and g_{xx} (II) (the smaller g_{xx}-value that appears at higher field), becomes visible. This splitting is most clearly seen in the spectrum of the S118C mutant, Figure 2.2.

Figure 2.2 J-band EPR spectra of azurin mutants and W-band spectra of S118 mutant at 40K (W-band) and 100K (J-band). Arrows at g_{xx}, g_{yy} and g_{zz} : resonance for magnetic field along the g-tensor x-, y-, and z-axes. A_{zz}: nitrogen hyperfine coupling along z-direction. Simulation for all spectra are shown (dotted lines).

To analyze this spitting, the J-band EPR spectra were simulated with two spectral components, which differ only with respect to the g_{xx} values and the relative contribution of the components to the total spectra. The respective components are given as g_{xx} (I) and g_{xx} (II) in the Table 2.1. To make sure that this splitting is not an artifact, simulations of the W-band spectra were performed using the two components obtained from J-band EPR.

These simulations agreed with the experimental spectra, confirming that the difference between the g_{xx} (I) and g_{xx} (II) values is too small to be resolved by W-band EPR.

Due to the higher resolution of J-band EPR, the errors in the simulation parameters at J-band are overall smaller than those at W-band. Partly, this is due to the larger separation of the individual components of the spectra. Furthermore, a frequent problem in the W-band EPR spectra of protein samples are signals of Mn(II) impurities. The signal of these impurities overlaps the lines of the spin-label spectra in W-band EPR, thus increasing the experimental errors in determining the position of these lines. This was the case for the W-band EPR spectra of the K27C mutant. In the J-band EPR spectra, the signal of the Mn(II) impurity does not overlap with the spectrum of the spin label, resulting in smaller errors.

Table 2.1 g and hyperfine tensor parameters of azurin mutants from W-band (95 GHz) and J-band (275 GHz) EPR

Mutant	band	g_{xx} (I) [a]	g_{xx}(II) [a]	g_{xx} resp. g_{xx}(av) [b]	g_{yy} [c]	g_{zz}	A_{zz} [d] mT
Q12C	W	n.a. [e]	n.a.	2.00775	2.00574		3.77
	J	2.00795(20%)	2.00765	2.00771	2.00567		3.75
K27C	W	n.a.	n.a.	2.00788	2.00583		3.73
	J	2.00806(30%)	2.00769	2.00780	2.00573	2.00198	3.73
N42C	W	n.a.	n.a.	2.00783	2.00579		3.77
	J	2.00803(35%)	2.00773	2.00783	2.00574		3.75
S118C	W	n.a.	n.a.	2.00794	2.00585		3.70
	J	2.00811(55%)	2.00771	2.00793	2.00576		3.67

For comparison, all g-values are adjusted to g_{zz} = 2.00198. No calibration of absolute g values was performed. Errors of g values are given with respect to the relative magnitude of g_{xx} and g_{yy} vs. g_{zz}:
    Error: $\pm 1 \cdot 10^{-5}$. In bracket: percentage of contribution of species.
    g_{xx}(av): weighted average of g values g_{xx}(I) and g_{xx}(II) from J-band; errors: $\pm 2 \cdot 10^{-5}$. For Q12, error: $\pm 4 \cdot 10^{-5}$.
    g_{xx}: principal value of g-tensor from W-band: only one component used in the simulations; error: $\pm 2 \cdot 10^{-5}$. For K27C, error: $\pm 6 \cdot 10^{-5}$ due to the presence of Mn(II) impurity in the sample.
    Error: W-band $\pm 6 \cdot 10^{-5}$; J-band $\pm 3 \cdot 10^{-5}$
    Error: ± 0.025 mT for W and J-band spectra except for J-band: K27: ± 0.03 mT. J-band values: 0.045 mT added to account for different magnet field sweep calibrations (see text)
    n.a.: not applicable

From J-band EPR, the order of the g_{xx} values, i.e. the weighted average g_{xx} (av) of g_{xx} (I) and g_{xx} (II) of the four mutants is S118C > K27C $\approx$ N42C > Q12C. The error of the determination of g_{xx} from the W-band spectra was too large to determine that order. The A_{zz} parameters of the four mutants are very similar. The largest A_{zz} values are found for Q12C and N42C. They are significantly larger than the value for S118C. The A_{zz} value of K27C agrees within experimental error with those of the three other mutants, not allowing to place the A_{zz} value of this mutant relative to the other mutants.

A plot of A_{zz} vs. g_{xx} illustrates the polarity/proticity properties (Figure 2.3), where proticity refers to the propensity of the protein environment to donate hydrogen bonds. The squares are values of the spin label MTSL in different solvents from Owenius *et al.*[6]. The dots are the J-band EPR data obtained on the Zn-azurin mutants.
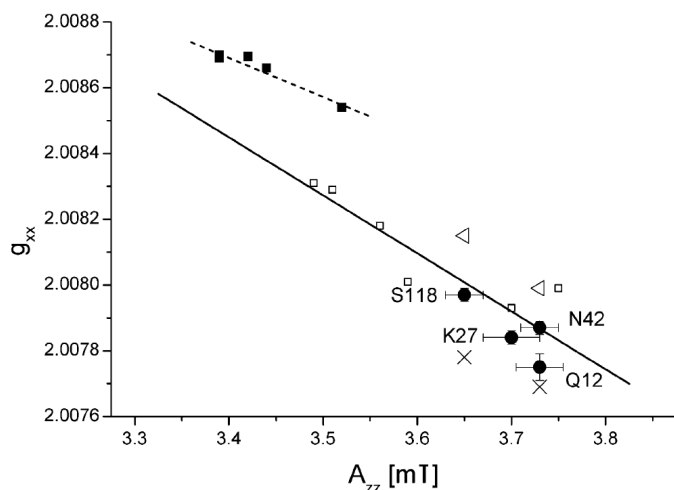
The mutants are located in a region of the plot where the more protic, polar solvents are found (see Discussion).

Shown are the values of g_{xx} (av) for all mutants, and for S118C and Q12C also the values of g_{xx} (I) and g_{xx} (II).

Figure 2.3 Plot of g_{xx} vs. A_{zz} of spin labels in Zn-azurin. Dots: g_{xx}(av) from J-band EPR, triangles: g_{xx}(I), crosses: g_{xx}(II) of S118C and Q12C. For reference the values of MTSL in different solvents are shown (filled squares, aprotic; open square, protic solvents). Dotted line: Linear correlation of g_{xx} vs. A_{zz} for non-hydrogen bonding solvents; solid line, linear correlation for hydrogen bonding solvents [5]. Figure modified from ref [7].

Discussion

Spin labels at four surface sites in Zn-azurin are investigated. The higher resolution of J-band EPR reveals the presence of two spectral components, not previously resolved in W-band EPR spectra of spin-labeled proteins. The signal-to-noise ratio of the J-band EPR spectra shows that the sensitivity of this new EPR spectrometer is sufficient to measure biological samples with realistic concentrations, i.e. around 0.5 mM. Remarkable is the very modest volume required for the sample (see Materials and methods), resulting in a total amount of protein needed of only 17 pmol.

The EPR signals can be simulated with regular powder line shapes, revealing the absence of spectral distortions due to dispersion admixture, which is a frequent problem in high-field EPR. Thus, reliable g- and hyperfine tensor parameters were obtained. The EPR results from W-band and J-band EPR are overall consistent (see Table 2.1). The remaining differences between the EPR parameters of the individual mutants derived from W-band and J-band EPR are attributed to the differences in measurement temperature and glycerol content in the two experiments (see Materials and methods). The J-band EPR spectra were simulated with a larger component linewidth, 1.6 mT, compared to 0.82 mT for the W-band EPR spectra, indicating that in addition to unresolved hyperfine couplings, which do not depend on field, g-strain and other inhomogeneities start to play a role at J-band.

The absence of spectral overlap in the J-band EPR spectra permits determination of the g-values with higher precision, enabling us to establish the order of the mutants with respect to g_{xx}, which is impossible by W-band EPR.

Two components of the spin-label spectra that differ with respect to their g_{xx} values can be resolved by J-band EPR. They are separated by $\Delta g_{xx} = 4 \times 10^{-4}$ (g_{xx}(I) - g_{xx}(II)), corresponding to 1.7 mT at that field. In W-band EPR, the same Δg_{xx} amounts to a splitting of ≈0.6 mT. As shown by the simulation of the W-band EPR spectra with two components (see Results) this separation is not large enough to resolve the two components. Previously, separations as small as 2×10^{-4} were resolved by W-band EPR, albeit in systems where spectra with significantly better signal-to-noise ratio could be obtained. One example was the investigation of MTSL in different solvents[6]. At small values of Δg_{xx} in W-band EPR, the second component appears as a shoulder at the low field edge of the spectrum, which cannot be distinguished in spectra of lower signal-to-noise ratio, such as the typical spin-labeled protein.

For the interpretation of the differences in the EPR parameters obtained for the different mutants, a plot of g_{xx} vs. A_{zz} is shown in Figure 2.3. Such plots serve to illustrate polarity/proticity profiles, as g_{xx} is most sensitive to differences in proticity, and A_{zz} to differences in polarity. In Figure 2.3 the data points obtained for the four mutants are compared with the parameters of MTSL in a series of solvents[6]. Unpolar/aprotic solvents are characterized by high g_{xx}/low A_{zz} values, polar/protic solvents by low g_{xx}/high A_{zz} values. Linear correlations of A_{zz} vs. g_{xx} for the data obtained in different solvents are shown. The dotted line corresponds to aprotic, the solid line to protic solvents. In this plot, the spin labels of Zn-azurin are located in a region close to the polar and hydrogen-bond-forming solvents. This agrees with the location of the spin labels close to the surface of the protein. According to the differences in polarity/proticity observed, the spin label in the S118C mutant is in the most apolar/aprotic environment, i.e. S118 is the most buried residue, whereas Q12 and N42 are the most solvent exposed residues. The X-ray structure of azurin[8], reveals that all residues are close to the surface. The difficulty to dimerize S118C-azurin has been interpreted as evidence for a low solvent accessibility of S118[9]. Also, mobility studies performed by W-band EPR reveal a significantly reduced mobility for S118C[10], suggesting that S118 is more buried than the other residues. Interestingly, the mobility of the spin label attached to Q12C is lower than that attached to K27C[10], whereas the present study reveals a more apolar/aprotic, i.e. more buried environment for K27C. This could suggest that the spin label attached to K27C is in a protein pocket that is shielded from outside water, but large enough to allow motion of the spin label. That proposition could be tested by molecular dynamics simulations, for example, but in the absence of those, any structural model has to remain speculation.

The higher resolving power of J-band compared to W-band EPR enables the differentiation of even more subtle differences in proticity. It reveals that each spin-label position in Zn-azurin results in two components in the J-band EPR spectra (cf. Figure 2.2), which differ with respect to the g_{xx} parameters. The spin label at position S118 possesses the largest g_{xx} (I) value and the largest relative contribution of that form, whereas in the mutant Q12C this component has a small contribution to the spectra. The mutants K27C and N42C are intermediate. For the K27C and the N42C mutants, the set of simulation parameters given in the table, i.e. the values of g_{xx} (I) and g_{xx} (II) and the respective spectral contributions, is not unique because of the strong interdependence of these parameters in the simulations.

We propose that the two spectral components are due to the spin label being exposed to slightly different micro-environments in the protein. Given that only the g_{xx}, and not the A_{zz} lines show two components, the two spectral components reveal that the spin-label environment corresponding to these components differs most with respect to the proticity and not the polarity of the protein. The magnitude of the splitting (Δg_{xx}) can be compared with models for the influence of hydrogen bonding and polarity on the spin label parameters[6,11,12]. These studies suggest, that the value of Δg_{xx} observed corresponds to one hydrogen bond (4×10^{-4} [6,11]) or a positive charge in the vicinity of the N-O-group of the spin label[11]. This would indicate that, in S118C, for one component, g_{xx} (I), the nitroxide group of the spin label is shielded from hydrogen bond donors, whereas for the other component, g_{xx} (II), it is exposed to a molecule or a group that can donate a hydrogen bond, such as a water molecule or an amino acid residue. For the other mutants, the weight of the component g_{xx} (I) decreases, as evidenced by the smaller percentage of the component with g_{xx} (I).

The nitroxide group can be exposed to different protein environments, if the linker connecting the spin label to the protein backbone has different conformations (rotamers), as has been proposed before. The X-ray structure of a spin-labeled protein[13] revealed different rotamers of the spin-label linker. The study [12] suggested that the two spectral components of these spin labels observed in EPR mobility studies were due to these groups of rotamers. We therefore propose that the two spectral components observed by J-band EPR correspond to different rotamers of the spin-label linker, which cause the spin label nitroxide group to have different hydrogen-bonding environments.

The present study reveals that small polarity/proticity differences can be resolved by high-field EPR. By increasing the field to 9 T in the novel 275 GHz spectrometer, two spectral components were observed that were previously not resolved in spin-labeled proteins. By comparing mobility studies[10] with the present investigation, subtle differences in the location of the

spin label can be resolved that will enable us to calibrate the result of molecular dynamics simulations and polarity calculations to be performed in the future.

Reference List

1. Steinhoff,H.J., Savitsky,A., Wegener,C., Pfeiffer,M. & Plato,M. High-field EPR studies of the structure and conformational changes of site-directed spin labeled bacteriorhodopsin. *Biochimica Et Biophysica Acta-Bioenergetics* **1457**, 253-262 (2000).

2. Lou,Y. & Ge,M.T. A multifrequency ESR study of the complex dynamics of membranes. *Journal of Physical Chemistry B* **105**, 11053-11056 (2001).

3. Altenbach,C., Marti,T., Khorana,H.G. & Hubbell,W.L. Transmembrane protein structure: spin labeling of bacteriorhodopsin mutants. *Science* **248**, 1088-1092 (1990).

4. Blok,H., Disselhorst,J.A.J.M. & Orlinskii,S.B. A continuous-wave and pulsed electron spin resonance spectrometer operating at 275 GHz. *Journal of Magnetic Resonance* **166**, 92-99 (2004).

5. van Amsterdam,I.M.C., Ubbink,M., Jeuken,L.J.C., Verbeet,M.P., Einsle,O. & Messerschmidt,A. Effects of dimerization on protein electron transfer. *Chemistry-A European Journal* **7**, 2398-2406 (2001).

6. Owenius,R., Engstrom,M., Lindgren,M. & Huber,M. Influence of solvent polarity and hydrogen bonding on the EPR parameters of a nitroxide spin label studied by 9-GHz and 95-GHz EPR spectroscopy and DFT calculations. *Journal of Physical Chemistry A* **105**, 10967-10977 (2001).

7. Finiguerra,M.G., Blok,H. & Ubbink,M. High-field (275 GHz) spin-label EPR for high-resolution polarity determination in proteins. *Journal of Magnetic Resonance* **180**, 197-202 (2006).

8. Nar,H., Messerschmidt,A., Huber,R., Vandekamp,M. & Canters,G.W. Crystal structure analysis of oxidized *Pseudomonas Aeruginosa* azurin at pH 5.5 and pH 9.0 - A pH-induced conformational transition involves a peptide bond flip. *Journal of Molecular Biology* **221**, 765-772 (1991).

9. van Amsterdam,I.M.C., Ubbink,M. & Canters,G.W. Anti-cooperativity in the two electron oxidation of the S118C disulfide dimer of azurin. *Inorganica Chimica Acta* **331**, 296-302 (2002).

10. Finiguerra,M.G., van Amsterdam,I.M.C., Alagaratnam,S. & Ubbink,M. Anisotropic spin label mobilities in azurin from 95 GHz electron paramagnetic resonance spectroscopy. *Chemical Physics Letters* **382**, 528-533 (2003).

11. Plato,M., Steinhoff,H.J., Wegener,C., Torring,J.T., Savitsky,A. & Möbius,K. Molecular orbital study of polarity and hydrogen bonding effects on the g and hyperfine tensors of site directed NO spin labelled bacteriorhodopsin. *Molecular Physics* **100**, 3711-3721 (2002).

12. Engstrom,M., Vaara,J., Schimmelpfennig,B. & Agren,H. Density functional theory calculations of electron paramagnetic resonance parameters of a nitroxide spin label in tissue factor and factor VIIa protein complex. *Journal of Physical Chemistry B* **106**, 12354-12360 (2002).

13. Hubbell,W.L., Gross,A., Langen,R. & Lietzow,M.A. Recent advances in site-directed spin labeling of proteins. *Current Opinion in Structural Biology* **8**, 649-656 (1998).

Chapter III

Accurate long-range distance measurements in a doubly spin-labeled protein by a four-pulse, double electron-electron resonance method

Abstract

Distance determination in disordered systems by a four-pulse double electron-electron resonance method (DEER or PELDOR) is becoming increasingly popular because long distances (several nm) and their distributions can be measured. From the distance distributions eventual heterogeneities and dynamics can be deduced. To make full use of the method, typical distance distributions for structurally well-defined systems are needed. Here, the structurally well-characterized protein azurin is investigated by attaching two 1-oxyl-2,2,5,5-tetramethylpyrroline-3-methyl)methanethiosulfonate spin labels (MTSL) by site-directed mutagenesis. Mutations at the surface sites of the protein Q12, K27, and N42 are combined in the double mutants Q12C/K27C and K27C/N42C. A distance of 4.3 nm is found for Q12C/K27C and 4.6 nm for K27C/N42C. For Q12C/K27C the width of the distribution (0.24 nm) is smaller than for the K27C/N42C mutant (0.36 nm). The shapes of the distributions are close to Gaussian. These distance distributions agree well with those derived from a model to determine the maximally accessible conformational space of the spin-label linker. Additionally, the expected distribution for the shorter distance variant Q12C/N42C was modeled. The width is larger than the calculated one for Q12C/K27C by 21%, revealing the effect of the different orientation and shorter distance. The widths and the shapes of the distributions are suited as a reference for two unperturbed MTSL labels at structurally well-defined sites.

Introduction

Distance determination by EPR techniques became gradually more important to solve structural problems that are not easily accessible by standard structural techniques. Usually, two spin labels are introduced such that their distance reflects the structural property of interest. Double electron-electron spin resonance (DEER or PELDOR[1-4]), a pulsed EPR method by which distances in the nm regime can be determined, is more and more used in that context, as reviewed recently[5,6]. Besides the long distance range accessible by the technique, the possibility to determine distance distributions is increasingly appreciated. Such distributions contain information about the uniformity of the molecular ensemble and can be used as a measure for flexibility, parameters that could cast light on the dynamics of macromolecules. Such dynamical aspects are of particular interest in a biological context. Here, DEER and related methods are spreading rapidly, also because methods to incorporate labels at the desired positions in many biological systems are now available.

Model systems in which the approach has been tested in a biological context are scarce. In particular, data of well characterized systems are needed as a reference for flexible, dynamic systems. We present distance measurements between two spin labels in the small protein azurin. The structure of this protein is well defined and known from X-ray crystallography[7]. Spin labels were introduced by spin label mutagenesis, as pioneered by Hubbell *et al.*[8] Two double mutants were investigated. The first one, in which Q12 and K27 were each replaced by a cysteine (Cys) (Q12C/K27C), and the second one, in which K27 and N42 were replaced by Cys (K27C/N42C). The singly labeled mutant protein K27C was used as a reference. All residues concern surface residues, i.e., residues that are expected to interfere least with the structure of the protein.

Two steps have to be accomplished. From experimental data, the distance (distribution) is determined, then, the distances are related to the protein structure. For the latter step, the length of the spin-label linker joining the spin label with the protein backbone is important[9-11].

Multiple conformations and dynamics can best be identified through the width of the distance distribution, but the uncertainty of the spin-label linker conformation makes it difficult to discriminate between the effect of the linker and the sought-for width of the distribution of the attachment points. For structurally well characterized proteins the former effect should dominate and therefore can be used to calibrate widths observed in unknown systems.

In the present study we show that distances in the 4 nm region can be measured with high accuracy. We propose a simple model to account for the conformation of the spin label linker (represented in Figure 3.1) and show that it yields a good agreement with the data.
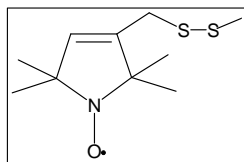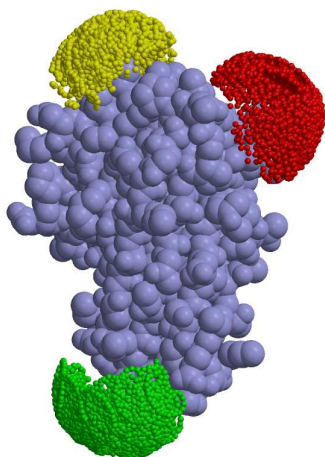
Figure 3.1 A surface model of azurin (PDB entry 4AZU[7]) is shown with the MTSL oxygens of all sterically allowed conformations of the spin labels. Red: spin label attached to C12; green: to C27; yellow: to C42. Insert: structure of MTSL, including cysteine sulphur and C$_\beta$ - atom.

Furthermore, we use the model to calculate the distance distribution of the spin-label combination Q12C/K42C to assess the effect of the location of the spin-labels, which are adjacent, i.e., on the same hemisphere of the protein, (Q12C/K42C) versus opposing, i.e., at opposite ends of the protein (Q12C/K27C and K27C/N42C) (Figure 3.1).

The range of the distance distributions is between 0.25 and 0.45 nm, where the latter value includes the effect of a wider distribution in the case of (Q12C/K27C).The width of these distance distributions is at the lower end of several of the distance distributions determined previously[12-17], suggesting that in the latter cases the flexibility of the protein plays an important role.

Materials and methods

Mutants and spin labeling

The mutation N42C was introduced in the gene encoding K27C azurin (plasmid pChH02, kindly provided by Prof. G. W. Canters, Leiden). First, part of the gene was amplified by PCR using an oligonucleotide containing the N42C mutation (CCTGCCGAAGTGCGTCATGGGTC ACAACTGGG) and an oligonucleotide binding downstream of the gene (CATGCACGGATCGTCGCGC). The resulting megaprimer was used in a second PCR reaction in combination with an oligonucleotide encoding a region upstream of the SalI restriction site at residue 22 (ACGACCAGATGCAGTTCAAC). The product was digested with *Kpn*I and *Sal*I and inserted into the pChH02, digested with the same enzymes, yielding pMGF02.

The Q12C/K27C double mutant was obtained by restriction of a fragment of the gene with only the Q12 mutation (pAZQ12C, kindly provided by Prof. G. W. Canters, Leiden) and insertion into the K27C azurin gene, taking advantage of the *Sal*I site, located between the mutation sites. This resulted in pMGF01. The mutations were confirmed by sequence analysis. Protein expression and purification was carried out under reducing conditions, as described[18]. The naturally present

metal ion Cu(II) was replaced by Zn(II) to avoid interference from spin interaction or redox chemistry[19]. Spin labeling of the mutants with the spin label 1-oxyl-2,2,5,5-tetramethylpyrroline-3-methyl)methanethiosulfonate (MTSL) was performed as described in ref. 20.

Sample preparation

The protein concentrations for the samples of the double mutants of azurin (0.175 mM, i.e. 0.35 mM in spin label, volume 150 µl, including 30% v/v glycerol) and the single mutant reference (K27C, 0.35 mM, volume 150 µl, including 30% v/v glycerol) were chosen according to the maximum concentrations suggested in reference [4] for the distance range of interest. Wilmad suprasil quartz tubes (inside diameter 3 mm, outside diameter 4 mm) were used.

DEER experiments

The DEER experiments were performed on a Bruker Elexsys 680 spectrometer (Bruker Biospin GmbH Rheinstetten, Germany) with the modifications described in reference[20]. Measurement conditions were analogous to those in reference[21]. The DEER experiment was performed at 40 K using a dielectric ring resonator and a helium flow system by Oxford, model CF 935. The four-pulse DEER sequence[2] p_1-t_1-p_2-t_2-p_3 with a pump pulse inserted after p_2 was employed. The pulse power of the observer pulses p_1, p_2 and p_3 (lengths: 32 ns) was adjusted to obtain a $\pi/2$ pulse for p_1 and π-pulses for p_2 and p_3. The pump-pulse (length: 36 ns) was adjusted for maximum inversion of the echo by varying the pump power. Delay times were t_1 = 200 ns, t_2 = 2000 ns and the time T, at which the pump pulse was inserted after p_2 was varied. The observer field was set to the low-field edge of the spin-label EPR spectrum and the pump frequency adjusted to coincide with the maximum of the electron-spin-echo detected EPR spectrum (frequency separation: $\Delta\nu$ = 65 MHz). The total measurement time for the DEER curves was 15 h.

Analysis of DEER results

For the analysis of the distance distributions, first, Gaussian distance distributions were simulated using the program DEERfit[2,22,23]. The parameters were adjusted manually; errors for single Gaussian distributions (Q12C/K27C: ± 0.03 nm; K27C/N42C: ± 0.02 nm) were estimated by determining the magnitude of the changes in the parameters that resulted in simulated curves outside the noise limit of the experiment. For the fitting procedure with arbitrary distance distributions, the methods provided in the program DeerAnalysis 2006 [24] were used. The background was calculated from the DEER curves with different starting times (Q12C/K27C: > 980 ns; K27C/N42C: > 1300 ns). Some of the characteristics in the data of the Q12C/K27C mutant also point to the possibility that the degree of double labeling is smaller in this mutant than in the

K27C/N42C mutant. Therefore, for the data of Q12C/K27C, also the experimental background from the K27C sample was tried but did not result in significant changes of the fits. Tikhonov regularization was employed and the first and second moments of the distance distributions are given.

Determining the conformational space of the spin label

Models of azurin with MTSL on Cys27 and either C12 or C42 were constructed using PDB entry 4AZU[7]. Then, using XPLOR-NIH,[25] the five torsion angles between the C_α of the Cys residue and the ring of the spin label were rotated systematically in steps of 30º. All orientations with steric clashes were discarded. Then, the distances from the MTSL nitrogens of all orientations of Cys27 to the nitrogens of all the MTSL orientations of C12 or C42 were determined and binned (binning classes: 0.1 nm).

Results

The intensity of the echo as a function of the time T (DEER time trace) for all three samples is shown in Figure 3.2. The modulations observed for the two double mutants reflect the spin-spin interaction. They are absent in the single mutant that contains only one spin label.
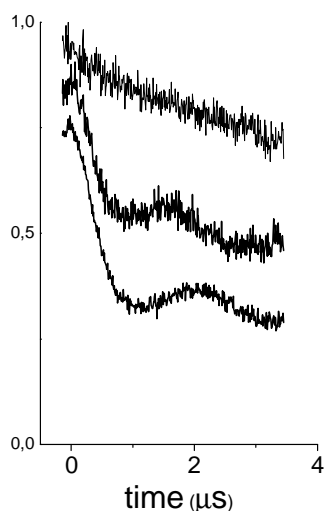

Figure 3.2 DEER time traces of K27C (top), Q12C/K27C (middle) and K27C/N42C (bottom). The traces are normalized and the traces of Q12C/K27C and K27C/N42C are shifted down for better visibility.

The difference in the modulation period of the two mutants is clearly visible, indicating a smaller dipolar interaction and thus a longer distance for the K27C/N42C mutant. For the analysis, the programs of Jeschke *et al.*[2,22-24] were used.

In Figure 3.3, panels a (Q12C/K27C) and b (K27C/N42C) the fits obtained are shown, superimposed on the baseline corrected time traces from Figure 3.2. The corresponding distance distributions are displayed in panels c (Q12C/K27C) and d (K27C/N42C).

For Q12C/K27C, the result of a single Gaussian fit is shown as trace 1 in Figure 3.3a. The deviation from the measured curve for the second period of the modulation around 2.5 µs is significant, suggesting that the distribution deviates from a single Gaussian. The agreement is better when two Gaussian functions are used, an example for which is shown in Figure 3.3a, trace 2 (distance distribution: Figure 3.3c, trace 2). Different combinations

of the two Gaussians give simulations of similar quality. The larger fraction peak is always centered at the value given in Table 3.1.
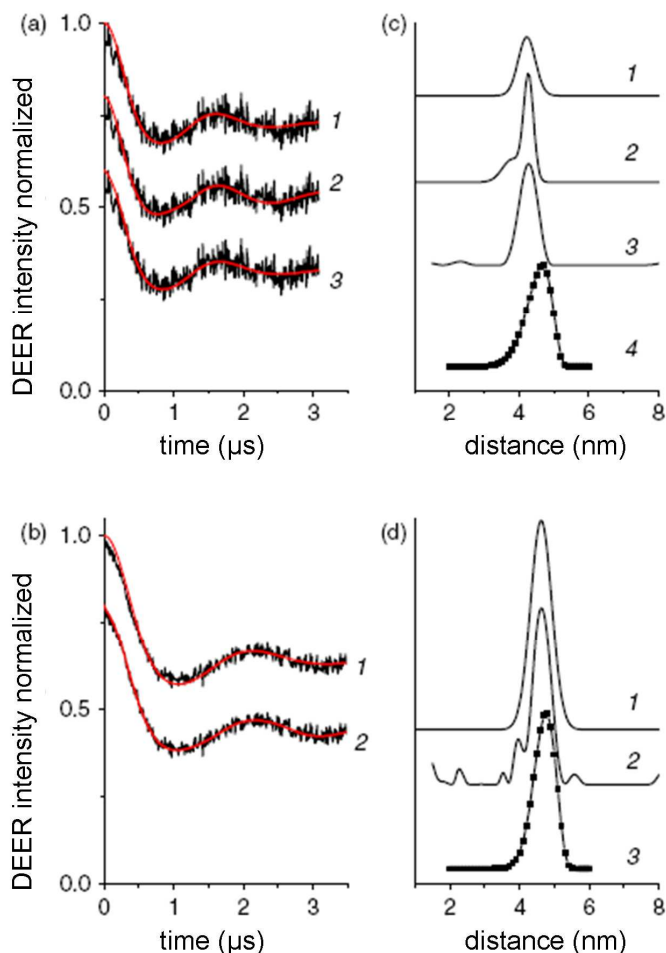

This peak has a position that is similar to that of the single Gaussian fit in trace 1 but it has a smaller width. Tikhonov regularization yields a fit (Figure 3.3a, trace 3) that is slightly better in quality than trace 2. The distribution (Figure 3.3c, trace 3) has a main peak that is similar to the main peak in trace 2 and an additional peak at 2.4 nm of low intensity. In Table 3.1, the distance parameters corresponding to the main peak of the Tikhonov regularization are also listed.

For K27C/N42C (Figure 3.3b) a single Gaussian distribution (trace 1 in Figure 3.3b and 3.3d) yields the proper period of the modulation albeit with larger damping than the experimental curve, suggesting that the width of the Gaussian distribution is too large. Tikhonov regularization results in the fits (Figure 3.3b, trace 2) and the distance distribution

Figure 3.3 DEER time traces (background corrected) and fits with different methods for Q12C/K27C (a) and K27C/N42C (b) (curves are shifted by constant amounts to avoid overlap); distance distributions for Q12C/K27C (c) and K27C/N42C (d). Models shown: (a, and c, trace 1): single Gaussian fit, parameters: 4.22 nm (centre), 0.35 nm (width), trace 2: two-Gaussian simulation, parameters see Table 3.1, trace 3: Tikhonov regularization, parameters see Table 3.1, trace 4: Distance distribution from model (see text). Panels b and d give the corresponding distance distributions. The distance distribution derived from the structural model is shown for Q12C/K27C in c, trace 4 and for K27C/N42C in d, trace 3.

shown (Figure 3.3d, trace 2). The agreement with the experimental data is slightly better than in the case of the single Gaussian (Figure 3.3b, trace 1). As seen from the parameters corresponding to these two distributions (Table 3.1) the peak resulting from Tikhonov regularization is indeed narrower than the single Gaussian.

Overall, a smaller distance and a smaller width of the distribution are found for the Q12C/K27C mutant than for the K27C/N42C mutant. There is some indication for a deviation of the distribution from Gaussian or a bimodal distribution for Q12C/K27C.

Table 3.1 Distances and parameters of distance distributions from the X-ray structure of azurin, DEER experiments, and the model

Mutant	Structure		Model		Gaussian		Tikhonov		$\Delta r(C_\beta)^e$
	C_α^a (nm)	C_β^b (nm)	Distance (nm)	Width[c] (nm)	Distance (nm)	Width[c] (nm)	Distance (nm)	Width[c] (nm)	
Q12C/K27C	3.38	3.50	4.58	0.42	4.27	0.2[f]	4.26	0.24	0.76
K27C/N42C	3.51	3.69	4.72	0.35	4.62	0.43	4.57[g]	0.36	0.88
Q12C/N42C	1.44	1.70	2.80[h]	0.53	nd[i]	nd[i]	nd[i]	nd[i]	na[i]

[a] C_α: $C_\alpha(1)$- $C_\alpha(2)$
[b] C_β: $C_\beta(1)$-$C_\beta(2)$
[c] half width at half-height
[d] standard deviation
[e] (distance from Tikhonov) – $(C_\beta(1)$-$C_\beta(2))$
[f] additional Gaussian, 31%: 3.8 nm centre, 0.4 nm width
[g] parameters of the central peak of the distribution
[h] maximum of distribution
[i] nd: not determined; na: not applicable

From the crystal structure[7], the distances between the C_β atoms of the two residues that are mutated were obtained. The measured distances are larger than the distances between the C_β atoms ($C_\beta(1)$-$C_\beta(2)$) listed in Table 3.1.

A simple model was used to determine the distribution of spin-label distances. By systematic rotation around the five torsion angles that connect the nitroxyl radical with the protein backbone, an ensemble of sterically allowed conformations was obtained for each spin label. The
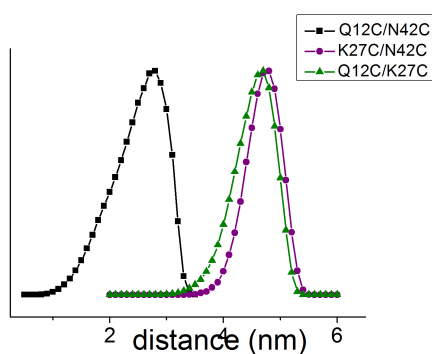

Figure 3.4 Distance distribution calculated from model. The distributions for Q12C/K27C and K27C/N42C are identical to those shown in Figure 3.3 (c) and (d).

model results in the distributions shown in Figure 3.3c, trace 4 and Figure 3.3d, trace 3.

The combination Q12C/K27C is also analyzed, and it is shown along with the other calculated distributions in Figure 3.4. These distributions are slightly skewed with a foot at shorter distances, but the deviation from a symmetrical Gaussian distribution is small. The distributions overlap the experimental ones and differences are discussed in more detail below.

Discussion

The distance distributions for two double mutants of Zn-azurin were obtained. In the following we will first discuss the analysis of the data and compare them to a model describing the spin-label linker conformations. The measured distances can then be related to the protein structure. Finally, we will compare the distance distributions to those obtained for other proteins.

The DEER data were analyzed using the currently available methods. For Q12C/K27C the parameters of the Gaussian distribution and the Tikhonov regularization agree within experimental uncertainties, for K27C/N42C the single Gaussian has a distance comparable to the Tikhonov regularization, but the smaller width of the latter yields a better agreement with the data. Thus, although the distance distributions from these approaches differ slightly, the overall deviation from Gaussians is small. The distributions are narrow and do not indicate significant bimodal character. The distance distribution of Q12C/K27C has a smaller distance and a smaller width than that of K27C/N42C.

As pointed out before[9-11], interpretation of the measured distances requires structural information about the spin-label. From the X-ray structure, only the position of the C_α and C_β atoms of the aminoacid-residue replaced by the cysteine is known, but the distance obtained from the experiment corresponds to the center of spin density on the two nitroxide groups of the spin label. The distance from the nitroxide group of the spin label to the C_β atom is between 0.5 and 0.6 nm for extended conformations of the spin-label linker[10]. Several approaches have been suggested to account for the conformation of the spin-label linker.

A straightforward approach [10] is to analyze the difference in the distances between the C_α and the C_β atoms of the two residues (residues (1) and (2)) that are mutated. If the $C_\alpha(1)-C_\alpha(2)$ distance is smaller than the $C_\beta(1)-C_\beta(2)$ distance, it is assumed that the spin labels are pointing away from each other, suggesting a distance larger than the $C_\beta(1)-C_\beta(2)$ distance, if the opposite is true the distance should be shorter. For both mutants, the $C_\alpha(1)-C_\alpha(2)$ distance is smaller than the $C_\beta(1)-C_\beta(2)$ distance (see Table 3.1), suggesting that the spin labels are pointing away from each other. In agreement with this, the measured distances are larger than the $C_\beta(1)-C_\beta(2)$ distances (see values $\Delta r(C_\beta)$ in Table 3.1). Assuming a spin-label-linker length of 0.5 nm per spin label, the distances observed experimentally, i.e. $\Delta r(C_\beta) < 1$ nm, are in the range of what the X-ray structure predicts.

To model the conformation of the linker directly, a model is proposed that is described in 'Experimental section'. It aims to explore the maximally accessible conformational space for the spin label by generating all possible conformations of the linker chain and only exclude those that have sterical clashes. The result may not represent the real distribution of distances, because any

molecular interactions that may result in preferred orientations of the MTSL are neglected (conformations, see Figure 3.1). For Q12C/K27C, the distance distribution derived from the model (Figure 3.3c) overlaps the distribution derived from the DEER experiment, but the model predicts a significant fraction at a larger distance that is not observed in the experiment. The trend towards model distributions that are broader than the experimental is also discussed in a recent publication[26]. For K27C/N42C (Figure 3.3d), the distribution from the model is closer in width and centre position to the experimental distribution than in the case of Q12C/K27C. It could thus be argued that the experimentally observed shift to shorter distances for Q12C/K27C represents conformations of the spin-labeled residue C12 that are determined by favorable molecular interactions. The good overall agreement of the model with the experimental results made it attractive to address the remaining combination of spin label positions Q12C/K42C *in silico*, to investigate the effect of a different relative orientation and a smaller distance of the spin labels. The comparison of the three distributions from the model (Figure 3.4) shows that the width of the distribution of Q12C/K42C is larger, which we attribute to the location of the two residues, which are adjacent rather than at opposing hemispheres of the protein, and the shorter distance between the nitroxides.

Previously, the model had been used in the context of distance determination in NMR, in which the paramagnetic relaxation caused by an MTSL spin label is used[27]. Because of the r^{-6} weighting of the distances in the NMR data, for the interpretation, particular attention has to be paid to the conformational space occupied by the spin label. The present data show that for the three positions of the spin label in the mutants a good agreement between the model and the experimental results is achieved as shown in Figure 3.3 and detailed in the *Results* section. This presents independent evidence for the validity of the model.

Other approaches to obtain the spin-label conformation are modelling the conformational degree of freedom of the spin label as free rotation about two bonds,[10] Molecular Dynamics (MD) simulations,[28-30] Monte Carlo energy minimization,[31] and rotamer libraries[32]. A comparison of different approaches has been discussed previously[32]. Recently[26], an approach has been presented that uses rotamer libraries and rigid-body refinement to determine the structure of a dimer by direct calculation of the DEER time traces. For *de novo*-structure determination the method has the advantage that it avoids the step to derive distance distributions from the DEER time traces. For the time being, we find the model employed in the present study a good compromise that allows us to include the local structure of the protein without having to pay the price of a full-fledged MD simulation.

The spin labels in the Zn-azurin mutants investigated here are on the surface of the protein and therefore not conformationally restrained. The protein azurin has a well-defined structure and,

as a consequence, should not contribute to the width of the distance distribution. Therefore, the widths of the distributions observed here, i.e. 0.24 nm and 0.36 nm, reflect exclusively the flexibility of the spin-label linkers. For a given range of conformations of the individual spin labels, the width of the distribution will, however, also depend on the relative location of the spin labels on the protein. Both the absolute distance but also the relative orientation of the protein surfaces can play a role. The distribution calculated for the pair Q12C/N42C gives an indication because, as seen in Figure 3.1, here two spin labels are in the same hemisphere of the protein, rather than at opposing ends of the protein. The calculated width of the distribution is 21 % larger than that of Q12C/K27C, which, in terms of the largest measured width (K27C/N42C, Tikhonov regularization), would correspond to 0.44 nm.

Several systems reported in the literature have comparable widths. A width of 0.3 nm was found for the interaction of two MTSL labels in ubiquitin[12], another structurally well characterized protein. In contrast, the buried spin-label sites in T4 lysozyme revealed broader, and in some cases bimodal distance distributions by continuous-wave EPR using a spectral-deconvolution method[13]. In one protein-oligomer system, a distribution with the parameters (6.15 ± 0.14) nm[14], was observed, however, in that case, the width may not be a reliable parameter given that the total length of the trace is shorter than the modulation period. Otherwise distance distributions in proteins tend to be broader. For example, in a membrane protein (LHCII), distance distributions with widths between 0.5-2 nm (width at half height) were found[15]. For the interaction between protein-monomers in an oligomeric system, depending on the conditions, distributions as narrow as 0.2 ± 0.1 nm, around 0.4 nm, or broad distance distributions ranging from 1.5 nm to 6 nm were found[17]. Almost structureless distributions with decreasing intensity between 2 and 4 nm were observed between spin labels attached to a single membrane protein[16]. Similarly, also DNA/RNA systems were investigated by DEER techniques, see for example reference [33], but chemically different spin labels and linkers used for these systems make the comparison difficult.

Our study indicates that broad distributions (> 0.45 nm) are not likely to be caused by the spin-label-linker conformations alone. This is not self evident because the length of the spin-label linker of 0.5 nm could, in principle, cause widths as large as 2 nm for the distance between two spin labels. Taking the widths measured for the relatively unrestricted spin labels at the surface of the protein of Q12C/K27C and K27C/N42C as a reference, structural heterogeneities or dynamics in the proteins investigated are the most likely source for distributions with widths larger than 0.45 nm.

Summary and conclusions

We measured the distance between two spin labels located at the surface of a well characterized protein, azurin. The system serves as a model for distance determination in a biological context. We applied different methods of analysis for the data and found relatively narrow distance distributions that are well described by Gaussians.

A model to determine the maximum conformational space of the spin-label linker yielded a good agreement with the experimental distance distribution, suggesting that the model gives a realistic picture of the linker conformation. We suggest that for proteins labeled with two MTSL spin labels that are not conformationally restricted, widths between 0.25 and 0.45 nm should be typical, indicating that larger widths are caused by flexibility or dynamics of the protein investigated.

The problem of absolute structure determination remains difficult as long as the label is attached by linkers of the given length, emphasizing the usefulness of conformationally rigid spin labels, such as used in synthetic peptides[34], proteins[35] and DNA or RNA systems[33,36]. The investigation of conformational changes or of interactions of protein subunits under different conditions suffers much less from the absolute distance uncertainty and has therefore been successfully addressed by the MTSL approach, as has been demonstrated in several studies[14-17].

Compared to Förster resonance energy transfer (FRET), a method that is well established for distance determination in biological systems, the spin label is smaller than the conventional fluorescent labels, and the spin density is localized on two atoms enabling structural determination to high precision. Also, there is no need for differential labeling, as required to introduce the FRET donor and acceptor pairs, and, in spin-label EPR, the same paramagnetic labels give access to the distance range from several Å to several nm.

The DEER method extends spin-label EPR to longer distances and thus has aided to turn spin-label EPR into a tool that complements the existing structural methods as NMR and FRET.

Reference List

1. Milov,A.D., Maryasov,A.G. & Tsvetkov,Y.D. Pulsed electron double resonance (PELDOR) and its applications in free-radicals research. *Applied Magnetic Resonance* **15**, 107-143 (1998).

2. Jeschke,G. Distance measurements in the nanometer range by pulse EPR. *Chemphyschem* **3**, 927-932 (2002).

3. Kurshev,V.V., Raitsimring,A.M. & Tsvetkov,Y.D. Selection of dipolar interaction by the 2+1 pulse train ESE. *Journal of Magnetic Resonance* **81**, 441-454 (1989).

4. Larsen,R.G. & Singel,D.J. Double electron-electron resonance spin-echo modulation: Spectroscopic measurement of electron-spin pair separations in orientationally disordered solids. *Journal of Chemical Physics* **98**, 5134-5146 (1993).

5. Borbat,P.P. & Freed,J.H. Measuring distances by pulsed dipolar ESR spectroscopy: Spin-labeled histidine kinases. (2007).

6. Schiemann,O. & Prisner,T.F. Long-range distance determinations in biomacromolecules by EPR spectroscopy. *Quarterly Reviews of Biophysics* **40**, 1-53 (2007).

7. Nar,H., Messerschmidt,A., Huber,R., Vandekamp,M. & Canters,G.W. Crystal structure analysis of oxidized *Pseudomonas Aeruginosa* azurin at pH 5.5 and pH 9.0 - A pH-induced conformational transition involves a peptide bond flip. *Journal of Molecular Biology* **221**, 765-772 (1991).

8. Hubbell,W.L. Investigation of structure and dynamics in membrane proteins using site-directed spin labeling. *Current Opinion in Structural Biology* **4**, 566-573 (1994).

9. Sale,K., Song,L.K., Liu,Y.S. & Perozo,E. Explicit treatment of spin labels in modeling of distance constraints from dipolar EPR and DEER. *Journal of the American Chemical Society* **127**, 9334-9335 (2005).

10. Borbat,P.P. & Mchaourab,H.S. Protein structure determination using long-distance constraints from double-quantum coherence ESR: Study of T4 lysozyme. *Journal of the American Chemical Society* **124**, 5304-5314 (2002).

11. Persson,M., Zhou,A., Mitri,R., Hammarstrom,P., Carlsson,U., Eaton,G.R. & Eaton,S.S. Distance determination between deeply buried position in human carbon anhydrase II. *Biophysical Journal* **78**, 2255Pos (2000).

12. Hara,H., Tenno,T. & Shirakawa,M. Distance determination in human ubiquitin by pulsed double electron-electron resonance and double quantum coherence ESR methods. *Journal of Magnetic Resonance* **184**, 78-84 (2007).

13. Altenbach,C., Oh,K.J., Trabanino,R.J., Hideg,K. & Hubbell,W.L. Estimation of inter-residue distances in spin labeled proteins at physiological temperatures: Experimental strategies and practical limitations. *Biochemistry* **40**, 15471-15482 (2001).

14. Jeschke,G., Abbott,R.J.M., Lea,S.M., Timmel,C.R. & Banham,J.E. The characterization of weak protein-protein interactions: Evidence from DEER for the trimerization of a von Willebrand factor A domain in solution. *Angewandte Chemie-International Edition* **45**, 1058-1061 (2006).

15. Jeschke,G., Bender,A., Schweikardt,T., Panek,G., Decker,H. & Paulsen,H. Localization of the N-terminal domain in light-harvesting chlorophyll a/b protein by EPR measurements. *Journal of Biological Chemistry* **280**, 18623-18630 (2005).

16. Jeschke,G., Wegener,C., Nietschke,M., Jung,H. & Steinhoff,H.J. Interresidual distance determination by four-pulse double electron-electron resonance in an integral membrane protein: the Na+/proline transporter PutP of Escherichia coli. *Biophysical Journal* **86**, 2551-2557 (2004).

17. Hilger,D., Jung,H., Padan,E., Wegener,C., Vogel,K.P., Steinhoff,H.J. & Jeschke,G. Assessing oligomerization of membrane proteins by four-pulse DEER: pH-dependent dimerization of NhaA Na^+/H^+ antiporter of *E. coli*. *Biophysical Journal* **89**, 1328-1338 (2005).

18. van Amsterdam,I.M.C., Ubbink,M., Einsle,O., Messerschmidt,A., Merli,A., Cavazzini,D., Rossi,G.L. & Canters,G.W. Dramatic modulation of electron transfer in protein complexes by crosslinking. *Nature Structural Biology* **9**, 48-52 (2002).

19. Ubbink,M., Lian,L.Y., Modi,S., Evans,P.A. & Bendall,D.S. Analysis of the ^{1}H-NMR chemical shifts of Cu(I)-, Cu(II)- and Cd-substituted pea plastocyanin - Metal-dependent differences in the hydrogen-bond network around the copper site. *European Journal of Biochemistry* **242**, 132-147 (1996).

20. van Amsterdam,I.M.C., Ubbink,M., Canters,G.W. & Huber,M. Measurement of a Cu-Cu distance of 26 a by a pulsed EPR method. *Angewandte Chemie-International Edition* **42**, 62-64 (2003).

21. Steigmiller,S., Borsch,M., Graber,P. & Huber,M. Distances between the b-subunits in the tether domain of F0F1-ATP synthase from *E. coli*. *Biochimica Et Biophysica Acta-Bioenergetics* **1708**, 143-153 (2005).

22. Jeschke,G., Koch,A., Jonas,U. & Godt,A. Direct conversion of EPR dipolar time evolution data to distance distributions. *Journal of Magnetic Resonance* **155**, 72-82 (2002).

23. Jeschke,G. Determination of the nanostructure of polymer materials by electron paramagnetic resonance spectroscopy. *Macromolecular Rapid Communications* **23**, 227-246 (2002).

24. Jeschke,G., Chechik,V., Ionita,P., Godt,A., Zimmermann,H., Banham,J., Timmel,C.R., Hilger,D. & Jung,H. DeerAnalysis2006 - a comprehensive software package for analyzing pulsed ELDOR data. *Applied Magnetic Resonance* **30**, 473-498 (2006).

25. Schwieters,C.D., Kuszewski,J.J., Tjandra,N. & Clore,G.M. The Xplor-NIH NMR molecular structure determination package. *Journal of Magnetic Resonance* **160**, 65-73 (2003).

26. Hilger,D., Polyhach,Y., Padan,E., Jung,H. & Jeschke,G. High-resolution structure of a Na^+/H^+ antiporter dimer obtained by pulsed election paramagnetic resonance distance measurements. *Biophysical Journal* **93**, 3675-3683 (2007).

27. Volkov,A.N., Worrall,J.A.R., Holtzmann,E. & Ubbink,M. Solution structure and dynamics of the complex between cytochrome *c* and cytochrome *c* peroxidase determined by paramagnetic NMR. *Proceedings of the National Academy of Sciences of the United States of America* **103**, 18945-18950 (2006).

28. Borovykh,I.V., Ceola,S., Gajula,P., Gast,P., Steinhoff,H.J. & Huber,M. Distance between a native cofactor and a spin label in the reaction centre of Rhodobacter sphaeroides by a two-frequency pulsed electron paramagnetic resonance method and molecular dynamics simulations. *Journal of Magnetic Resonance* **180**, 178-185 (2006).

29. Steinhoff,H.J., Muller,M. & Beier,C. Molecular dynamics simulation and EPR spectroscopy of nitroxide side chains in bacteriorhodopsin. *Journal of Molecular Liquids* **84**, 17-27 (2000).

30. Beier,C. & Steinhoff,H.J. A structure-based simulation approach for electron paramagnetic resonance spectra using molecular and stochastic dynamics simulations. *Biophysical Journal* **91**, 2647-2664 (2006).

31. Sale,K., Sar,C., Sharp,K.A., Hideg,K. & Fajer,P.G. Structural determination of spin label immobilization and orientation: A Monte Carlo minimization approach. *Journal of Magnetic Resonance* **156**, 104-112 (2002).

32. Jeschke,G. & Polyhach,Y. Distance measurements on spin-labelled biomacromolecules by pulsed electron paramagnetic resonance. *Physical Chemistry Chemical Physics* **9**, 1895-1910 (2007).

33. Schiemann,O., Piton,N., Mu,Y.G., Stock,G., Engels,J.W. & Prisner,T.F. A PELDOR-based nanometer distance ruler for oligonucleotides. *Journal of the American Chemical Society* **126**, 5722-5729 (2004).

34. Sartori,E., Corvaja,C., Oancea,S., Formaggio,F., Crisma,M. & Toniolo,C. Linear configuration of the spins of a stable trinitroxide radical based on a ternary helical peptide. *Chemphyschem* **6**, 1472-1475 (2005).

35. Becker,C.F.W., Lausecker,K., Balog,M., Kalai,T., Hideg,K., Steinhoff,H.J. & Engelhard,M. Incorporation of spin-labelled amino acids into proteins. *Magnetic Resonance in Chemistry* **43**, S34-S39 (2005).

36. Piton,N., Mu,Y., Stock,G., Prisner,T.F., Schiemann,O. & Engels,J.W. Base-specific spin-labeling of RNA for structure determination. *Nucleic Acids Research* **35**, 3128-3143 (2007).

Chapter IV

Paramagnetic NMR using spin-labeled proteins to study the structure of the complex between cytochrome f and plastocyanin

Abstract

Using site-specific spin-labeling in combination with paramagnetic relaxation enhancement (PRE) NMR spectroscopy, the physiological transient complex between cytochrome f (Cyt f) and plastocyanin (Pc) from cyanobacterium *Nostoc* sp. has been investigated and the interaction of Pc with five Cyt f cysteine mutants has been analyzed. In this work, the large magnetic dipolar interaction existing between unpaired electrons and nearby nuclear spins has been employed. The structure obtained has been compared to the results of a previous study performed using other NMR techniques, specifically pseudocontact shifts (PCSs) and chemical shift perturbations (CSPs). The conclusion of the present work is that a single structure does not satisfactorily represent the complex as previously proposed.

Introduction

In biomolecular research the understanding of the mechanism of biological processes at the molecular level is one of the main goals. Many biological processes involve protein-protein complexes. To understand how proteins interact to form a complex, and therefore how they react to undertake their functions, knowledge of the static complex structure alone, even at the atomic level, is not enough. A complete description of the protein-protein complex formation requires thinking of interacting proteins as 'objects in action'; thus, the study of protein dynamics becomes fundamental. The extension of the structure-function paradigm to include time as a fourth dimension, in addition to the three spatial dimensions, is required for the description of a complete protein-protein reaction mechanism.

In general, when two proteins meet each other to form a complex, they form a static complex if the affinity between the proteins is high. Conversely, if it is low they form a transient complex. The model of the process of protein-protein association, proved by kinetic and NMR studies recently reviewed[1], assumes that the complex formation begins with the proteins approaching by diffusion; they then start random collisions, which may develop into an initial association, the so-called *encounter complex*, which is in equilibrium with the final specific complex, - see Ubbink[1] and references therein (Fig. 4.1). In a transient complex the relative orientation of the proteins may vary from a single well-defined state to a highly dynamic cluster of orientations[2-10] which constitute the encounter complex[1]. Many studies[11-23] have provided evidence for the existence of encounter complexes both in transient protein-protein interactions and in protein-DNA interactions.
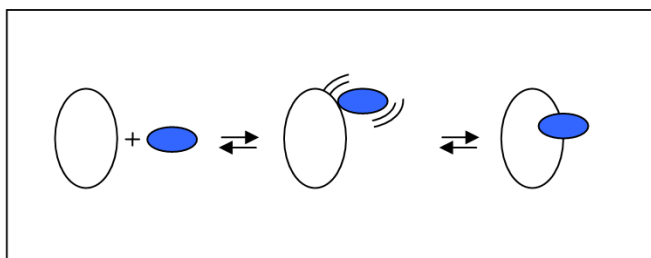

Figure 4.1 Protein complex formation model: the final single-oriented complex (right shape) is preceded by the ensemble of protein orientation middle, the so-called encounter complex[2].

To clarify the term "encounter complex", it is interesting to describe the evolution of its meaning over time, as reviewed by Volkov[11]. In 1968, Adam and Delbrück defined an *encounter complex* as two proteins occupying the same solvation shell as a result of a diffusion-driven collision process[24,25]. A later definition distinguished between a simple collision, happening when the distance of two proteins is small, and precisely equal to one hydration radius (*ca.* 2 Å), and an

actual encounter, *i.e.* the entire set of interactions from the initial collision to the final separation of the two proteins[26]. A refined version of the second definition further specifies an encounter complex as the state in which the protein touches the surface of the partner, via multiple microcollisions, and a specific active, *single-orientation complex* formed as a result of some of these collisions[25]. The character of transient protein complexes can vary from highly-dynamic to well-defined depending on the equilibrium between the encounter and the specific state. The transientness of protein complexes is related to their function. Some biological processes, such as electron transfer processes or processes related to signal transduction require the existence of transient protein complexes. In redox processes, usually one of the partners is a small carrier protein that shuttles electrons between its partners in the reaction chain.

The lifetime of complexes, in weakly bound electron transfer processes, can be very short (of the order of milliseconds), since it is essential that the complex rapidly dissociates. A balance between protein specificity and affinity is reached, and a high turnover can be achieved if both the association and dissociation rate constants of the complex (k_{on} and k_{off}, respectively) are high. If the lifetime of the complex is in the millisecond range, then the dissociation rate constant (k_{off}) is $\geq 10^3 s^{-1}$. The maximal association rate constant is the diffusion limit (10^7-10^9 M^{-1} s^{-1})[27-29]. These values for k_{on} and k_{off} imply a dissociation constant ($K_d = k_{off}/k_{on}$) in the µM–mM range. Conversely, the main characteristic of proteins performing their diverse set of functions through stable complexes is their ability to bind to other molecules specifically and tightly. For these protein complexes the specificity of the binding is determined by the complementary geometry of the protein surface (lock and key model); they are characterized by much lower dissociation rate constants (k_{off}) and, as a result, by long lifetimes.

In which way specificity is achieved has been a central question of studies for many years. Its answer is not completely known yet.[1-3,7-12,14,15,21,22,30,31,31]

Computational analysis of the crystal structures of redox protein complexes available revealed that fast dissociation is characterized by low geometric complementarity of the protein partners in the complex, which allows only a poor packing[32]. Protein-protein complexes are stabilized by a variety of non-covalent interactions, including van der Waals, electrostatic, hydrophobic interactions, net dipoles, intermolecular hydrogen bonds and salt bridges. Long-range electrostatic interactions are generally implicated in the early step of transient protein-protein association, while short-range hydrophobic interactions play a main role in the second step, allowing the protein to recognize its partners, to achieve specificity for carrying out a particular function, and to achieve stability. In electron transfer protein complexes, whose biological function requires them to be highly transient, a patch of hydrophobic residues is often found on the surface close to the active site, allowing for

protein-protein contact and, thus rapid electron transfer. Complete desolvation is not productive to carry out their function; therefore the hydrophobic patch usually represents a small fraction of the total surface of the protein and is surrounded by a ring of polar residues that promotes the dissociation of the complex[16,31]. Electron transfer partners react quickly and do not achieve high specificity, leading to low affinity and high k_{off}. In many cases electron transfer proteins have multiple partners reacting at the same binding site and, in those cases, a compromise in binding specificity is required. In other cases proteins form much more stable complexes, which require high specificity. The encounter complex is an integral part of the protein complex and plays different roles in the two complex formation types. A recent review[1] containing a summary of the relevant theoretical considerations and the discussion of the experimental results on the encounter state of protein complexes came to the conclusion that a complete description of protein complexes requires the study of both the well-defined, productive complex and of the dynamic encounter complex. To understand how specificity is achieved in weak and transient complexes requires therefore the ability to get insights into the interplay of the non-covalent interactions in the protein complexes, and the simultaneous knowledge of the productive complex and the dynamic encounter complex.

The complex between plastocyanin (Pc) and cytochrome f (Cyt f), studied in this thesis, is a transient complex involved in the electron transfer processes of the oxygenic photosynthesis[34-37]. The Cyt f is a transmembrane protein with a large soluble domain that is part of the cytochrome b_6f complex, which is embedded in the thylakoid membrane. In the photosynthesis of the oxygen-evolving photosynthetic organisms (plants, cyanobacteria and green algae), from the energetic point of view, the b_6f complex is situated
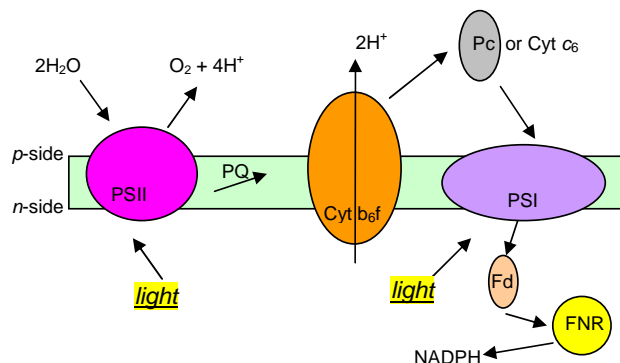

Figure 4.2 Schematic representation of the electron pathway in the oxygenic photosynthesis. The integral membrane protein complexes responsible for electron transport and proton translocation in oxygenic photosynthesis. The reaction centers of PSI (purple) and PSII (magenta), and the cytochrome b_6f complex (orange) are shown. Luminal (p) and stromal (n) -side soluble electron transfer proteins are plastocyanin (green) or cytochrome c_6, ferredoxin (pink), and ferredoxin-NADP reductase (yellow)[33].The idea and the layout of the figure was taken from ref. 33 in modified form.

between the two photosystems and transfers electrons from photosystem II-plastoquinone to plastocyanin-photosystem I (Fig. 4.2). Looking in more detail, Pc accepts an electron from the Cyt f of the cytochrome b_6f complex and transfers it to the pigment P700[+] from photosystem I[38]. Thus, Cyt f acts as an electron donor while P700[+] accepts electrons from reduced Pc. The cytochrome b_6f

complex and P700$^+$ are both membrane-bound proteins with exposed domains positioned on the lumen-side of the thylakoid membrane of cyanobacteria or chloroplasts (for plants and eukaryotic algae) in which the Pc is located. In the same cellular space another soluble protein, the cytochrome c_6, is also located, serving, in certain conditions, as an alternative electron carrier.

While Pc is the only electron carrier in higher plants and the cytochrome c_6 is the only one in some cyanobacteria[39], certain eukaryotic algae and cyanobacteria are capable of synthesizing either Pc or cytochrome c_6, depending on the availability of copper in the culture medium[40-43]. The two proteins, Pc and Cyt c_6, have different structures but carry out the same physiological function, the transfer of electrons from the cytochrome b_6f complex to PSI.

Besides being interesting for its physiological function, the Cyt f-Pc complex, due to the large amount of data available, represents an excellent model system for the understanding of transient interactions between proteins[44,45]. The lifetime of this type of complex is about 1 ms. Previous studies suggested that, depending on the organism from which it is derived (i.e. plants, algae or cyanobacteria), the kinetics of the Cyt f - Pc complex may vary greatly, highlighting in some cases differences in the reaction mechanism between *in vivo* and *in vitro* experiments[31,46-54] Extensive structural investigation of the transient Cyt f-Pc complex showed also differences in the orientations of the two proteins from different organisms in the complex[2,4,31,44,46,49,55-59]. This complex being transient, it requires the analysis of the time-dependent dynamics of the protein complex formation and the experimental characterization of the encounter complex. Recent studies on different protein complexes showed that a computational approach associated with restraints derived from experimental data, is a very promising way for the study of the elusive encounter complex[1,14,23]. Several spectroscopic techniques can be used for experimental investigations, including paramagnetic relaxation enhancement (PRE), pseudocontact shift and residual dipolar coupling NMR.

The PRE technique provides long-range distance information (up to 25-35 Å)[61]. Distances between a paramagnetic centre containing unpaired electrons, like a spin label or a metal ion, and a nucleus can be determined from the increased nuclear T_2 relaxation rate. The effect of the unpaired electron of a spin label on the relaxation rates is very strong at short distances between the nucleus and the paramagnetic centre, and it falls off with the sixth power of the distance. The PRE technique can detect conformations that represent only a small percentage of the complex. In this way, information on the surface area sampled by the protein partner can be obtained. The PRE is an average over all conformations, so it may represent either a heavily populated state far from the paramagnetic centre or a lowly populated state at short distance. Distinguishing between these two situations is impossible[1].
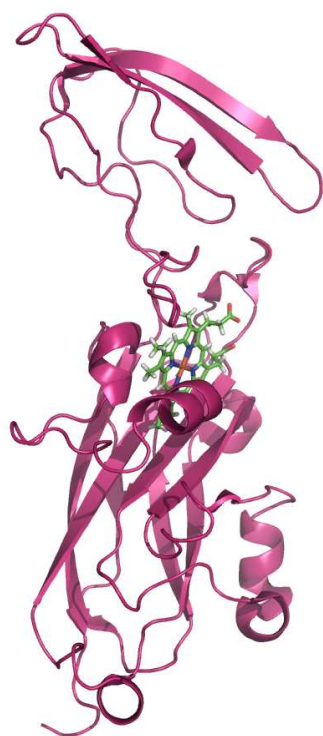

Figure 4.3 Three-dimensional structure of Cyt *f*. The protein is shown in pink and the haem, with the Fe in the center (red), is shown as sticks. The figure has been generated from the NMR structure of the complex between Pc and Cyt *f* from the cyanobacterium *Nostoc* sp. PCC 7119 (PDB entry 1tu2)[56]. The figure has been made with PyMOL v 0.98[60].

The larger protein used in this investigation is the truncated Cyt *f* subunit (Fig. 4.3), consisting of a ca. 28 kDa N-terminal soluble domain that in the cyanobacterium *Nostoc* sp. PC 7119 is anchored to the membrane by a C-terminal helix[62]. It is an atypical *c*-type cytochrome, having an unusual haem axial coordination (the N-terminus being one of the haem ligands). The secondary structure is mainly β-sheet.

The partner protein, Pc, is a small (11 kDa) type I copper protein with the metal ion coordinated by two histidines, one cysteine and one methionine[48] (Fig. 4.4). Two functional regions, the hydrophobic and the electrostatic patch, have been identified on Pc. The first one, site 1, is positioned at the so-called north end surface of the molecule surrounding a copper-ligand histidine and is involved in the electron transfer[2]. The second one, site 2, is situated at the 'east side' of the molecule, playing in some cases, like in plants, a key role in electrostatic interactions with the redox partners[62]. Generally, the structures of Cyt *f* and Pc are well conserved among plants, algae and cyanobacteria, although differences are observed in the distribution of charges on both proteins, permitting in all cases electrostatic attractions with the partner protein in the complex.[33,48,63,64] In plants and *P. laminosum* the Pc is an acidic protein (pI = 5.5 and pI = 5.0, respectively), while in Pc from the cyanobacterium *Nostoc*, it is basic (pI = 8.8). A comparison between the amino acid sequences of the Pc partner, Cyt *f* from *P.*

laminosum and Cyt *f* from *Nostoc*, reveals a high similarity, with the exception of a range of about sixty residues, found between position 170 and 230, which correspond to the small domain of the soluble part of the protein. The surface charge of *Nostoc* Cyt *f* is different from that of *Phormidium* Cyt *f*, and is involved in the interactions within the complex, even though this effect is much more evident *in vitro* then *in vivo*[65]. Differences in surface charge distributions are reflected in the modality of

approach between the two proteins and in their mutual orientation in the complex.[4,55,56,65]

In the Cyt *f*-Pc complex from cyanobacterium *Nostoc sp.*, significant structural differences have been found with respect to equivalent complexes from other sources[2,56]. The three-dimensional structure of the *Nostoc* Pc-Cyt *f* complex has been characterized by NMR spectroscopy[56] using intermolecular pseudo-contact shifts caused by the heme iron and chemical shift perturbation data, thus revealing that this complex adopts a conformation similar to the one found in plants, which is in the side-on binding mode, but with opposite charge[2]. The interface of the *Nostoc* Pc-Cyt *f* complex is similar to that of the cyanobacterium *Phormidium laminosum* complex. The latter, though, shows an atypical head-on orientation[4,65]. At the interface region of the complex, the
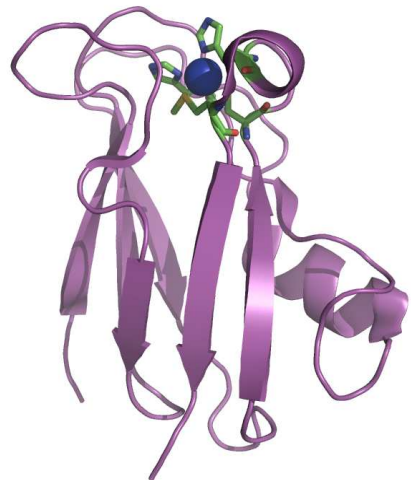
Figure 4.4 Three-dimensional structure of Cu-Pc. The copper atom is shown as blue sphere and the four ligands, a cysteine, methionine and two histidines, are shown as sticks. The figure has been generated from the crystal structure of plastocyanin from the cyanobacterium *Anabaena variabilis* (PDB entry 2gim)[66].

binding site involves the hydrophobic areas close to the metal sites in both proteins[56]. But whereas in *Phormidium* the interaction in the complex is weakly salt dependent, in *Nostoc* it varies greatly with the ionic strength; in fact, the binding constant for the complex of *Nostoc* at low ionic strength becomes an order of magnitude larger compared to the one at physiological ionic strength[65]. A mutagenesis study of the complex demonstrated that Pc protein dictates the specificity of the electrostatic interaction. Specific short-range electrostatic interactions are present as well and, as already mentioned above, these are due essentially to the Cyt *f*[67].

In Cyt *f* five acidic residues (pink residues in figure 4.5) play a relevant role in the electrostatic interactions with the positive groups of Pc. These residues are: Asp-64 and Glu-189, located on the small domain region of Cyt *f*, containing an acidic patch; Asp-100 and Glu-108, which are on the large domain; and Glu-165, located near the hydrophobic patch[56]. The charged residues are located at the border of a group of 20 residues (some of them being at least partially

buried) involved in the recognition site, most of which are hydrophobic or uncharged polar. Five aromatic residues are present on this patch and three of them, specifically Tyr 1, Phe 3, and Tyr 102, constitute about 31% of the recognition surface of Cyt *f*. Six proline residues (which are amino acids with very low propensity in protein-protein interfaces)[68-70] are located in the interface. The inability of Pro to form hydrogen bonds may be employed to limit the affinity in such complex[56]. Furthermore, 4.3% of the recognition sites of the complex are derived from the polar, uncharged amino acid glutamine, which, surrounding the hydrophobic patch, may improve dissociation by facilitating resolution of the interface, as suggested by Crowley and Ubbink[31].

In Pc, the interface region comprises 14 residues (Fig. 4.5). Ten from the hydrophobic patch (Leu-14, Val-36, Pro-37, Pro-38, Leu-64, Met-66, Pro-68, Pro-91, His-92, and Ala-95, indicated in blue in Fig. 4.5), three from the nearby region of site 2 (Lys-62, Gln-63, and Glu-90), and the Lys-35 which is adjacent to the hydrophobic patch[56]. A second, minor recognition site on Pc corresponds to residues Asp-54 and Lys-57, interacting with the acidic patch of the above mentioned small domain of the Cyt *f* [56].

Kinetic studies of the *Nostoc* Cyt *f*-Pc complex to investigate the contribution of the charged residues to the interaction energy and to identify specific short-range electrostatic interactions between charged residues have been carried out[67]. To this purpose a series of site-directed mutants of Cyt *f*, neutralizing the charge of negative residues with alanine or reverting it upon substitution by lysine, were
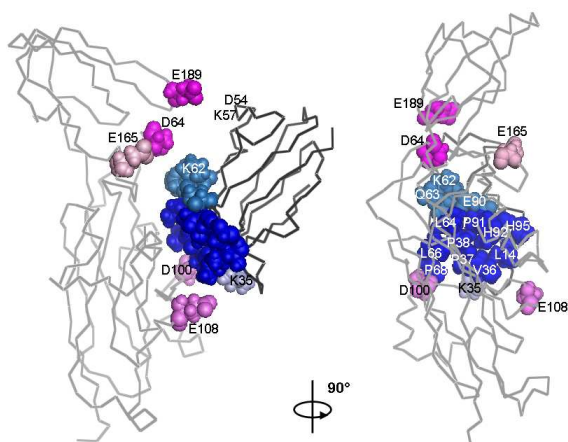

Figure 4.5 *Nostoc* Cyt *f* – Pc interface. In pink, the five Cyt *f* residues playing a relevant role in the electrostatic interactions with the positive group of Pc (dark pink: residues located on the small domain of Cyt *f*; light pink: residue close to the hydrophobic patch; medium pink: residues located on the large domain). In blue, the 14 Pc residues on the interface region (dark blue: the 10 hydrophobic residues from the hydrophobic patch; medium blue: residues located in site 2; light blue: basic residue 35 close to the hydrophobic patch). On the left figure, adjacent to E189 of Cyt *f*, the positions of the two Pc residues of the second recognition site are also shown[56].

constructed. The effects of mutations on the kinetics of electron transfer to wild-type and mutant forms of Pc were measured by laser flash absorption spectroscopy. The results showed that in the *Nostoc* complex the main contribution to the electrostatic interaction with Pc in the complex is provided by the small domain of Cyt *f*. The Cyt *f* mutants, with some negative charges replaced with neutral residues, revealed an apparent electron transfer rate constant with wild-type Pc similar to (or

slightly higher than) that of the wild-type species. Mutants, in which negative charges were replaced by positive residues exhibited instead a significantly lower reactivity. Furthermore, in contrast with the more defined surface found in Pc[71], a wide electrostatic area was involved, as the result of an additive effect of multiple specific interactions. As a consequence the substitution of a single charged residue in the Cyt *f* does not promote drastic changes in the interaction with the Pc. A similar outcome was obtained by mutating specific residues in *Phormidium* Cyt *f* [55]. Different results were obtained from the analysis of the interaction of Cyt *f* (wt) with site-directed mutants of charged residues in the positive patch of *Nostoc* Pc[71]. In that case, the neutralization or the charge inversion of the key residues promoted significant changes in complex formation and electron transfer, suggesting that the specificity of the Cyt *f*-Pc interaction is mainly determined by the electrostatic features of Pc. These results are in agreement with the particular orientation of the two partners described in NMR studies[56]. The parallel kinetic behaviour showed that Pc uses the same surface area to interact with both its redox partners, Cyt *f* and Photosystem I (PSI)[67,71,72]. The electrostatic patch enhances the association rate, and the hydrophobic area is used for electron transfer.

Several structural studies on electron transfer (ET) complexes like that between Pc and Cyt *f* have been performed, as recently reviewed[1]. Some ET complexes appear to be mostly specific[2,11,73], while others are completely or mainly non-specific[3,6,9,10,15,74], and the encounter state is the most populated form. The structure of the ET *Nostoc* Pc-Cyt *f* complex was found to be well-defined, as it is in the case of plants[2,56], in contrast with the highly dynamic structures found in the case of *P. laminosum*[4] and of *Prochlorothrix Hollandica*[58]. All these complexes, which are transient, were studied using paramagnetic NMR spectroscopy, which is a powerful technique for *in vitro* studies of structure and dynamics of soluble biological macromolecules. If a nucleus approaches a paramagnetic tag like a stable free radical or a paramagnetic metal ion, a shift of the nuclear resonance or a change in its relaxation time results. Different paramagnetic NMR techniques can be used for experimental investigations, including paramagnetic relaxation enhancement (PRE), pseudocontact shift (PCS) and residual dipolar couplings (RDCs). In the work of Diaz-Moreno and collaborators, the *Nostoc* Pc-Cyt *f* complex was studied using PCSs and chemical shift perturbation (CSP)[56]. In the present work, we use PRE NMR with the purpose of complementing this study, acquiring independent constraints for complex structure determination, and getting information concerning the encounter complex. Paramagnetic Relaxation Enhancement is isotropic and inversely dependent on the sixth power of the distance between nucleus and paramagnetic centre, while the PCS depends on the orientation of nucleus within the frame set by the magnetic susceptibility tensor, and is inversely dependent on the third power of distance between nucleus and

paramagnetic centre. The observable RDC, on the other hand, does not depend on the nucleus-tag distance. All these techniques, therefore, provide different views of the complex dynamics[14,75].

The PRE technique provides long-range distance information (15-24 Å). Distances between a paramagnetic centre containing unpaired electrons, like a spin label, can be determined from the increased T_2 relaxation rates. The effect of an unpaired electron on the relaxation rate is very strong at short distances. Consequently, the PRE technique is able to detect also conformations representing only a small percentage of the complex in which the paramagnetic centre is close to the active nuclei.

When spin labels are attached to different positions on the protein surface, it is possible to acquire information about the surface sampled by the partner protein in the encounter complex[11,23]. Such effects are, however, an average over time and space. Hence, the information obtainable from this technique could be caused by either a heavily populated state characterized by long-distance interactions, or by a lowly populated state with short distance interactions; it is not possible to distinguish between these two situations[1]. Still, it must be taken into account that an important advantage of this technique is that it also allows to study sparsely populated conformational ensembles in solution[75], as it happens in some cases for the encounter complex. This method has been extensively used to demonstrate the existence of the encounter complex by Clore and coworkers[13,76] and Ubbink and coworkers[11,23].

In the present work, therefore, we aim to investigate the structural aspects of the transient complex between Pc and Cyt f from the cyanobacterium *Nostoc* sp. PC 7119 (formerly *Anabaena variabilis*) using the PRE technique, in combination with site-directed spin labelling (SDSL). The Pc has been uniformly ^{15}N labeled and was used to form a complex with its physiological partner, the Cyt f. The results of this study indicate that the Cyt f – Pc complex cannot be described only as a single structure, but must be depicted as the equilibrium between a specific and an encounter complex, a view that was recently suggested also for the Pc-Cyt f complex from other species[58], as well as for a complex between Cyt f and cytochrome c_6[77].

Materials and Methods

Site Directed Spin Labeling of Cyt f

- *Mutagenesis*

The pEAF-wt[71] expression plasmid encoding the soluble domain of Cyt f from *Nostoc* sp. PCC7119 was kindly provided by Prof. Miguel De la Rosa, Instituto de Bioquímica Vegetal y Fotosíntesis, Universidad de Sevilla, Spain. To avoid changes in the pI, which could affect the

protein-protein interactions, only neutral amino acid residues (N, Q, S, A) were replaced by cysteine. In order to prepare the single-cysteine Cyt *f* variants Q7C, A63C, N71C, Q104C and S192C, mutations were introduced in the Cyt *f* gene using the Quik Change™ polymerase chain reaction protocol (Stragene, La Jolla, CA) with the plasmid pEAF-wt as a template and the primers indicated in Table 4.1. All constructs were verified by DNA sequencing.

Table 4.1. **Primers used in site–directed mutagenesis of Cyt *f*. Codon-changing (bold italic underlined) and silent (highlighted) mutations are indicated.**

Q7C (34 bp; restriction enzyme: ApaL I)

forward   5'– GCATATCCTTTCTGGGCGCAG***TGC***ACTTACCCAG – 3'

reverse   3'– GACCCATTCA***CGT***GACGCGGGTCTTTCCTATACG – 5'

A63C (36 bp; restriction enzyme BstX I)

forward   5'– CCAGCGTCCAACAAGTTGGT***TGC***GATGGCTCTAAGG – 3'

reverse   3'– GGAATCTCGGTAG***CGT***TGGTTGAACAACCTGCGACC – 5'

N71C (31 bp; restriction enzyme: Sty I)

forward   5' – GGCTCCAAGGTCGGCTTA***TGC***GTCGGTGCTG – 3'

reverse   3'– GTCGTGGCTG***CGT***ATTCGGCTGGAACCTCGG – 5'

Q104C (32 bp; restriction enzyme: Bgl I)

Forward   5' – CGGCGATGTTTACTTC***TGC***CCCTACGGCGAAG – 3'

Reverse   3' – GAAGCGGCATCCC***CGT***CTTCATTTGTAGCGGC – 5'

S192C (36 bp; restriction enzyme: Sal I)

Forward 5'– GGCGAAGATGGT***TGC***GTTAAATATTTAGTCGACATC – 3'

Reverse 3' – CTACAGCTGATTTATAAATTG***CGT***TGGTAGAAGCGG – 5'

For A63C and N71C a silent mutation was designed to introduce an extra BstX I and Sty I restriction site respectively, located close to the *5'* end of the primer (Table 4.1). In the case of the S192C mutant a Sal I restriction site was introduced at the *3'* end of the primer (Table 4.1). The mutagenesis for preparing Q7C and Q104C mutant has been described previously[78]: to introduce a cysteine instead of the asparagines at the position 71 the direct primer (see table 4.1) was designed inserting at the same time the Sty I restriction site next to the *5'* end of the primer. Analogously, to introduce a cysteine instead of the glutamine at the position 104 the direct primer was designed, inserting an extra Bgl I restriction site respect to the wild type.

Protein production and purification

- *Cytochrome f variants*

To improve the yield of holocytochrome *f* and promote the correct insertion of the haem group, *E. coli* strain MV1190 (Bio-Rad) was co-transformed with plasmids pEC86[79] and (mutated) pEAF plasmid. The cells were plated on Luria-Bertani (LB) medium plates and incubated at 37° C for 24 hours. This medium and those mentioned below were supplemented with 20 mg/L ampicillin (amp) and chloamphenicol (cam). Several pre-cultures were prepared in 100 mL flasks with 20 mL of LB medium and incubated at 37 °C and 250 rpm for 5-6 hours. The pre-cultures with the highest OD_{600} were used to inoculate 1.7 L (in 2 L Erlenmeyer flasks) of LB, ratio 1:100. The cultures were incubated at 25 °C and 150 rpm for more a 72 h under semi-anaerobic conditions and high antibiotics pressure by adding further amp and cam after 20 h and 40 h. Expression was induced 20h after the inoculation of the large culture using 1 mM IPTG (isopropyl-β-thiogalactopyranoside). More than 80 h after the induction the cultures appeared brown for the presence of the Cyt *f*. The cells were harvested by centrifugation and the periplasmic fraction was extracted by osmotic shock[80]. The pink water fraction (about 200 mL *per* 1.7 L of culture), tested for the presence of Cyt *f* by UV/vis analysis, was dialyzed against 2 L of 5 mM Tris-HCl buffer, pH 8 and 3 mM dithiothreitol (DDT). The resulting dialysate was cleared by centrifugation and loaded on a DEAE column equilibrated in the same buffer. Elution was performed with a gradient of 20–500 mM NaCl and 3 mM DTT. The fraction containing the Cyt *f* was concentrated and loaded on a gel-filtration (G75 Superdex) column and eluted in the same buffer containing 150 mM NaCl. The protein fractions were pooled, concentrated, dialysed against 5 mM Mes, pH 6 and 3 mM DTT and loaded on a DEAE column equilibrated in the same buffer. The Cyt *f* was eluted with a gradient 0-500 mM NaCl. Pure fractions showed a A_{280}/A_{556} of 1.3 under reducing conditions. The protein concentration was determined using $\varepsilon_{556} = 31.5$ mM^{-1}cm^{-1}. The yield of the pure proteins was 36 mg/L for Q7C, 16 mg/L for Q104C, 14 mg/L for N71C, 18 mg/L for S192C and 2.4 mg/L for A63C, referred to the volume of the culture.

- *Plastocyanin*

Uniformly ^{15}N-labeled Pc (^{15}N-Pc) was produced in *E. coli* JM109 transformed with pEAP-wt[81]. A 10 mL LB/amp (100 μg/mL) pre-culture was incubated at 37°C for 8 h. Then 1 mL was used to inoculate 500 mL of room temperature ^{15}N-labeled OD2 Silantes media purchased from *Buchem* B.V. (formerly ARC Laboratories B.V. – The Netherlands) containing 100 μg/mL AMP and 1 mM copper citrate at pH 6. The culture was incubated at 37 °C/225 rpm overnight to OD_{600} = 2.5. Isolation and purification of the protein was performed as described previously[81]. For *Nostoc*

Pc, a ratio A_{278}/A_{598} of 1.0 of the oxidized protein indicated sufficient purity for characterization by NMR and further applications[65]. The solution containing the ^{15}N-labeled Pc protein was concentrated to the required volume by ultrafiltration (Amicon, YM3 membrane). The protein concentration was determined by absorption spectroscopy using an ε_{598} of 4.5 mM^{-1} cm^{-1} for the oxidized forms of ^{15}N-Pc[65]. The yield of the pure proteins was 7 mg *per* litre of culture.

Zn-substitution of Pc

For the study of the interaction of Pc with Cyt *f* without interference from possible electron transfer reactions and to avoid the paramagnetism of the Cu(II), the Cu in Pc was replaced by the redox inactive substitute Zn(II). The Zn substitution was performed in a way similar to the one previously described for the incorporation of Cd into Pc[82], with the following modifications. To produce Pc(Zn), 6 mg of oxidised Pc(Cu) were concentrated to a volume of 0.5 mL. The solution containing the concentrated protein was kept on ice. A solution of 200 mM KCN in 500 mM Tris-HCl pH 7 (200 μL) was slowly added to the protein solution. The blue colour gradually disappeared. The solution was left on ice for 10 min. Then, 1 mM ZnCl$_2$ in 50 mM MES pH 7 (buffer A) was added to the sample to get a total volume of 1-1.5 mL. The solution was loaded on a PD10 column, equilibrated with buffer A, and eluted with up to 3.5 mL of buffer A. Fractions of 0.5 ml with the Zn protein were collected and the absorption at 280 nm was measured. To avoid Zn precipitation, the solution of the fractions containing the protein was first exchanged against water, then against 10 mM sodium phosphate buffer, at pH 6.0. The protein was concentrated to 1 mM. The concentration was checked at 280 nm using an extinction coefficient ε_{280} of 5.1 mM^{-1} cm^{-1}.

Spin-labelling of Cyt f mutants

Before adding the spin labels the excess DTT, used to avoid disulfide bridge formation, was removed from the Cyt *f* cysteine mutant solution, by several concentration/redilution cycles with degassed 10 mM sodium phoshate buffer pH 6. To avoid reduction of the disulfide group by the Fe(II) haem resulting in loss of the spin label, the protein was oxidized by adding a 100-fold excess of K$_3$[Fe(CN)$_6$] to the solution before adding a 10 fold excess of MTSL [(1-Oxyl-2,2,5,5,-tetramethyl-3-pyrroline-3-methyl)-methanethiosulfonate] or MTS [(1-Acetyl-2,2,5,5,-tetramethyl-3-pyrroline-3-methyl)-methanethiosulfonate], both purchased from Toronto Research Chemicals, Ontario, Canada (Figure 1, Chapter I). Stock solutions of 0.1 M MTSL or MTS in DMSO were used. The solution containing the protein and the spin label was left for 2 h at room temperature and then overnight at 4° C. The excess K$_3$[Fe(CN)$_6$] and MTSL were removed by several concentration/redilution cycles with degassed 10 mM sodium phosphate buffer pH 6. The degree of

labeling of the protein was estimated by EPR experiments[11]. The percentage of bound Pc was calculated to be 27% using $K_a = 16 \times 10^3$ M^{-1} [56]. This fraction was estimated on the basis chemical CSP and PCS values, by comparison with the *w.t.* values, for which the binding curves in known[56].

NMR spectroscopy

The NMR samples contained 1 mM of 1:1 complex of ^{15}N Pc and Cyt *f* – MTSL or Cyt *f* – MTS in 20 mM sodium phosphate pH 6.0, 6% of D_2O for lock, and 0.1 mM $CH_3CO^{15}NH_2$ as internal reference. The pH of the sample was adjusted to the pH 6.00 using small aliquots of 0.1 M HCl or 0.1 M NaOH, as required. All measurements were performed at 301 K on a Bruker DMX600 spectrometer equipped with a triple-resonance TXI-Z-GRAD probe (Bruker, Karlsruhe, Germany). Performing 2D [^{15}N, ^1H] HSQC experiments, spectra were obtained with 1024 and 256 complex points in the direct and indirect dimensions, respectively, and spectral widths of 32 ppm (^{15}N) and 16 ppm (^1H). All data were processed with AZARA 2.7 [83] and analysed in ANSIG for Windows[84,85]. Assignments of the ^{15}N and ^1H nuclei of Pc were based on 3D NOESY and TOCSY-HSQC spectra (not shown) and are listed in Appendix A. Several Pc amides were either not observed or not analysed due to spectral overlap.

Determination of distance restraints

The unpaired electron of the spin label enhances the relaxation rate of the nuclei in its proximity by the magnetic dipolar interactions. The magnitude of the effect, reflected in line broadening, depends on the distance, providing structural information[86]. In the present work, the PRE was calculated using equation 4.1[86]:

$$\frac{I_{para}}{I_{dia}} = \frac{R_{2,dia} \exp(-tR_{2,para})}{R_{2,dia} + R_{2,para}} \qquad \text{(Eq. 4.1)}$$

where I_{para} and I_{dia} are the resonance intensity of an amide group in [^1H, ^{15}N] HSQC spectra for Pc in the complex containing Cyt *f* – MTSL and Cyt *f* – MTS, respectively; $R_{2,dia}$ is the transverse relaxation rate of Pc amide protons in the complex with Cyt *f* – MTS; $R_{2,para}$ is the paramagnetic contribution to the relaxation rate (PRE) and *t* is the INEPT evolution time of the HSQC (9 ms). For residues whose resonances disappear in the paramagnetic spectrum, the maximal I_{para} value was set to the noise level of the spectrum. The I_{para} / I_{dia} ratios were normalized as previously described[11]. For all amide protons, the $R_{2,dia}$ was determined from the HSQC peaks of the Pc in the complex with Cyt *f* – MTS. The FIDs in the HSQC spectra were zero-filled up to 2048 and 512 complex points in

the direct and indirect dimensions, respectively, and processed with a 2 Hz line-broadening exponential multiplication window-function in the ^{1}H dimension. For each peak the width at half-height ($\Delta v_{1/2}$) in the proton dimension was extracted from a Lorentzian fit using MestRec-C 4.8.6.0 (Mestrelab Research S.L., Santiago de Compostela, Spain). After correction for the artificial line-broadening, the $\Delta v_{1/2}$ was used to calculate $R_{2,dia}$ ($R_{2,dia} = \pi\Delta v_{1/2}$). $R_{2,para}$ was then obtained by a fit of data to equation 4.1. The PREs values were converted into distances using equation 4.2:

$$r = \sqrt[6]{\frac{\gamma^2 g^2 \beta^2 f_b f_e}{20 R_{2,para}}\left(4\tau_c + \frac{3\tau_c}{1+\omega_h^2\tau_c^2}\right)} \qquad \text{(Eq. 4.2)}$$

where r is the distance between the unpaired electron of the MTSL bound to the Cyt f and a given amide proton of Pc; γ is the gyromagnetic ratio of ^{1}H; g is the electronic g-factor; β is the Bohr magneton; f_b and f_l are fraction Pc bound and fraction Cyt f spin labeled, respectively; τ_c the correlation time of the electron-nucleus vector and ω_h is the proton Larmor frequency. The τ_c values were determined from EPR spectra of each Cyt f mutant in the presence of Pc (see Results).

Docking

The intermolecular distance restraints obtained from the PREs were employed to guide the docking of Pc onto Cyt f. The distance restraints were categorized in three classes[86]. The spin label-amide distances for residues for which the resonances disappeared in the paramagnetic spectrum were restrained only with an upper limit. For those not affected by MTSL only a lower limit was set. Finally, for the residues affected by the spin-label and for which resonances were observed in the paramagnetic spectra the distances were restrained with both upper and lower limits. Restrained rigid-body docking of the protein molecules was carried out using Xplor-NIH 2.13[87] as described previously[2,4,11,49,56]. Dr. A. Volkov is kindly acknowledged for performing these computations. The coordinates of Cyt f and Pc were taken from the NMR structure of the complex (PDB entry 1tu2[56]) and from the crystal structure (PDB entry 2GIM[66]), respectively.

The spin label is very mobile because of the possible rotation around the five single bonds of the chain linking the protein to the pyrrolidinic ring which contains the paramagnetic nitroxide, (see Introduction, Fig. 2). This mobility was accounted for in the calculations by selecting four orientations from the sterically allowed conformers, and obtaining, for each mutant, the averaged position of the oxygen atom of MTSL. As reported in the literature, using a greater number of orientations did not modify the final result[11,88].

The coordinates of Cyt *f* were fixed, whereas Pc was placed at a random position and left to move under the action of two energy terms, the PRE restraints and van der Waals repel forces, which were defined for the protein atoms but set to zero for the spin labels. After that, the 30 – 40 best structures were further minimised in energy allowing only side-chain dynamics, with the repel function now also including the spin labels. Finally, the whole docking procedure was repeated till the lowest energy was obtained.

Results

The complex between Pc and Cyt *f* from cyanobacteria *Nostoc* sp. PC 7119 (formerly *A. variabilis*) has been investigated by NMR, using the PRE technique in combination with SDSL. The structure of the Pc-Cyt *f* complex was previously investigated by Diaz-Moreno *et al.*[56]. In that study pseudo-contact shifts of Pc amide resonances, caused by the haem iron, and the chemical-shift perturbation data were used to determine the structure of the complex (PDB entry 1tu2). The aim of the present work was to obtain independent structural restraints for validation and refinement of the structure as well as information about the encounter complex.

Five variants of Cyt *f* were created in which a single surface exposed residue was replaced by a cysteine for attachment of a thiol specific paramagnetic spin label (MTSL), or its diamagnetic homologue (MTS). The Cyt *f* does not contain other free thiol groups, making the engineered cysteine residue a unique position for spin label linkage. The positions 7, 63, 71 and 104 are in proximity of the haem. Residue 192 is more distant, positioned on the small domain of Cyt *f* (Fig. 4.6). Table 4.2 lists the distances between the mutated residues and the haem iron of the Cyt *f*, or the Cu of the Pc, using the published structure of the complex.
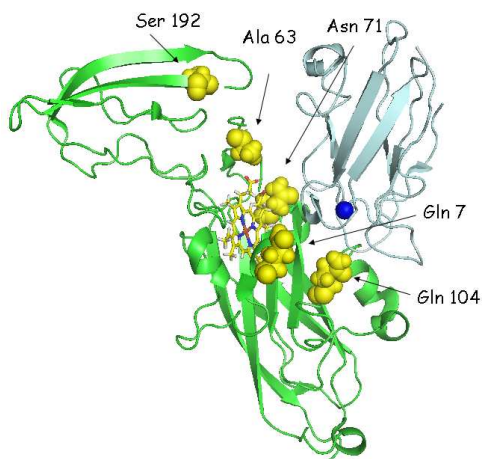

Figure 4.6 Ribbon model of the Cyt *f*-Pc complex from *Nostoc*. The residues represented in space filling have been replaced, one at time, by cysteine. Cyt *f* is shown in green, with the haem sticks. Pc is in light blue, with the copper shown as a blue sphere. Coordinates from PDBdata bank, accession codes 1tu2[56].

Table 4.2. Distances (Å) from the C_α atom of the mutated residue to the haem iron and copper in the Cyt *f* –Pc complex (ref 22)

Residue	Haem	Cu
N71C	10.0	18.0
Q104C	15.4	13.5
Q7C	12.0	14.1
A63C	12.7	19.0
S192C	24.7	30.7

All Cyt f variants could be produced in the same recombinant expression system as for w.t. Cyt f. To avoid interference from electron transfer reactions and paramagnetism of Cu(II) the Pc copper ion was substituted with Zn(II) (see material and methods).

PREs in the ^{15}N ZnPc - Cyt f-MTSL complexes

To produce an intermolecular paramagnetic relaxation enhancement on the amide protons of the ^{15}N-Pc, the spin labels were linked to the cysteine residues on Cyt f. Previous EPR[89] and NMR[86] spectroscopy studies have demonstrated that nitroxide spin labels typically perturb only negligibly the structures of soluble proteins. To measure the PRE accurately, parallel labeling with paramagnetic and diamagnetic compounds of very similar structures was performed[11,90]. Hence, the spin labels MTSL [(1-Oxyl-2,2,5,5,-tetramethyl-3-pyrroline-3-methyl)-methanethiosulfonate] (see Figure 1, Chapter I), and its diamagnetic homologue MTS [(1-Acetyl-2,2,5,5,-tetramethyl-3-pyrroline-3-methyl)-methanethiosulfonate], in which the oxygen on the nitroxide of MTSL is replaced with an acetyl group, were used.

For each Cyt f variant, ^{15}N-^{1}H HSQC spectra were acquired of ^{15}N-Pc in complex with Cyt f labeled with MTSL or MTS, under identical conditions. The resonance intensities (based on peak heights) were measured for all amides to obtain I_{para} and I_{dia}. From the ratio of these values, as well as the linewidth of the peaks in the Cyt f MTS spectra ($R_{2,dia}$), the PRE ($R_{2,para}$) was derived (eq. 4.1 in material and methods). The normalized I_{para} / I_{dia} ratios are shown in Fig. 4.7 and the data are summarized in Tables 1 in Appendix B.
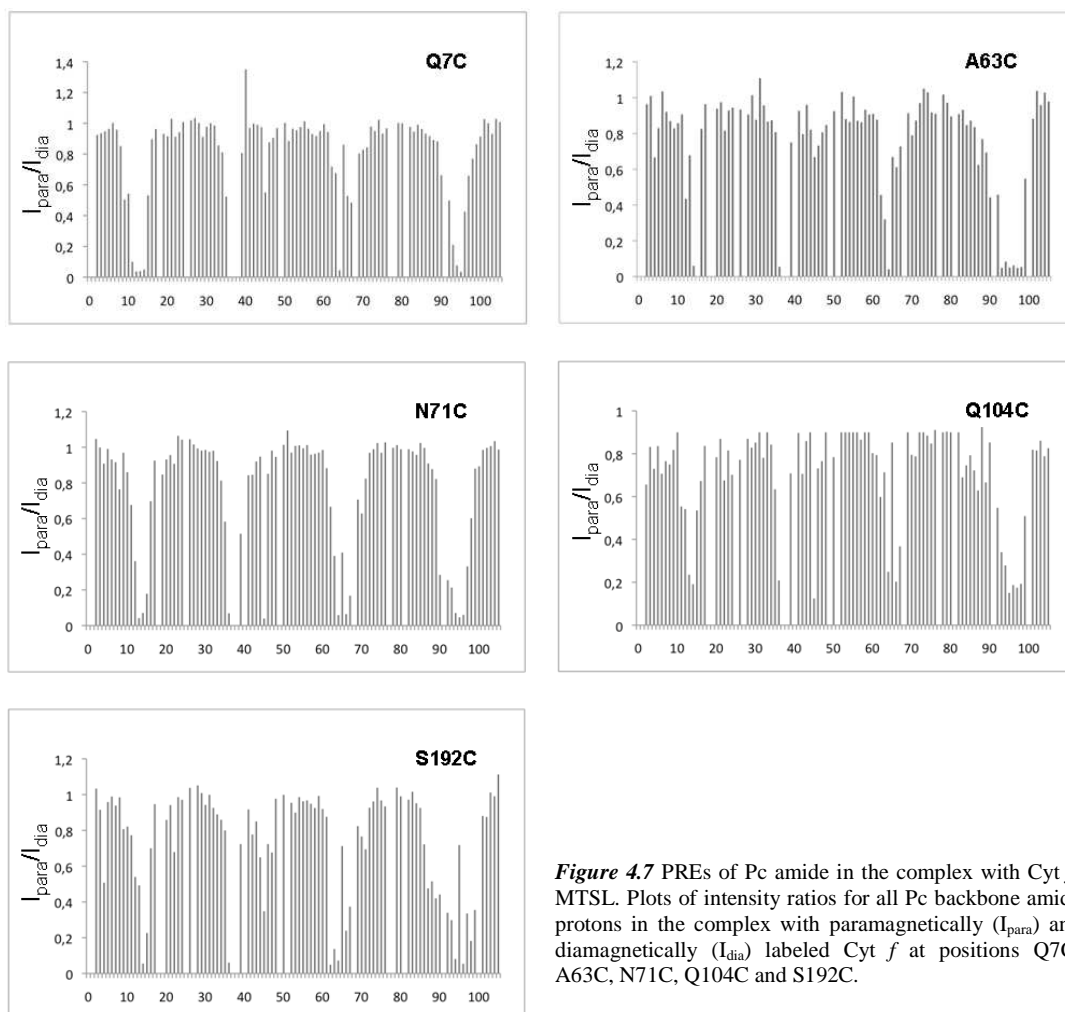
Figure 4.7 PREs of Pc amide in the complex with Cyt *f*-MTSL. Plots of intensity ratios for all Pc backbone amide protons in the complex with paramagnetically (I_{para}) and diamagnetically (I_{dia}) labeled Cyt *f* at positions Q7C, A63C, N71C, Q104C and S192C.

The relaxation effects have been visualized in Fig. 4.8. This figure shows the surface of Pc coloured according to the size of the observed PREs. Surprisingly all Cyt *f* variants affect the same region of the Pc surface. This is remarkable, because each spin label would be expected to enhance relaxation of nuclei in different regions and to different degrees if the complex were in a single conformation. Fig 4.6 shows that the spin label positions are spread around the interface of the Cyt *f* - Pc complex. The chemical shift perturbations observed for Pc bound to the Cyt *f*-MTS variants are quite comparable to that of w.t. Cyt *f* [56] (data not shown), indicating that affinity and interface were not affected by the introduction of the SL. Only for variants A63C some deviations were observed, suggesting small changes in binding in this complex. The general effects observed on the hydrophobic patch of Pc and surrounding region cannot be explained by a single orientation and strongly suggest the complex is dynamic to some extent. Furthermore, it must be underlined that on

the Pc always the same interface is affected, suggesting that Pc uses this area to interact with a large portion of the Cyt *f* surface.
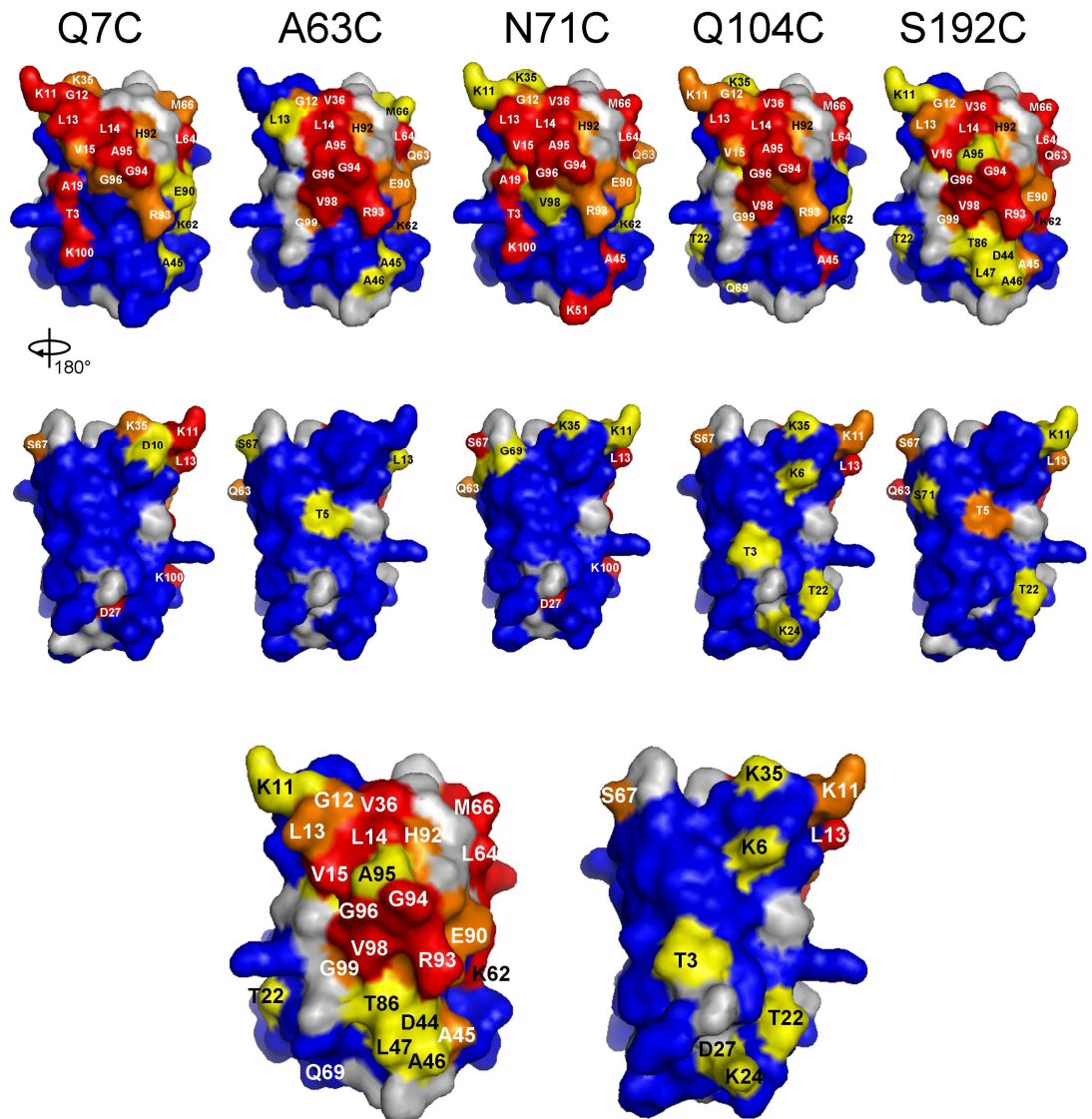

Figure 4.8 Surface representation of *Nostoc* Pc coloured according to $R_{2,para}$ observed in complex with the Cyt *f*-MTSL variant indicated at the top of the panel. The following classes have been used. Residues that disappear or experience a $R_{2,para} > 60/s^{-1}$ in red; $60\text{-}25/s^{-1}$ in orange; $25\text{-}15/s^{-1}$ in yellow; $<15/s^{-1}$ in blue. The residues for which no data are available are in grey. At the bottom, the S192C mutant (bottom left, front; bottom right, back) is shown enlarged for an easier reading of the name of the residues.

Comparing the PREs perturbation map of the Pc surface with the chemical shift perturbation map reported in the work of Diaz-Moreno and co-workers, a new region of the Pc appears to be affected

by the interaction with Cyt *f*. This is the lower region of Pc around residue A45 in A63C and especially in S192C (Figure 4.8, up). A similar perturbation is also detected for residue K24 in Q104C (Figure 4.8, bottom).

Structure calculation

Structure calculations were performed by Dr A. Volkov. The method used for the determination of the protein complex structure is based on the theory that the NMR resonance intensity of one of the proteins is influenced by a paramagnetic centre, for example a SL covalently attached to the partner protein. The unpaired electron on the SL produces an increase of the relaxation rate of nearby nuclei, because of the dipolar magnetic interactions induced between each nucleus and the SL. The influence of the paramagnetic centre depends on the inverse of the sixth power of the distance between the SL and the nucleus, averaged over all the positions adopted by the nuclei and the SL. The paramagnetic effects can then be converted into distance restraints[9,11] , which can be used to determine the relative orientation of the proteins[12]. Therefore, for every amide proton observed on Pc the PRE due to the MTSL has been determined, using the equation 4.1 [9,86]. From this equation R_2^{para} was obtained, so that the distance r could be obtained through the equation 4.2 [86]. This procedure has been applied to each of the five Cyt *f* mutants studied in this work in the complex with the Zn-Pc. The relaxation effect is very strong when the nuclei are in close proximity to the SL; under these conditions even lowly populated states, existing for only a small fraction of the lifetime of the complex, can be revealed. Still, it has to be considered that PRE data result from an average of the nuclear positions relative to the SL of both space and time. The structures that can be obtained, therefore, represent an average over all the adopted orientations[1].

In equation 4.2 τ_c is the rotational correlation time of the electron-nucleus vector. The total, effective rotational correlation time (τ_c) is determined by a contribution from the electron relaxation time τ_s and the rotational correlation time due to the tumbling of the molecule τ_r, according to $1/\tau_c = 1/\tau_s + 1/\tau_r$. In the case of proteins where the paramagnetic center is a stable radical $\tau_r < \tau_s$[75], therefore the value of τ_c is dominated by τ_r. The τ_c values used here were determined from the EPR spectra of each Cyt *f* mutant in the presence of Pc (Fig. 4.9) which were reported in the thesis of Dr. F. Scarpelli (Leiden University 2009). They are listed in Table 4.3[*].

---

[*] Subsequent studies have shown that it may be more appropriate to use τ_c for the entire complex[11]. However, the value of τ_c has been shown not to be critical[11]. For further details, see the concluding remarks of this chapter.
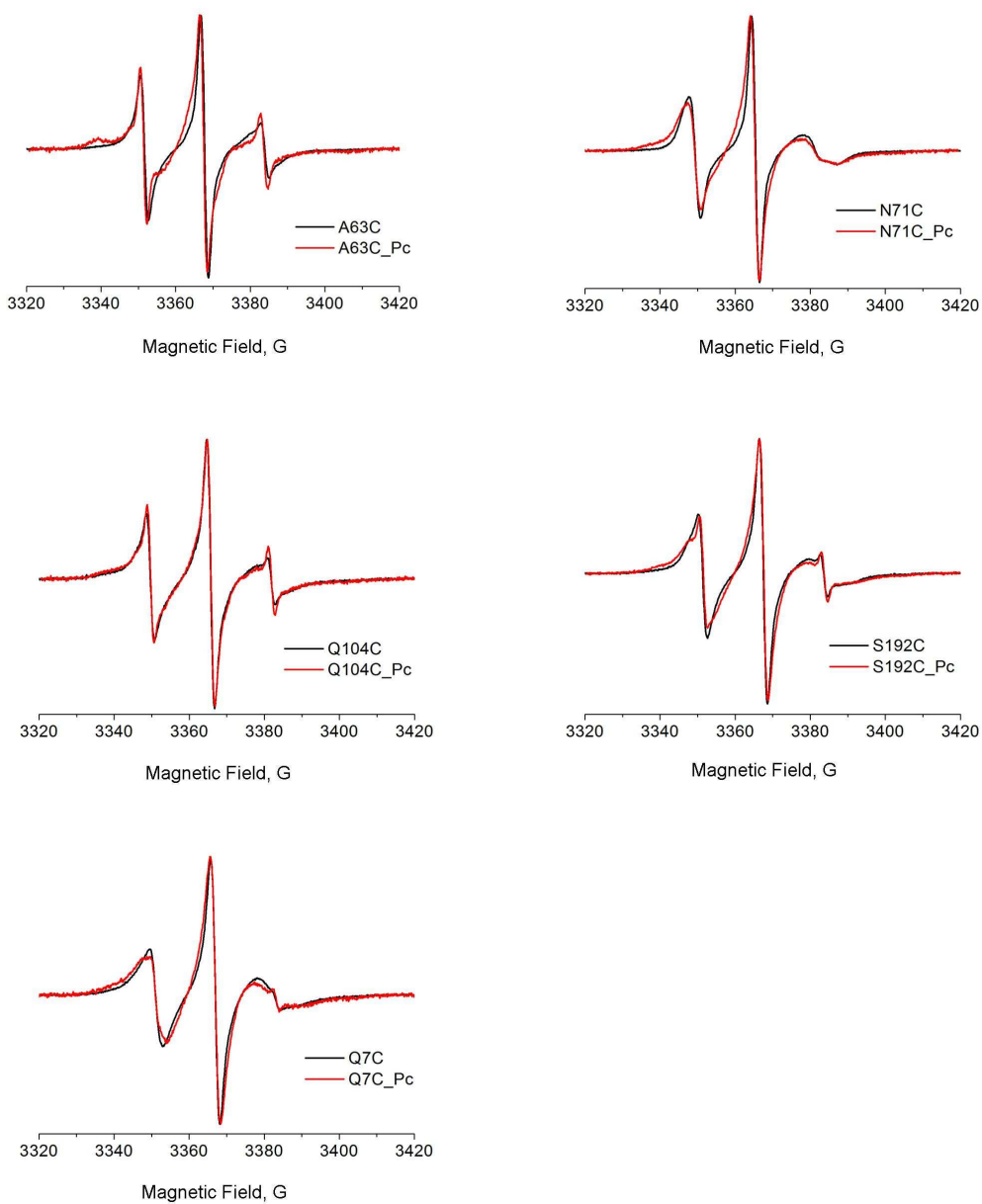
Figure 4.9 X band EPR at room temperature of the five mutated free Cyt *f* (black) and the corresponding Pc – Cyt *f* complexes (red).

The intermolecular distance restraints obtained from the PRE between the measured position of the oxygen atom of MTSL and the backbone amide protons of Pc have been employed to determine the docking of Pc onto Cyt *f* and get independent information on the complex structure. A set of distance restraints for MTSL attached to five positions on Cyt *f* was used in a rigid-body docking protocol[11] with the aim to deduce the relative orientation of the two protein backbones in

the complex. Two low-energy clusters of Pc orientations separated by ca. 25 Å were found. Figure 4.10 B + C show the docking results for the case in which distance constraints from all 5 Cyt *f* variants are used. It is clear that both solutions differ significantly from the published orientation[56]

Table 4.3. Rotational correlation time (τ_c, ns) for the spin label for each Cyt *f* mutant determined from EPR spectra

Cytochrome *f* mutant	Rotational correlation time (ns)
A63C	14
S192C	7
Q7C	6
Q104C	3
N71C	6

(Figure 4.10, A). However, to value the relevance of the docking results, the agreement between the measurement and the back-predicted distances needs to be evaluated. The violation analysis of the solution structure (Figure 4.11) shows that many restraints are not satisfied.
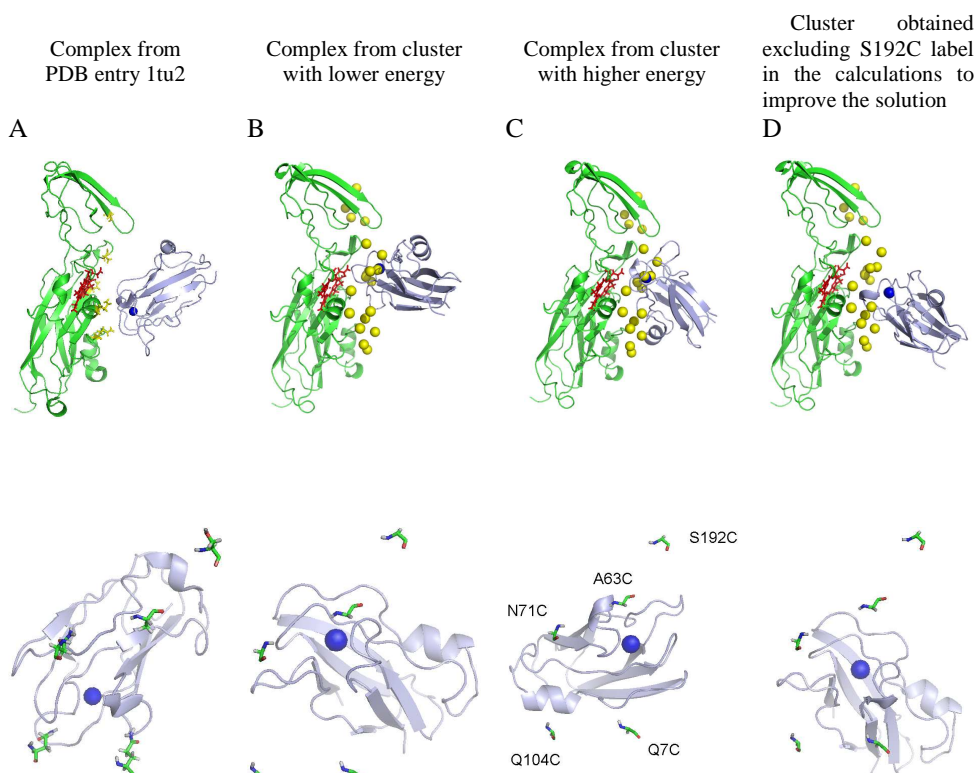
Complex from PDB entry 1tu2

Complex from cluster with lower energy

Complex from cluster with higher energy

Cluster obtained excluding S192C label in the calculations to improve the solution

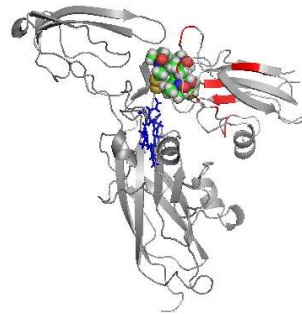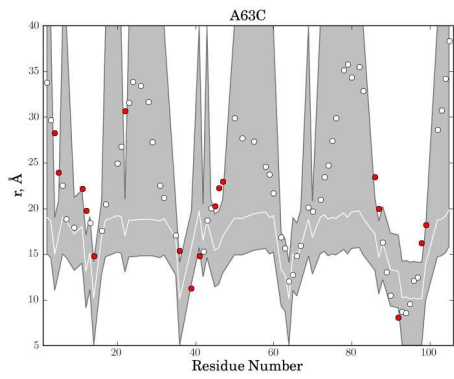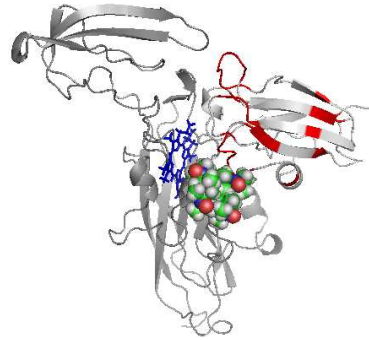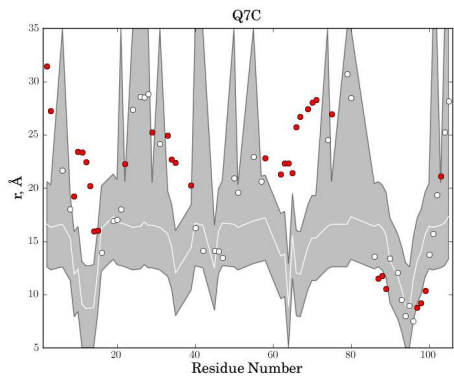**Figure 4.10** Comparison of Cyt *f* – Pc relative orientations. Above: the whole complex. In A: the residues where the spin labels have been attached are indicated in yellow. In B, C and D: the yellow spheres represent the oxygen atom of the spin labels in the four chosen conformations. Below: detail of each complex obtained looking at the Pc from the Cyt *f* position.
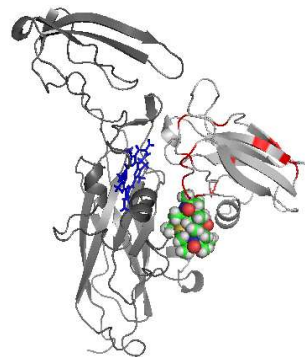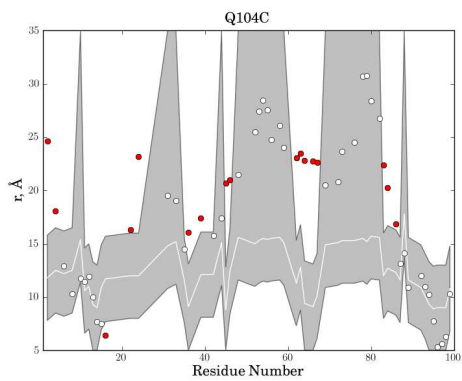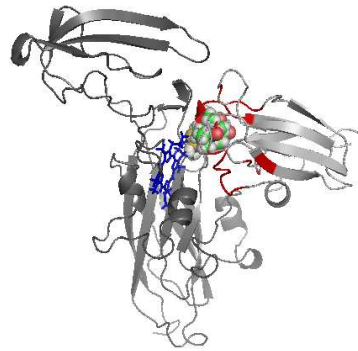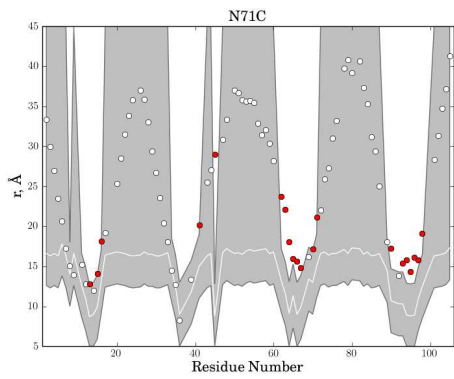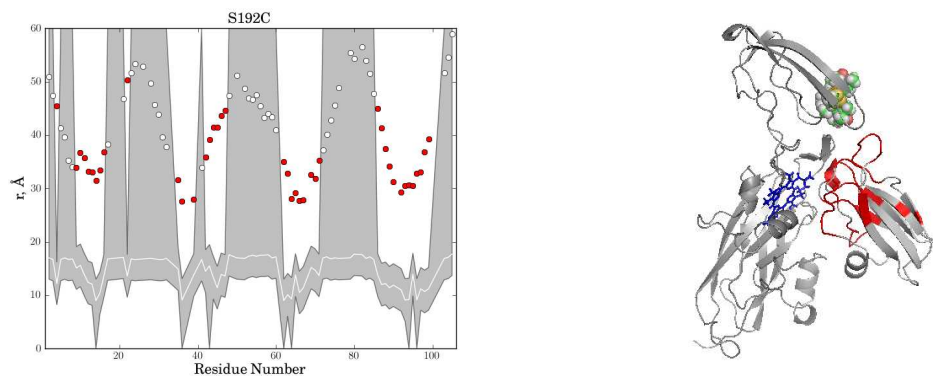
Figure 4.11 Violation analysis of the best structure solution for the Cyt *f* –Pc complex. The plots illustrate the distances from the Pc backbone amide protons in the best structure solution (circles) to the averaged position of the oxygen atom of MTSL attached to Cyt *f* at Q7C, A63C, N71C, Q104C and S192C positions. The white line and the shaded area indicate the PRE-derived distances and error margins, respectively, used in the structure calculations. Violations are represented as red circles. On the right cartoon representations of the best solution structure are shown, indicating the residues with satisfied (light gray) and violated (red) restraints. The haem group is in blue. For each of the MTSL positions, four conformations representing the freedom of the group are represented as spheres. These were used for ensemble averaging in the structure calculations.

The plots in Fig. 4.11 show the distances from the Pc backbone amide protons in the best solution structure (open circles) to the averaged position (calculated as explained in Materials and Methods) of the oxygen atom of MTSL attached to Cyt *f* for each of the Q7C, A63C, N71C, Q104C and S192C positions[11,88]. The white line and the shaded area indicate the PRE-derived distances and error margins, respectively, used in the structure calculations. For a given residue, the restraint is satisfied if the corresponding circle is inside the shaded area and violated if the circle is outside (red circles). The relative amount of violated restraints are similar for three mutants (16 % for A63C - Cyt *f* and Q104C - Cyt *f* ; 19 % for N71C). For the other two complexes, Q7C - Cyt *f* and S192C - Cyt *f*, the quantity of violated restraints is again similar (32 and 39 % respectively), and higher compared to the first group. For all variants, mainly positive violations are observed. Positive violations imply that the actual distances for residues in the single-orientation complex are larger than those determined experimentally.

The effects of leaving out the restraints of one spin label at a time during the docking calculations were studied. Only taking out the distant S192C label improved the quality of the fit, while for all other spin labels it did not make any difference, with many restraints yet to be satisfied. The orientation found (Fig. 4.10 D) is very similar to one of the solutions found with five SLs (Fig. 4.10 B). Then another spin label (in addition to S192C) was taken out. Runs with only 3 spin labels give solutions similar to the calculations excluding S192C only, irrespective of what spin labels were used. These observations suggest that it is not possible to meet all restraints in a single structure. Instead, the observed violations are evidence of additional protein-protein orientations sampled in the dynamic encounter state of the complex, in which the violated residues come close to the spin-

label. In that case, for each residue, the measured PRE (reflected in $R_{2,obs}^{para}$) is the sum of contributions from all protein-protein orientations (each contributing with R_2^{para}), weighted by the fraction of time (*f*) spent in each form, according to the equation 4.3[11], provided that all orientations are in fast exchange compared to the R_2^{para} values. Such an analysis was not performed in the present study.

$$R_{2,obs}^{para} = \sum_{i=1}^{n} f_i R_{2,i}^{para} \qquad \text{(Eq. 4.3)}$$

In summary, the experimental results proved that the conformational search of Pc in the encounter complex extends further than just the region in the Cyt *f* nearby the interface of the well-defined complex found by Diaz-Moreno[56]. This is particularly evident looking at the perturbation map of the Pc bound to the S192C Cyt *f* mutant (see Figure 4.8). The sampled area resembles a valley in Cyt *f* situated between the small and big domains; this valley seems to be delineated by the five acidic residues (Asp-64, Glu-189, Asp-100, Glu-108 and Glu 165) that allow the electrostatic interactions with the positive groups of Pc. The hydrophobic patch of the Pc is oriented differently in cluster 1 and 2, but in both cases its edge is directed toward the Cyt *f* Tyr-1, like in the structure determined by Diaz-Moreno *et al*. Compared to this structure, in cluster 1 there is an additional positive electrostatic interaction between Lys-11 on Pc and Glu 189 in Cyt *f*, with the Cyt *f* Tyr-102 hydrophilic residue being very close to these two residues, while in the structure previously described it was found close to the hydrophobic patch. In cluster 2, the Pc K-51 and Cyt *f* D-100 residues are located in a way that makes it possible to form an additional electrostatic interaction between the two partner proteins, and also in this case Cyt *f* Tyr-102 is very close to these residues. In the Pc site 2 (indicated by light blue colour in Fig. 4.12), the Asp-54 and Lys-57 residues were found to be close to Cyt *f* E-189 by Diaz-Moreno. Here, they are more distant by it in cluster 1, but remain in the same region. In cluster 2, they are found between the E-108 and D-100 residues; in this latter case it seems that Pc is rotated by 180 degrees compared to the previous study, and that the hydrophobic patch is slid within the valley described above (Fig. 4.12, bottom), so that it is surrounded by the Cyt *f* E-189, K-35, E-165 acidic residues.

In order for the ET process to be fast enough (10^3-10^4 s^{-1}), the maximum distance between the redox centres should be in the order of 16 Å[91]. In the literature, in two plant complexes this distance was found to be 11.0 and 13.9 Å, while in the *Phormidium* complex it was 15.0 Å[56 and therein]. Our results show that the distance between Fe and Zn is 16.07 Å in cluster 1 (similar to the 16.1 Å previously found for *Nostoc* Cyt *f* – Cd Pc), and 14.1 Å in cluster 2. The structure described

here is therefore compatible with fast ET, although the distance in cluster 1 is close to the upper theoretical limit for efficient ET.
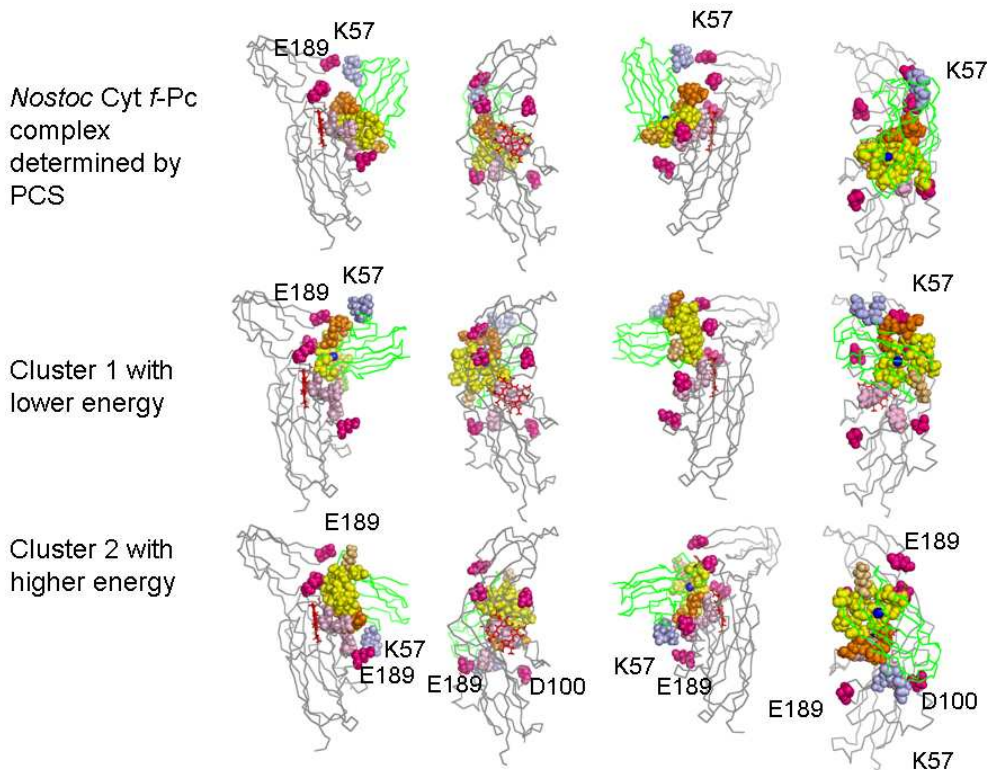

Figure 4.12 Comparison of Cyt *f* – Pc structures, obtained with PCS (top) and PRE NMR (middle and bottom). Pc and Cyt *f* are shown as green and grey ribbon, respectively; the five Cyt *f* acidic residues are in pink; the Pc hydrophobic patch is in yellow; the first electrostatic recognition site on Pc is in orange; the secondary recognition site on Pc is in light blue. On each row, the structure is observed through progressive 90 degrees rotations around the vertical axis.

Discussion

Previous studies to determine the orientation of Cd-plastocyanin (Pc-Cd) relative to Cyt *f* were performed[56] using chemical-shift perturbation data and intermolecular pseudo-contact shifts as experimental restraints, which were observed for the Pc amide nuclei and caused by the haem iron. The results showed that the hydrophobic patch, surrounding tyrosine 1 in Cyt *f*, docks the hydrophobic patch of Pc. The respective recognition sites of Cyt *f* and Pc give evidence for charge complementarities at the interface area. Further studies revealed that the binding affinity is independent of the oxidation state of Cyt *f*, but varies to some extent between Pc with a singly and doubly charged metal[56,65]. The interface map analysis showed a large perturbed area that, together with the localized nature of the binding map, indicates that the complex between Cyt *f* and Pc-Cd is well-defined, in agreement with the classification for "well defined" versus "dynamic" suggested by

Worrall *et al.*[8] and Prudencio and Ubbink[16]. Details about the conformation that the Pc assumes during most of the lifetime of the complex have been investigated; it was found that the orientation is the same as observed in plant complexes, rather than the one found for another cyanobacterial complex, that from *Phormidium*. The conclusion of that work, namely that in solution the proteins spend most of their time in a well-defined single-orientation complex, is in contrast with what was found in the present work. Here, the complex generated from the interaction of Cyt *f* and Pc in solution, investigated by the PRE NMR technique, cannot be explained by a single structure. In fact, all five Cyt *f* mutants prepared in the present study give similar results, which is unexpected for a complex with a single structure as proposed by Diaz-Moreno *et al.*[56].

This observation can be related to a particular step of the protein-protein interaction, the encounter complex. It should be underlined that kinetic studies of the *Nostoc* Cyt *f*-Pc complex by Albarran *et al.*, in which the effects of mutations on the kinetics of electron transfer to wild-type and mutant forms of Pc were measured by laser flash absorption spectroscopy, showed that a wide area is involved in the electrostatic interaction with Pc in the complex; this was explained to be the result of an additive effect of multiple specific interactions[71]. This observation is in agreement with our hypothesis. In fact, the results of the present work also suggest that the orientation of the two proteins in the complex is such that Pc searches the negatively charged, long face of Cyt *f,* while being aligned along its long axis, exploring a large Cyt *f* surface always with the same area. Proteins, and macromolecules in general, recognize partners through short-range biophysical interactions, like hydrogen bonding, hydrophobic and van der Waals forces at the binding interface, usually representing only a small fraction of the total surface of the protein[1]. The process of complex formation involves two phases. In the first, the protein meets its partner and forms a transient intermediate involving non-specific binding modes, which is a dynamic encounter state that produces the encounter complex. The latter may then follow two paths, forming the final complex or dissociating again[1]. Suh *et al*. stressed the importance of electrostatic interactions in the initial phase of the protein formation[19]; in the same work it was shown that distinguishing between specific and non-specific conformations may be difficult, due to the small energy difference between the two.

The results of the present work, although different from what was published by Diaz-Moreno, are not incompatible with it: due to the PRE technique used in this work, we were able to detect ensembles of sparsely populated conformations that contribute to the encounter complex of the two proteins. This conclusion is in line with recent studies performed on protein dynamics[1]. In particular, it was found that proteins may form an entirely dynamic complex, like that between adrenoxin and cytochrome *c*[15]. Although it is generally difficult to crystallize ET complexes, this

has been possible for cytochrome *c* and cytochrome *c* peroxidase from yeast. Since the crystallized complex was ET active, this suggested that the complex was fully specific. In contrast, it was recently found that only 70% of the complex is well-defined, with 30% representing the encounter complex[11,23]. Similar results have been reported by Tang *et al.* on other protein complexes[12].

Concluding remarks

The experimental data are best interpreted by the presence of a dynamic ensemble of protein-proteins orientations within the complex rather than a single, well-defined structure. Perhaps the most important result of the present work is that the effects observed with the PRE technique cannot be modelled by a single structure. This conclusion will not be affected by the choice of different τ_c values for the different mutants as discussed in detail by Volkov *et al.*[11]. In fact, the comparison made by these authors shows that the exact correlation time used is not critical. However, structure calculations should be performed with the τ_c of the complex.

Visualizing an encounter complex is a complex task, since this involves taking into account non-specific interactions and dynamics, leading to many orientations. Future work is needed, and a promising possibility is to associate experimental data with computational dynamics to provide more detailed insights into the nature of protein complex formation, of which the encounter complex is an important part.

Reference List

1. Ubbink,M. The courtship of proteins: Understanding the encounter complex. *Febs Letters* **583**, 1060-1066 (2009).

2. Ubbink,M., Ejdeback,M. & Karlsson,B.G. The structure of the complex of plastocyanin and cytochrome *f*, determined by paramagnetic NMR and restrained rigid-body molecular dynamics. *Structure* **6**, 323-335 (1998).

3. Hoffman,B.M., Celis,L.M., Cull,D.A., Patel,A.D., Seifert,J.L., Wheeler,K.E., Wang,J.Y., Yao,J., Kurnikov,I.V. & Nocek,J.M. Differential influence of dynamic processes on forward and reverse electron transfer across a protein-protein interface. *Proceedings of the National Academy of Sciences of the United States of America* **102**, 3564-3569 (2005).

4. Crowley,P.B., Otting,G., Schlarb-Ridley,B.G., Canters,G.W. & Ubbink,M. Hydrophobic interactions in a cyanobacterial plastocyanin-cytochrome *f* complex. *Journal of the American Chemical Society* **123**, 10444-10453 (2001).

5. Garrett,D.S., Seok,Y.J., Peterkofsky,A., Gronenborn,A.M. & Clore,G.M. Solution structure of the 40,000 M-r phosphoryl transfer complex between the N-terminal domain of enzyme I and HPr. *Nature Structural Biology* **6**, 166-173 (1999).

6. Worrall,J.A.R., Reinle,W., Bernhardt,R. & Ubbink,M. Transient protein interactions studied by NMR spectroscopy: The case of cytochrome *c* and adrenodoxin. *Biochemistry* **42**, 7068-7076 (2003).

7. Liang,Z.X., Jiang,M., Ning,Q. & Hoffman,B.M. Dynamic docking and electron transfer between myoglobin and cytochrome b_5. *Journal of Biological Inorganic Chemistry* **7**, 580-588 (2002).

8. Worrall,J.A.R., Liu,Y.J., Crowley,P.B., Nocek,J.M., Hoffman,B.M. & Ubbink,M. Myoglobin and cytochrome b_5: A nuclear magnetic resonance study of a highly dynamic protein complex. *Biochemistry* **41**, 11721-11730 (2002).

9. Liang,Z.X., Nocek,J.M., Huang,K., Hayes,R.T., Kurnikov,I.V., Beratan,D.N. & Hoffman,B.M. Dynamic docking and electron transfer between Zn-myoglobin and cytochrome b_5. *Journal of the American Chemical Society* **124**, 6849-6859 (2002).

10. Volkov,A.N., Ferrari,D., Worrall,J.A.R., Bonvin,A.M.J.J. & Ubbink,M. The orientations of cytochrome *c* in the highly dynamic complex with cytochrome b_5 visualized by NMR and docking using HADDOCK. *Protein Science* **14**, 799-811 (2005).

11. Volkov,A.N., Worrall,J.A.R., Holtzmann,E. & Ubbink,M. Solution structure and dynamics of the complex between cytochrome *c* and cytochrome *c* peroxidase determined by paramagnetic NMR. *Proceedings of the National Academy of Sciences of the United States of America* **103**, 18945-18950 (2006).

12. Tang,C., Iwahara,J. & Clore,G.M. Visualization of transient encounter complexes in protein-protein association. *Nature* **444**, 383-386 (2006).

13. Iwahara,J. & Clore,G.M. Detecting transient intermediates in macromolecular binding by paramagnetic NMR. *Nature* **440**, 1227-1230 (2006).

14. Xu,X.F., Keizers,P.H.J., Reinle,W., Hannemann,F., Bernhardt,R. & Ubbink,M. Intermolecular dynamics studied by paramagnetic tagging. *Journal of Biomolecular NMR* **43**, 247-254 (2009).

15. Xu,X.F., Reinle,W.G., Hannemann,F., Konarev,P.V., Svergun,D.I., Bernhardt,R. & Ubbink,M. Dynamics in a pure encounter complex of two proteins studied by solution scattering and paramagnetic NMR spectroscopy. *Journal of the American Chemical Society* **130**, 6395-6403 (2008).

16. Prudencio,M. Transient complexes of redox proteins: structural and dynamic details from NMR studies. *Journal of Molecular Recognition* **17**, 524-539 (2004).

17. Fawzi,N.L., Doucleff,M., Suh,J.Y. & Clore,G.M. Mechanistic details of a protein-protein association pathway revealed by paramagnetic relaxation enhancement titration measurements. *Proceedings of the National Academy of Sciences of the United States of America* **107**, 1379-1384 (2010).

18. Harel,M., Spaar,A. & Schreiber,G. Fruitful and futile encounters along the association reaction between proteins. *Biophysical Journal* **96**, 4237-4248 (2009).

19. Suh,J.Y., Tang,C. & Clore,G.M. Role of electrostatic interactions in transient encounter complexes in protein-protein association investigated by paramagnetic relaxation enhancement. *Journal of the American Chemical Society* **129**, 12954-12955 (2007).

20. Kim,Y.C., Tang,C., Clore,G.M. & Hummer,G. Replica exchange simulations of transient encounter complexes in protein-protein association. *Proceedings of the National Academy of Sciences of the United States of America* **105**, 12855-12860 (2008).

21. Northrup,S.H., Boles,J.O. & Reynolds,J.C.L. Brownian dynamics of cytochrome *c* and cytochrome *c* peroxidase association. *Science* **241**, 67-70 (1988).

22. Volkov,A.N., Bashir,O., Worrall,J.A.R. & Ubbink,M. Binding hot spot in the weak protein complex of physiological redox partners yeast cytochrome *c* and cytochrome *c* peroxidase. *Journal of Molecular Biology* **385**, 1003-1013 (2009).

23. Bashir,Q., Volkov,A.N., Ullmann,G.M. & Ubbink,M. Visualization of the encounter ensemble of the transient electron transfer complex of cytochrome *c* and cytochrome *c* peroxidase. *Journal of the American Chemical Society* **132**, 241-247 (2010).

24. Adam,G. & Delbruck,M. Structural Chemistry and Molecular Biology. Freeman, San Francisco, (1968).

25. Volkov, A. Transient Complexes of Haem Proteins. Ph.D. thesis. Leiden University, Leiden, The Netherlands, 2007

26. Northrup,S.H. & Erickson,H.P. Kinetics of protein protein association explained by Brownian dynamics computer simulation. *Proceedings of the National Academy of Sciences of the United States of America* **89**, 3338-3342 (1992).

27. Radic,Z., Kirchhoff,P.D., Quinn,D.M., McCammon,J.A. & Taylor,P. Electrostatic influence on the kinetics of ligand binding to acetylcholinesterase - Distinctions between active center ligands and fasciculin. *Journal of Biological Chemistry* **272**, 23265-23277 (1997).

28. Schreiber,G. & Fersht,A.R. Rapid, electrostatically assisted association of proteins. *Nature Structural Biology* **3**, 427-431 (1996).

29. Smoluchowski,M.V. Veruch einer mathematischen theorie der koagulationkinetik kolloider losungen. *Z. Phys. Chem* 129-168 (1917).

30. Crowley, P. B. Transient Protein Interactions of Photosynthetic Redox Partners. Ph.D. thesis. Leiden University, Leiden, The Netherlands, 2002

31. Crowley,P.B. & Ubbink,M. Close encounters of the transient kind: Protein interactions in the photosynthetic redox chain investigated by NMR spectroscopy. *Accounts of Chemical Research* **36**, 723-730 (2003).

32. Crowley,P.B. & Carrondo,M.A. The architecture of the binding site in redox protein complexes: Implications for fast dissociation. *Proteins-Structure Function And Bioinformatics* **55**, 603-612 (2004).

33. Kurisu,G., Zhang,H.M., Smith,J.L. & Cramer,W.A. Structure of the cytochrome b_6f complex of oxygenic photosynthesis: Tuning the cavity. *Science* **302**, 1009-1014 (2003).

34. Nelson,N. & Ben Shem,A. The complex architecture of oxygenic photosynthesis. *Nature Reviews Molecular Cell Biology* **5**, 971-982 (2004).

35. Kruse,O., Rupprecht,J., Mussgnug,J.R., Dismukes,G.C. & Hankamer,B. Photosynthesis: a blueprint for solar energy capture and biohydrogen production technologies. *Photochemical & Photobiological Sciences* **4**, 957-970 (2005).

36. Noy,D., Moser,C.C. & Dutton,P.L. Design and engineering of photosynthetic light-harvesting and electron transfer using length, time, and energy scales. *Biochimica Et Biophysica Acta-Bioenergetics* **1757**, 90-105 (2006).

37. Iverson,T.M. Evolution and unique bioenergetic mechanisms in oxygenic photosynthesis. *Current Opinion in Chemical Biology* **10**, 91-100 (2006).

38. Martinez,S.E., Huang,D., Szczepanink,A. & Cramer,W.A. Crystal-structure of chloroplast cytochrome *f* reveals a novel cytochrome fold and unexpected heme ligation. *Structure* **2**, 95-105 (1994).

39. Sandmann,G. Formation of plastocyanin and cytochrome c_{553} in different species of blue-green algae. *Archives of Microbiology* **145**, 76-79 (1986).

40. Merchant,S., Hill,K. & Howe,G. Dynamic interplay between 2 copper-titrating components in the transcriptional regulation of cyt c_6. *Embo Journal* **10**, 1383-1389 (1991).

41. Bovy,A., Devrieze,G., Borrias,M. & Weisbeek,P. Transcriptional regulation of the plastocyanin and cytochrome c_{553} genes from the cyanobacterium *Anabaena* species PCC 7937. *Molecular Microbiology* **6**, 1507-1513 (1992).

42. Zhang,L., Mcspadden,B., Pakrasi,H.B. & Whitmarsh,J. Copper-mediated regulation of cytochrome c_{553} and plastocyanin in the cyanobacterium *Synechocystis* 6803. *Journal of Biological Chemistry* **267**, 19054-19059 (1992).

43. Navarro,J.A., Hervas,M. & DelaRosa,M.A. Co-evolution of cytochrome c_6 and plastocyanin, mobile proteins transferring electrons from cytochrome b_6f to photosystem I. *Journal of Biological Inorganic Chemistry* **2**, 11-22 (1997).

44. Gross,E.L. & Pearson,D.C. Brownian dynamics simulations of the interaction of *Chlamydomonas* cytochrome *f* with plastocyanin and cytochrome c_6. *Biophysical Journal* **85**, 2055-2068 (2003).

45. Bendall,D.S. Interprotein electron transfer in Protein Electron Transfer , Bendall,D.S. (ed.) pp. 43-64 (BIOS Scientific Publishers Ltd.,Oxford,1996).

46. Kannt,A., Young,S. & Bendall,D.S. The role of acidic residues of plastocyanin in its interaction with cytochrome *f*. *Biochimica Et Biophysica Acta-Bioenergetics* **1277**, 115-126 (1996).

47. Soriano,G.M., Ponamarev,M.V., Tae,G.S. & Cramer,W.A. Effect of the interdomain basic region of cytochrome *f* on its redox reactions in vivo. *Biochemistry* **35**, 14590-14598 (1996).

48. Hope,A.B. Electron transfers amongst cytochrome *f*, plastocyanin and photosystem I: kinetics and mechanisms. *Biochimica Et Biophysica Acta-Bioenergetics* **1456**, 5-26 (2000).

49. Lange,C., Cornvik,T., Diaz-Moreno,I. & Ubbink,M. The transient complex of poplar plastocyanin with cytochrome *f*: effects of ionic strength and pH. *Biochimica Et Biophysica Acta-Bioenergetics* **1707**, 179-188 (2005).

50. Niwa,S., Ishikawa,H., Nikai,S. & Takabe,T. Electron-transfer reactions between cytochrome *f* and plastocyanin from *Brassica komatsuna*. *Journal of Biochemistry* **88**, 1177-1183 (1980).

51. Takenaka,K. & Takabe,T. Importance of local positive charges on cytochrome *f* for electron transfer to plastocyanin and potassium ferricyanide. *Journal of Biochemistry* **96**, 1813-1821 (1984).

52. Beokubetts,D., Chapman,S.K., Knox,C.V. & Sykes,A.G. Kinetic studies on 1:1 electron-transfer reactions involving blue copper proteins. 11. Effects of pH, competitive inhibition, and Chromium(III) modification on the reaction of plastocyanin with cytochrome *f*. *Inorganic Chemistry* **24**, 1677-1681 (1985).

53. Takabe,T. & Ishikawa,H. Kinetic studies on a cross-linked complex between plastocyanin and cytochrome *f*. *Journal of Biochemistry* **105**, 98-102 (1989).

54. Zhou,J.H., FernandezVelasco,J.G. & Malkin,R. N-terminal mutants of chloroplast cytochrome *f* - Effect on redox reactions and growth in *Chlamydomonas reinhardtii*. *Journal of Biological Chemistry* **271**, 6225-6232 (1996).

55. Hart,S.E., Schlarb-Ridley,B.G., Delon,C., Bendall,D.S. & Howe,C.J. Role of charges on cytochrome *f* from the cyanobacterium *Phormidium laminosum* in its interaction with plastocyanin. *Biochemistry* **42**, 4829-4836 (2003).

56. Diaz-Moreno,I., Diaz-Quintana,A. & De la Rosa,M.A. Structure of the complex between plastocyanin and cytochrome *f* from the cyanobacterium *Nostoc* sp PCC 7119 as determined by paramagnetic NMR - The balance between electrostatic and hydrophobic interactions within the transient complex determines the relative orientation of the two proteins. *Journal of Biological Chemistry* **280**, 18908-18915 (2005).

57. Gross,E.L. & Rosenberg,I. A brownian dynamics study of the interaction of *Phormidium* cytochrome *f* with various cyanobacterial plastocyanins. *Biophysical Journal* **90**, 366-380 (2006).

58. Hulsker,R., Baranova,M.V., Bullerjahn,G.S. & Ubbink,M. Dynamics in the transient complex of plastocyanin-cytochrome *f* from *Prochlorothrix hollandica*. *Journal of the American Chemical Society* **130**, 1985-1991 (2008).

59. Qin,L. & Kostic,N.M. Electron-transfer reactions of cytochrome *f* with flavin semiquinones and with plastocyanin - Importance of protein-protein electrostatic interactions and of donor-acceptor coupling. *Biochemistry* **31**, 5145-5150 (1992).

60. DeLano, W. L. The PyMOL Molecular Graphics System, http://www.pymol.org (2002)

61. O'Connell,M.R., Gamsjaeger,R. & Mackay,J.P. The structural analysis of protein-protein interactions by NMR spectroscopy. *Proteomics* **9**, 5224-5232 (2009).

62. Gray,J.C. Cytochrome *f* - Structure, function and biosynthesis. *Photosynthesis Research* **34**, 359-374 (1992).

63. Hervas,M., Navarro,J.A. & De la Rosa,M.A. Electron transfer between membrane complexes and soluble proteins in photosynthesis. *Accounts of Chemical Research* **36**, 798-805 (2003).

64. De la Rosa,M.A., Molina-Heredia,F.P., Hervas,M. & Navarro,J.A. Convergent evolution of plastocyanin and cytochrome c_6 in Photosystem I: The light-driven, plastocyanin: ferredoxin oxidoreductase, Golbeck,J.H. (ed.) pp. 683-696 (Springer, New York,2006).

65. Diaz-Moreno,I., Diaz-Quintana,A., De la Rosa,M.A., Crowley,P.B. & Ubbink,M. Different modes of interaction in cyanobacterial complexes of plastocyanin and cytochrome *f*. *Biochemistry* **44**, 3176-3183 (2005).

66. Schmidt,L., Christensen,H.E.M. & Harris,P. Structure of plastocyanin from the cyanobacterium *Anabaena variabilis*. *Acta Crystallographica Section D-Biological Crystallography* **62**, 1022-1029 (2006).

67. Albarran,C., Navarro,J.A. & De la Rosa,M.A. The specificity in the interaction between cytochrome *f* and plastocyanin from the cyanobacterium *Nostoc* sp. PCC 7119 is mainly determined by the copper protein. *Biochemistry* **46**, 997-1003 (2007).

68. Jones,S. & Thornton,J.M. Analysis of protein-protein interaction sites using surface patches. *Journal of Molecular Biology* **272**, 121-132 (1997).

69. Chakrabarti,P. & Janin,J. Dissecting protein-protein recognition sites. *Proteins-Structure Function and Genetics* **47**, 334-343 (2002).

70. Janin,J. & Wodak,S.J. Protein modules and protein-protein interaction - Introduction. *Advances in Protein Chemistry* **61**, 1-8 (2003).

71. Albarran,C., Navarro,J.A., Molina-Heredia,F.P., Murdoch,P.S., De la Rosa,M.A. & Hervas,M. Laser flash-induced kinetic analysis of cytochrome *f* oxidation by wild-type and mutant plastocyanin from the cyanobacterium *Nostoc* sp. PCC 7119. *Biochemistry* **44**, 11601-11607 (2005).

72. Molina-Heredia,F.P., Hervas,M., Navarro,J.A. & De la Rosa,M.A. A single arginyl residue in plastocyanin and in cytochrome c_6 from the cyanobacterium *Anabaena* sp. PCC 7119 is required for efficient reduction of photosystem I. *Journal of Biological Chemistry* **276**, 601-605 (2001).

73. Vlasie,M.D., Fernandez-Busnadiego,R., Prudencio,M. & Ubbink,M. Conformation of pseudoazurin in the 152 kDa electron transfer complex with nitrite reductase determined by paramagnetic NMR. *Journal of Molecular Biology* **375**, 1405-1415 (2008).

74. Ubbink,M. & Bendall,D.S. Complex of plastocyanin and cytochrome *c* characterized by NMR chemical shift analysis. *Biochemistry* **36**, 6326-6335 (1997).

75. Keizers,P.H.J. & Ubbink,M. Paramagnetic tagging for protein structure and dynamics analysis. *Progress in Nuclear Magnetic Resonance Spectroscopy* **58**, 88-96 (2011).

76. Iwahara,J., Zweckstetter,M. & Clore,G.M. NMR structural and kinetic characterization of a homeodomain diffusing and hopping on nonspecific DNA. *Proceedings of the National Academy of Sciences of the United States of America* **103**, 15062-15067 (2006).

77. Hulsker, R. Transient interactions between photosynthetic proteins. Ph.D. thesis. Leiden University, Leiden, The Netherlands, 2008

78. Milikisyants,S., Scarpelli,F., Finiguerra,M.G., Ubbink,M. & Huber,M. A pulsed EPR method to determine distances between paramagnetic centers with strong spectral anisotropy and radicals: The dead-time free RIDME sequence. *Journal of Magnetic Resonance* **201**, 48-56 (2009).

79. Thony-Meyer,L. Haem-polypeptide interactions during cytochrome *c* maturation. *Biochimica Et Biophysica Acta-Bioenergetics* **1459**, 316-324 (2000).

80. Neu,H.C. & Heppel,L.A. The release of enzymes from *Escherichia Coli* by osmotic shock and during formation of spheroplasts. *Journal of Biological Chemistry* **240**, 3685-3692 (1965).

81. Molina-Heredia,F.P., Hervas,M., Navarro,J.A. & De la Rosa,M.A. Cloning and correct expression in *Escherichia coli* of the petE and petJ genes respectively encoding plastocyanin and cytochrome c_6 from the cyanobacterium *Anabaena* sp. PCC 7119. *Biochemical and Biophysical Research Communications* **243**, 302-306 (1998).

82. Ubbink,M., Lian,L.Y., Modi,S., Evans,P.A. & Bendall,D.S. Analysis of the H-1-NMR chemical shifts of Cu(I)-, Cu(II)- and Cd-substituted pea plastocyanin - Metal-dependent differences in the hydrogen-bond network around the copper site. *European Journal of Biochemistry* **242**, 132-147 (1996).

83. Boucher, W. AZARA 2.7, www.bio.cam.ac.uk/pub/azara (2002)

84. Helgstrand,M., Kraulis,P., Allard,P. & Hard,T. Ansig for Windows: An interactive computer program for semiautomatic assignment of protein NMR spectra. *Journal of Biomolecular NMR* **18**, 329-336 (2000).

85. Kraulis,P.J. Ansig - A program for the assignment of protein H-1 2D-NMR spectra by interactive computer-graphics. *Journal of Magnetic Resonance* **84**, 627-633 (1989).

86. Battiste,J.L. Utilization of site-directed spin labeling and high-resolution heteronuclear nuclear magnetic resonance for global fold determination of large proteins with limited nuclear overhauser effect data. *Biochemistry* **39**, 5355-5365 (2000).

87. Schwieters,C.D., Kuszewski,J.J., Tjandra,N. & Clore,G.M. The Xplor-NIH NMR molecular structure determination package. *Journal of Magnetic Resonance* **160**, 65-73 (2003).

88. Iwahara,J., Schwieters,C.D. & Clore,G.M. Ensemble approach for NMR structure refinement against H-1 paramagnetic relaxation enhancement data arising from a flexible paramagnetic group attached to a macromolecule. *Journal of the American Chemical Society* **126**, 5879-5896 (2004).

89. Hubbell,W.L., Mchaourab,H.S., Altenbach,C. & Lietzow,M.A. Watching proteins move using site-directed spin labeling. *Structure* **4**, 779-783 (1996).

90. Liang,B.Y., Bushweller,J.H. & Tamm,L.K. Site-directed parallel spin-labeling and paramagnetic relaxation enhancement in structure determination of membrane proteins by solution NMR spectroscopy. *Journal of the American Chemical Society* **128**, 4389-4397 (2006).

91. Moser,C.C., Keske,J.M., Warncke,K., Farid,R.S. & Dutton,P.L. Nature of biological electron-transfer. *Nature* **355**, 796-802 (1992).

Concluding Remarks

The main theme of the present thesis is the application of complementary paramagnetic approaches to obtain restraints for structural and dynamic determination in protein studies.

High-field EPR for detailed investigation of local polarity in proteins

Spin labeled proteins and EPR techniques have long been simultaneously used as tools for the study of structure and dynamics of proteins[1-3]. A spin label specifically attached to the surface of a protein is affected by conformational restrictions arising from sterical constraints or from interactions with the neighboring amino-acid residues. The conformational restrictions are reflected in the spin-label motion that can be detected by EPR techniques. These provide a way to investigate, with high accuracy, the microenvironment around the position to which the spin label is attached[2]. In fact, EPR spectra provide parameters that can be used to explore both the polarity and the propensity of the protein environment to donate hydrogen bonds (i.e. the proticity). When EPR spectroscopy of a spin labeled protein is performed at 95 GHz (W-band EPR), the spectral resolution is significantly improved compared to conventional, 9 GHz EPR (X-band EPR). The polarity profiles of membrane proteins have been determined in this way[2]. Also, the usefulness of multi- and high-frequency EPR to determine the dynamics of biological membranes[4] was demonstrated on a model system using spin-labeled lipids.

To further improve the spectral resolution, J-band EPR has been applied in the present work with the goal to discriminate even small differences in the local polarity. This is the first J-band EPR study made with the aim to investigate local polarity at specific positions on the surface of a protein. In a well known protein, azurin, spin labels were attached at four different surface positions. Indeed, the higher resolving power of J-band compared to W-band EPR made it possible to reveal the subtle differences in proticity. We expect that this work will allow calibrating the result of structure and polarity calculations, and that it will be the basis for investigations of these parameters in other, less well characterized protein systems.

Most remarkable was the finding that all EPR spectra of the surface positions of azurin appeared to be single component in W-band EPR, whereas the higher resolution of J-band EPR revealed two components. It seems likely that many "single component spectra" from lower field EPR could turn out to be multiple component, when investigated at J-band or higher.

Long-range distance measurement through double electron-electron resonance

In the study of biomolecules, distance determination provides crucial information for structural and functional investigations. Dipolar EPR spectroscopy of doubly labeled biological systems offers a

complementary method for distance determination, which is particularly useful when other techniques, like X-ray crystallography, FRET and NMR, are not applicable, or when the results are not completely understood[5,6]. In this situation, the possibility to perform measurements of the distance between spin labels becomes very interesting. Pulsed double electron-electron resonance (DEER, also known as PELDOR[7-10]) has been introduced about 30 years ago but only in the last decade has its application in structural biology increased significantly[5], due to widespread use of site directed mutagenesis. Very recently, the integration of the DEER with PRE NMR and conventional NMR intrachain NOESY-based distance constraints has been used for the structure determination of the homodimer Dsy0195 protein[11].

One of the advantages of DEER is that in addition to being sensitive to long, i.e. nm-distances, it produces distance distributions. The width of the distance distribution reflects different conformations of the proteins, and therefore provides information on the flexibility of the protein. This width, however, contains a contribution deriving from rotational isomers of the spin label linker. To consider this point, different approaches have been used in the past[12-17] in the interpretation of experimental data. The accurate interpretation of the results requires a biological model. In the present thesis we use the azurin protein as model system for which we have produced two doubly spin-labeled proteins. The conformation of the spin labels were modelled using XPLOR-NIH[18], already used in the NMR field. The appropriate conformers were selected from all rotamers by only excluding orientations that clash with other atoms in the protein structure. The distances between the nitrogen atoms of the two spin label linkers of allowed spin label orientations yield the modelled distance distribution. Surprisingly, this simple model gives realistic widths, but these seem to be centered at too long a distances, a clear indication that side chain modelling needs to be improved. The width of the distribution obtained experimentally (3 - 5 Å) is also a concern, since it limits the intrinsic accuracy of structure determination by this approach. Therefore, the use of other spin labels, such as the backbone incorporated TOAC label or shorter tether lablels should be considered. The price to be paid is the more difficult biochemical incorporation of such labels.

Structure of spin labeled proteins by paramagnetic NMR

Protein-protein associations give rise to either stable or transient complexes, which control most of the cellular activities. Electron-transfer protein complexes are an example of macromolecules interacting transiently because of their physiological role. The conditions that must be satisfied for this transient behavior are high reaction efficiency and low affinity. This ensures an adequate reaction rate for the electron transfer. Transient protein complexes are therefore at the boundary between specific and non-specific complexes. The encounter complex, preceding the formation of

the final complex with which is in equilibrium, has been demonstrated to be of dynamic nature. Nevertheless, a comprehensive understanding of the encounter complex is difficult; in fact, its nature is rather elusive, since it is formed by multiple orientations of the partner proteins, which interact in an aspecific way. For this reason, studying the encounter complex requires specific methods, able to detect differently populated states. Using spin labeled proteins and PRE NMR fits well in this framework. In general, the validity of this technique, which is based on paramagnetic tags for intermediate and long range distance measurements was proven[19]; it also demonstrated the complementarity of this approach with other established techniques. This approach exploits the large magnetic dipolar interaction existing between unpaired electrons and nearby nuclear spins.

In the present thesis, the physiological complex between Cyt *f* and Pc from cyanobacterial *Nostoc* sp. has been investigated and the interaction of Pc with five Cyt *f* cysteine mutants has been analyzed. The structure obtained was compared to the results of other NMR based approaches, namely pseudocontact shifts (PCSs) and chemical shift perturbations (CSPs). The conclusion of the present thesis is that a single structure does not adequately represent the complex. To proceed from the results presented here to a real picture of the dynamic encounter complex, the route outlined in several recent studies[20-24] can be taken. The results presented in the present thesis will provide the basis for such an interpretation and should cast a new light on the encounter complex structure.

Reference List

1. Hubbell,W.L., Gross,A., Langen,R. & Lietzow,M.A. Recent advances in site-directed spin labeling of proteins. *Current Opinion in Structural Biology* **8**, 649-656 (1998).

2. Owenius,R., Engstrom,M., Lindgren,M. & Huber,M. Influence of solvent polarity and hydrogen bonding on the EPR parameters of a nitroxide spin label studied by 9-GHz and 95-GHz EPR spectroscopy and DFT calculations. *Journal of Physical Chemistry A* **105**, 10967-10977 (2001).

3. Berliner L.J & Reuben J. Biological Magnetic Resonance, Vol. 8. Plenum Press, New York (1989).

4. Lou,Y. & Ge,M.T. A multifrequency ESR study of the complex dynamics of membranes. *Journal of Physical Chemistry B* **105**, 11053-11056 (2001).

5. Borbat,P.P. & Freed,J.H. Measuring distances by pulsed dipolar ESR spectroscopy: Spin-labeled histidine kinases. (2007).

6. Schiemann,O. & Prisner,T.F. Long-range distance determinations in biomacromolecules by EPR spectroscopy. *Quarterly Reviews of Biophysics* **40**, 1-53 (2007).

7. Milov,A.D., Maryasov,A.G. & Tsvetkov,Y.D. Pulsed electron double resonance (PELDOR) and its applications in free-radicals research. *Applied Magnetic Resonance* **15**, 107-143 (1998).

8. Kurshev,V.V., Raitsimring,A.M. & Tsvetkov,Y.D. Selection of dipolar interaction by the 2+1 pulse train ESE. *Journal of Magnetic Resonance* **81**, 441-454 (1989).

9. Larsen,R.G. & Singel,D.J. Double electron-electron resonance spin-echo modulation: Spectroscopic measurement of electron-spin pair separations in orientationally disordered solids. *Journal of Chemical Physics* **98**, 5134-5146 (1993).

10. Jeschke,G. Distance measurements in the nanometer range by pulse EPR. *Chemphyschem* **3**, 927-932 (2002).

11. Yang,Y.H. *et al.* Combining NMR and EPR Methods for Homodimer Protein Structure Determination. *Journal of the American Chemical Society* **132**, 11910-11913 (2010).

12. Borbat,P.P. & Mchaourab,H.S. Protein structure determination using long-distance constraints from double-quantum coherence ESR: Study of T4 lysozyme. *Journal of the American Chemical Society* **124**, 5304-5314 (2002).

13. Borovykh,I.V. *et al.* Distance between a native cofactor and a spin label in the reaction centre of Rhodobacter sphaeroides by a two-frequency pulsed electron paramagnetic resonance method and molecular dynamics simulations. *Journal of Magnetic Resonance* **180**, 178-185 (2006).

14. Steinhoff,H.J., Muller,M. & Beier,C. Molecular dynamics simulation and EPR spectroscopy of nitroxide side chains in bacteriorhodopsin. *Journal of Molecular Liquids* **84**, 17-27 (2000).

15. Beier,C. & Steinhoff,H.J. A structure-based simulation approach for electron paramagnetic resonance spectra using molecular and stochastic dynamics simulations. *Biophysical Journal* **91**, 2647-2664 (2006).

16. Sale,K., Sar,C., Sharp,K.A., Hideg,K. & Fajer,P.G. Structural determination of spin label immobilization and orientation: A Monte Carlo minimization approach. *Journal of Magnetic Resonance* **156**, 104-112 (2002).

17. Jeschke,G. & Polyhach,Y. Distance measurements on spin-labelled biomacromolecules by pulsed electron paramagnetic resonance. *Physical Chemistry Chemical Physics* **9**, 1895-1910 (2007).

18. Schwieters,C.D., Kuszewski,J.J., Tjandra,N. & Clore,G.M. The Xplor-NIH NMR molecular structure determination package. *Journal of Magnetic Resonance* **160**, 65-73 (2003).

19. Ubbink,M. The courtship of proteins: Understanding the encounter complex. *Febs Letters* **583**, 1060-1066 (2009).

20. Xu,X.F. *et al.* Dynamics in a pure encounter complex of two proteins studied by solution scattering and paramagnetic NMR spectroscopy. *Journal of the American Chemical Society* **130**, 6395-6403 (2008).

21. Harel,M., Spaar,A. & Schreiber,G. Fruitful and futile encounters along the association reaction between proteins. *Biophysical Journal* **96**, 4237-4248 (2009).

22. Kim,Y.C., Tang,C., Clore,G.M. & Hummer,G. Replica exchange simulations of transient encounter complexes in protein-protein association. *Proceedings of the National Academy of Sciences of the United States of America* **105**, 12855-12860 (2008).

23. Bashir,Q., Volkov,A.N., Ullmann,G.M. & Ubbink,M. Visualization of the encounter ensemble of the transient electron transfer complex of cytochrome *c* and cytochrome *c* peroxidase. *Journal of the American Chemical Society* **132**, 241-247 (2010).

24. Volkov,A.N., Ferrari,D., Worrall,J.A.R., Bonvin,A.M.J.J. & Ubbink,M. The orientations of cytochrome *c* in the highly dynamic complex with cytochrome b_5 visualized by NMR and docking using HADDOCK (vol 14, pg 799, 2005). *Protein Science* **15**, 1563 (2006).

Appendices

The appendices concern the analysis of NMR data on the Cyt f – Pc complex, Chapter 4.

Appendix A – Assignments of the ^{15}N and ^1H nuclei of Pc, taken from 3D NOESY and TOCSY-HSQC spectra.

Assignments	N (ppm)	H (ppm)
THR 2	119.27	8.540
TYR 3	126.19	8.674
THR 4	117.75	8.530
VAL 5	128.94	9.224
LYS 6	126.05	9.020
LEU 7	120.78	8.868
GLY 8	115.40	7.549
SER 9	119.04	8.401
ASP 10	120.84	9.419
GLY 12	108.18	8.183
LEU 13	116.85	7.352
LEU 14	124.39	8.539
VAL 15	112.14	7.544
PHE 16	120.27	8.765
GLU 17	122.12	8.864
ALA 19	116.95	8.067
LYS 20	115.61	7.307
LEU 21	121.44	7.648
THR 22	121.22	8.163
ILE 23	120.44	8.842
LYS 24	119.08	8.877
GLY 26	113.52	7.035
ASP 27	120.36	7.818
THR 28	114.86	8.517
VAL 29	126.10	9.100
GLU 30	128.04	9.083

Assignments	N (ppm)	H (ppm)
PHE 31	125.24	9.086
LEU 32	124.47	8.748
ASN 33	127.11	9.420
ASN 34	129.07	8.570
LYS 35	115.55	7.709
VAL 36	116.54	9.134
HIS 39	111.76	7.245
ASN 40	123.61	8.846
VAL 41	111.14	7.094
VAL 42	127.64	9.027
PHE 43	125.69	8.695
ASP 44	123.67	8.302
ALA 45	127.93	8.562
ALA 46	116.99	8.338
LEU 47	122.50	8.475
ASN 48	114.24	7.946
ALA 50	115.01	6.869
LYS 51	120.08	7.839
SER 52	109.36	8.113
ALA 53	133.55	9.100
ASP 54	119.71	8.317
LEU 55	123.48	8.048
ALA 56	119.18	7.452
LYS 57	120.48	8.409
SER 58	114.92	7.653
LEU 59	120.20	6.756
SER 60	110.63	6.831
HIS 61	119.82	9.357
GLN 63	120.99	8.579
LEU 64	121.54	8.269

LEU 65	124.59	9.133
MET 66	121.86	8.134
SER 67	112.67	7.816
GLY 69	112.07	8.858
GLN 70	118.86	7.265
SER 71	115.43	8.579
THR 72	115.52	8.620
SER 73	116.91	8.001
THR 74	120.49	9.370
THR 75	126.55	9.035
PHE 76	131.29	9.102
ALA 78	122.70	8.738
ASP 79	112.70	7.885
ALA 80	124.17	7.452
ALA 82	124.19	8.288
GLY 83	106.96	8.748
GLU 84	119.31	8.373
TYR 85	125.02	10.042
THR 86	120.91	8.463
PHE 87	125.16	8.453
TYR 88	113.83	8.742
CYS 89	121.23	7.705
GLU 90	127.29	9.993
HIS 92	114.29	8.416
ARG 93	128.76	8.013
ALA 95	120.66	7.248
GLY 96	105.31	7.910
MET 97	122.03	7.635
VAL 98	126.57	8.014
GLY 99	118.01	8.844
LYS 100	116.97	8.102
ILE 101	126.96	9.340
THR 102	125.58	9.160

VAL 103	128.15	9.208
ALA 104	133.31	9.165
GLY 105	113.45	7.693

Appendix B – List of normalized I_{para} / I_{dia} ratios for each mutant of Cyt f. Missing values refer to Pc amids that were either not observed or not analysed due to spectral overlap.

Residues	A63C	N71C	S192C	Q7C	Q104C
1	–	–	1.03	0.83	0.66
2	0.96	1.05	0.92	0.84	0.83
3	1.01	1.00	0.51	0.85	0.73
4	0.67	0.91	0.96	0.87	0.84
5	0.83	0.99	0.99	0.90	0.71
6	1.04	0.93	0.94	0.86	0.77
7	0.92	0.92	0.98	0.77	0.75
8	0.87	0.76	0.81	0.45	0.82
9	0.83	0.97	0.82	0.49	0.90
10	0.86	0.86	0.77	0.09	0.55
11	0.91	0.68	0.54	0.03	0.54
12	0.43	0.36	0.49	0.04	0.24
13	0.68	0.04	0.06	0.04	0.19
14	0.06	0.07	0.23	0.48	0.54
15	–	0.18	0.70	0.81	0.67
16	0.83	0.70	0.95	0.87	0.84
17	0.96	0.93	–	–	–
18	–	–	–	0.84	–
19	–	0.85	0.86	0.82	0.78
20	0.94	0.93	0.94	0.93	0.87
21	0.97	0.96	0.68	0.82	0.68
22	0.82	0.91	0.99	0.85	0.82
23	0.93	1.06	0.97	0.91	0.70
24	0.94	1.04	–	–	–
25	–	–	1.04	0.92	0.77
26	0.93	1.04	–	0.93	–
27	–	1.02	1.05	0.90	0.87
28	0.91	0.99	1.01	0.82	0.83
29	1.01	0.98	0.94	0.88	0.85
30	0.88	0.98	1.00	0.90	0.90
31	1.11	0.97	0.93	0.89	0.78
32	0.96	0.98	0.89	0.77	0.90
33	0.87	0.92	0.86	0.73	0.84
34	0.87	0.81	0.80	0.47	0.63
35	0.81	0.58	0.06	–	0.21
36	0.06	0.07	–	–	–
37	–	–	–	–	–
38	–	–	0.72	0.73	0.71
39	0.75	0.51	–	1.22	–
40	–	–	0.92	0.87	0.90
41	0.93	0.84	0.78	0.90	0.71
42	0.80	0.85	0.85	0.89	0.86
43	0.96	0.92	0.65	0.88	0.90
44	0.82	0.95	0.35	0.50	0.12
45	0.67	0.04	0.72	0.79	0.73
46	0.73	0.85	0.68	0.81	0.77
47	0.81	0.98	0.98	0.87	0.90
48	0.85	0.95	–	–	–
49	–	–	1.00	0.90	0.78
50	0.93	1.01	–	0.80	–
51	–	1.09	0.95	0.87	0.90

52	1.03	0.97	0.90	0.86	0.90
53	0.88	1.01	0.99	0.88	0.90
54	0.86	1.01	0.96	0.91	0.90
55	1.01	0.99	0.97	0.87	0.90
56	0.87	1.01	0.95	0.84	0.87
57	0.86	0.96	0.93	0.83	0.90
58	0.93	0.96	0.99	0.85	0.90
59	0.91	0.97	0.92	0.89	0.80
60	0.91	0.98	0.88	0.85	0.79
61	0.88	0.88	0.05	0.65	0.60
62	0.46	0.67	0.14	0.61	0.71
63	0.32	0.39	0.07	0.04	0.25
64	0.04	0.06	0.71	0.77	0.85
65	0.67	0.41	0.24	0.48	0.20
66	0.61	0.06	0.37	0.44	0.37
67	0.73	0.17	–	–	–
68	–	–	0.82	0.72	0.90
69	0.91	0.71	0.77	0.75	0.79
70	0.79	0.63	0.69	0.76	0.79
71	0.87	0.82	0.93	0.88	0.90
72	0.97	0.97	0.96	0.85	0.90
73	1.05	0.99	1.04	0.92	0.88
74	1.03	1.02	0.97	0.84	0.85
75	0.92	0.97	0.93	0.87	0.91
76	0.91	1.03	–	–	–
77	–	–	–	–	0.90
78	1.02	1.00	1.04	0.90	0.90
79	0.97	1.01	0.99	0.90	0.90
80	0.90	0.99	–	–	–
81	–	–	0.97	0.88	0.90
82	0.91	0.99	1.02	0.85	0.69
83	0.93	0.98	0.95	0.89	0.75
84	0.85	0.96	0.93	0.87	0.79
85	0.87	1.02	0.72	0.84	0.72
86	0.84	1.00	0.48	0.82	0.63
87	0.62	0.91	0.52	0.80	0.96
88	0.77	0.88	0.42	0.79	0.67
89	0.69	0.82	0.44	0.60	0.85
90	0.44	0.28	–	–	–
91	–	–	0.34	0.45	0.55
92	0.46	0.25	0.30	0.19	0.34
93	0.05	0.21	0.08	0.07	0.28
94	0.08	0.07	0.72	0.03	0.15
95	0.05	0.05	0.05	0.38	0.19
96	0.06	0.06	0.34	0.59	0.17
97	0.05	0.33	0.18	0.69	0.19
98	0.05	0.60	0.36	0.78	0.51
99	0.55	0.88	–	0.82	–
100	–	0.89	0.88	0.92	0.82
101	0.88	0.99	0.88	0.90	0.82
102	1.04	1.00	1.01	0.84	0.86
103	0.96	1.01	0.99	0.93	0.79
104	1.03	1.03	1.11	0.91	0.83
105	0.978349	0.99	–	–	–

Appendix C – R2,para values *versus* residue number
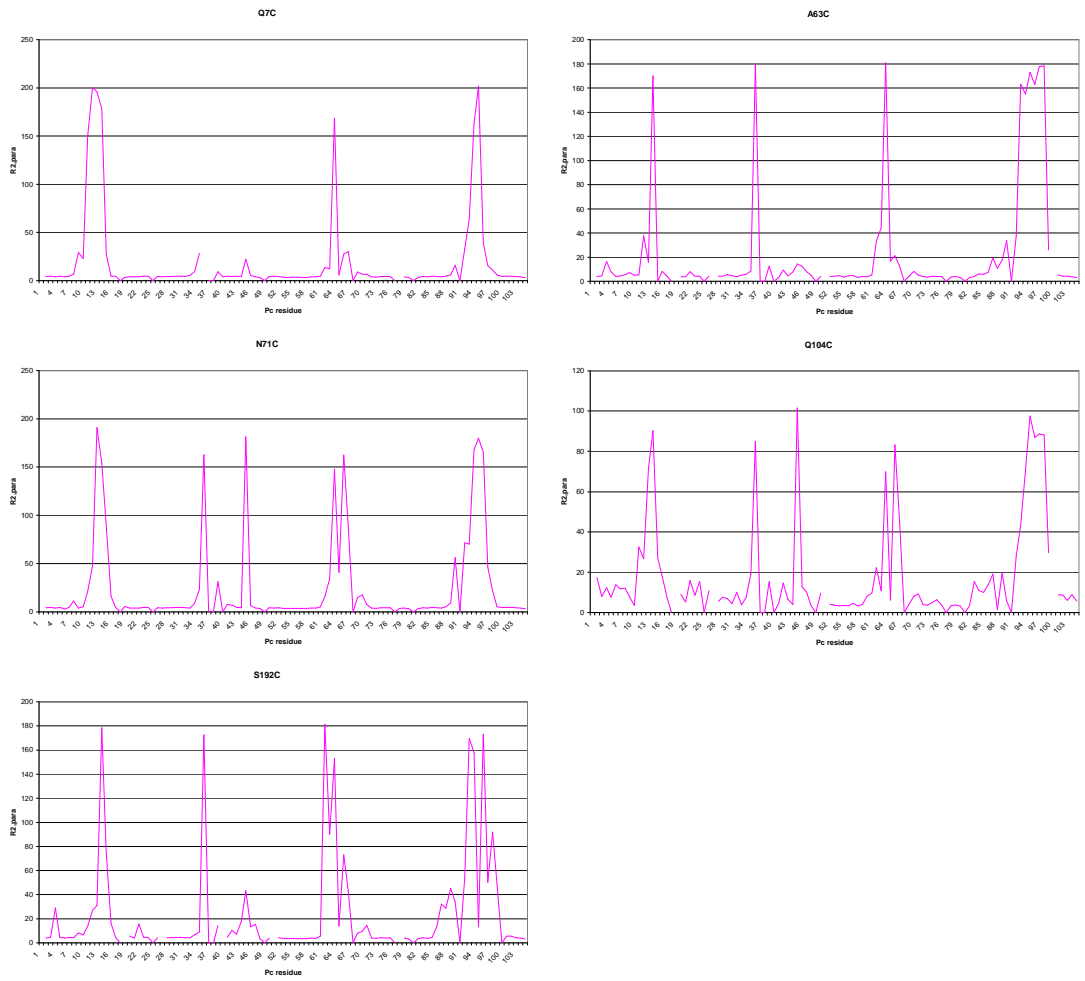
Summary

Since a long time, spin labeling and electron paramagnetic resonance (EPR) have been employed together as tools to study both the structure and dynamics of macromolecules, such as proteins. The general principle behind these techniques is that when a spin label is attached to a protein, it is no longer free, but is affected by its environment, for example by steric constraints either of the protein to which it is attached, or by possible interactions with binding partners or surrounding molecules. These interactions restrict the motion of the spin label and become visible in the EPR spectrum of the spin label. So the EPR spectrum returns information on the surroundings of the area of the protein to which the spin label is attached. By choosing different areas of attachment of the spin label, it is possible to analyze considerable parts of the molecule. Among the forces driving the interactions between proteins, the properties of their surface are crucial, in particular, the polarity of the surface. Electron paramagnetic resonance provides also information on the polarity and proticity (tendency to form hydrogen bonds) of the area around the spin label. In the present thesis, 275 GHz EPR (J-band) was employed to this end. The advantage of J-band EPR compared to conventional 9 GHz (X-band), and even 95 GHz (W-band), is that it allows differentiating between sites exhibiting only small differences in polarity, such as expected for different surface sites of a protein.

In Chapter II of this thesis, I report on our EPR studies of the polarity of the surface of Zn-azurin. Here, four single cysteine mutations were introduced at surface sites of Zn-azurin, specifically at positions 12, 27, 42 and 118. The proteins were analyzed in frozen solution. All mutants revealed two spectral components which differed mainly in one g-tensor parameter, the g_{xx} value. The differences were so small that they could not be resolved using W-band EPR. Since the g_{xx}-value is very sensitive to proticity, our measurements suggest that the spin label is in a position where the environment differs in proticity for the two observed spectral components. The absence of two components with respect to the A_{zz} values, sensitive to the polarity, suggests that the environment has a similar polarity for these two components. The two spectral components reveal two different populations of the spin label, each with its own microenvironment that differs mostly in proticity. Plotting g_{xx} vs. A_{zz}, the polarity/proticity profiles of the four mutants have been obtained and compared with data of spin labels in different solvents, already reported in literature. This comparison reveals that all positions refer to an overall protic/polar environment. Remarkably, a higher mobility for mutant K27C than for mutant Q12C was found in a related study, while according to data presented in this study K27C reveals a more apolar, aprotic environent than Q12C. This suggests that position 27 is located in the interior of the protein. The attached spin label is situated in a protein pocket which is big enough to allow it to move relatively free, but shielding it from the polar buffer environment.

Distance determination by the EPR technique on doubly spin labeled systems allows to complement existing structural methods like NMR and Förster resonance energy transfer (FRET). Double electron-electron spin resonance (DEER or PELDOR) is a pulsed EPR method which allows to detect distances in the nm regime. For this method to be used in the biological field, a model system was needed. Here we used azurin as such a model system, since its structure is known by X-ray crystallography. Two spin labels were attached to each of two double mutants (Q12C/K27C and K27C/N42C) of Zn-azurin. The results of our study are presented in Chapter III. The analysis of these results performed with different methods provided a distance distribution which can be described by a Gaussian. The length of the spin label linker must be considered, because it can influence the results. We propose a simple model to account for the conformation of the spin-label linker, which is in good agreement with the experimental distance distribution. Our results can be extended to other proteins. We propose that widths of the distance distributions larger than 0.45 nm indicate that the studied protein is flexible or exhibits enhanced dynamics.

In biology, understanding the mechanism of protein-protein interactions is fundamental. The process of protein-protein association can lead to static or transient complexes. In a transient complex, the relative orientation of the proteins may vary from a single well-defined state to a highly dynamic cluster of orientations which constitute the encounter complex. In Chapter IV the dynamics of the transient complex of *Nostoc* sp. PCC 7119 cytochrome *f* – plastocyanin (Cyt *f*-Pc) is described as investigated by NMR. The paramagnetic relaxation enhancements (PREs) from five spin labels on Cyt *f* were used as distance restraints in docking calculations. The experimental data are best interpreted by the presence of a dynamic ensemble of protein-protein orientations within the complex, rather than by a single, well-defined structure. This result appears to be in contrast with a previous study performed using a different NMR technique. We suggest that both results can be explained with an encounter complex model. Future work will probably be needed to obtain a better picture of the encounter complex. This is a complex task, since it involves taking into account non-specific interactions and dynamics, which leads to many possible orientations.

Samenvatting

Spin-labelen en elektron paramagnetische resonantie (EPR) worden al lange tijd samen gebruikt voor het bestuderen van de structuur en dynamiek van macromoleculen zoals eiwitten. Het algemene principe achter deze technieken is dat wanneer een spin-label aan een eiwit is gekoppeld, deze niet meer vrij beweegt maar hinder ondervindt door zijn omgeving, bijvoorbeeld door sterische hindering van het eiwit waar het aan gehecht is, of mogelijke interacties met bindende partners of omliggende moleculen. Deze interacties beperken de bewegingen van het spin-label en worden zichtbaar in het EPR spectrum. Dit levert informatie op over de omgeving van de positie waar het spin-label is geplaatst. Door verschillende locaties te kiezen voor het spin-label is het mogelijk grotere delen van het molecuul te analyseren. Voor de krachten die de interacties tussen eiwitmoleculen sturen zijn de eigenschappen van de moleculoppervlakken cruciaal, in het bijzonder de polariteit van het oppervlak. Via EPR is het mogelijk om informatie over de polariteit en proticiteit (de neiging om waterstofbruggen te vormen) van het gebied rond het spin-label te verkrijgen. In dit onderzoek is hiervoor gebruik gemaakt van 275 GHz EPR (J-band). Het voordeel van J-band EPR vergeleken met de conventionele 9 GHz (X-band) en zelfs 95 GHz (W-band) is dat het mogelijk is om onderscheid te maken tussen plekken met slechts zeer kleine verschillen in polariteit, zoals verwacht voor verschillende posities op het oppervlak van een eiwit.

In hoodstuk II van dit proefschrift beschrijf ik het EPR onderzoek gericht op het in kaart brengen van de verschillen in de polariteit aan het oppervlak van Zn-azurine. Via mutagenese werden vier enkele cysteïne mutaties aangebracht op de oppervlakte van Zn-azurine, op postities 12, 27, 42 en 118. Deze eiwitten werden voorzien van spin-labels en vervolgens geanalyseerd in een bevroren oplossing. Alle mutanten lieten twee spectrale componenten zien die voornamelijk verschilden in één g-tensor component, de g_{xx} waarde. De verschillen waren zo klein dat deze niet konden worden onderscheiden in de W-band EPR spectra. Aangezien de g_{xx} waarde zeer gevoelig is voor proticiteit suggereert dit dat voor de waargenomen spectrale componenten het spin-label in een positie zit waar de omgeving verschilt in proticiteit. De afwezigheid van twee componenten met betrekking tot de A_{zz} waarden, gevoelig voor polariteit, suggereert dat de omgeving een soortgelijke polariteit heeft voor deze twee componenten. De twee spectrale componenten onthullen twee verschillende populaties van het spin-label, elk met een eigen micro-omgeving die voornamelijk verschilt in proticiteit. Door de g_{xx} waarden grafisch tegen A_{zz} uit te zetten werden polariteit/proticity profielen voor de vier mutanten verkregen welke vervolgens werden vergeleken met de profielen verkregen voor het spin-label MTSL in diverse oplosmiddelen, die reeds eerder waren gerapporteerd in de literatuur. Deze vergelijking liet zien dat alle posities een

protische/polaire omgeving betreffen. Opmerkelijk is dat in een gerelateerde studie voor mutant K27C een hogere mobiliteit dan voor Q12C werd gerapporteerd, terwijl volgens data in deze studie K27C een meer apolaire, aprotische omgeving laat zien dan Q12C, een resultaat dat suggereert dat K27 zich binnen in het eiwit bevindt. Deze twee resultaten zijn te verklaren als het spin-label in positie K27 zich bevindt in een holte in het eiwitmolecuul die groot genoeg is om het relatief vrij te laten bewegen, maar het tegelijkertijd afschermt van de polaire bufferomgeving.

Afstandsbepaling door middel van toepassing van de EPR techniek op dubbel spin-gelabelde systemen is een aanvulling op bestaande methodes voor structuurbepaling zoals NMR en Förster resonantie energie overdracht (FRET). Dubbel elektron-elektron spin-resonantie (DEER of PELDOR) is een gepulste EPR methode die het mogelijk maakt afstanden te bepalen op nanometerschaal. Om deze methode toe te passen in biologisch onderzoek was het noodzakelijk om over modelsystemen te beschikken. Hier hebben we gebruik gemaakt van azurine als een dergelijk modelsysteem, aangezien de structuur hiervan bekend is via Röntgen kristallografie. Twee spin-labels werden vastgemaakt aan elk van twee dubbele mutanten (Q12C/K27C en K27C/N42C) van Zn-azurine. Dit onderzoek is beschreven in hoofdstuk III. De analyse van de resultaten met behulp van diverse methodes gaf een distributie van afstanden die beschreven kan worden met een Gaussische functie. De lengte van de spin-label linker moet meegenomen worden in de berekening aangezien deze de resultaten kan beïnvloeden. We stellen een simpel model voor om rekening te houden met de conformatie van de spin-label linker, dat goed overeenkomt met de experimentele afstandsdistributie. Deze conclusies zijn relevant voor eiwitten die minder goed bestudeerd zijn dan azurine. Het suggereert dat breedtes van de afstandsdistributie groter dan 0.45 nm aangeven dat het bestudeerde systeem een grotere flexibiliteit of dynamica heeft dan azurine.

In de biologie is inzicht in het mechanisme van eiwit-eiwit interacties van fundamenteel belang. Het proces van eiwit-eiwit associatie resulteert in statische of kortlevende complexen. In een kortlevend complex kunnen de relatieve oriëntaties van de eiwitmoleculen variëren van een duidelijk gedefinieerde toestand tot een zeer dynamisch cluster van oriëntaties die het ontmoetingscomplex vormen. Hoofdstuk IV beschrijft de studie van de dynamica van het kortlevende complex van *Nostoc* sp. PCC 7119 cytochroom *f* – plastocyanine (Cyt *f*-Pc) met behulp van NMR. De paramagnetische relaxatie versterkingen (PREs) van vijf spin-labels op Cyt *f* werden gebruikt als afstandsbeperkingen in docking berekeningen. De experimentele data kunnen het best geïnterpreteerd worden door de aanwezigheid van een dynamisch ensemble van eiwit-eiwit oriëntaties binnen het complex, in plaats van een enkele, duidelijk gedefinieerde structuur. Dit resultaat lijkt de resultaten van een eerdere studie met een andere NMR techniek tegen te spreken. Wij suggereren dat beide kunnen worden verklaard met een ontmoetingscomplex model.

Aanvullende studies zijn waarschijnlijk nodig om een beter beeld te krijgen van dit complex. Dit is een ingewikkelde taak, aangezien er rekening gehouden dient te worden met aspecifieke interacties en dynamica, waardoor vele oriëntaties mogelijk zijn.

List of publications

Milikisyants S, Scarpelli F, Finiguerra MG, Ubbink M, Huber M. A pulsed EPR method to determine distances between paramagnetic centers with strong spectral anisotropy and radicals: The dead-time free RIDME sequence. *Journal of Magnetic Resonance* 201, **2009**, 48-56.

Finiguerra MG, Prudencio M, Ubbink M, Huber M. Accurate long-range distance measurements in a doubly spin-labeled protein by a four-pulse, double electron-electron resonance method. *Magnetic Resonance in Chemistry* 46, **2008**, 1096-1101.

Finiguerra MG, Blok H, Ubbink M, Huber M. High-field (275 GHz) spin-label EPR for high-resolution polarity determination in proteins. *Journal of Magnetic Resonance* 180, **2006**, 197-202.

Finiguerra MG, Blok H, Ubbink M, Orlinskii SB, Alagaratnam S, van Amsterdam IMC, Schmidt J, Huber M. Spin-label electron paramagnetic resonance (EPR) at very high field resolves local polarity differences in azurin. *Biophysical Journal* 86, **2004**, 485A-485A.

Finiguerra MG, van Amsterdam IMC, Alagaratnam S, Ubbink M, Huber M. Anisotropic spin label mobilities in azurin from 95 GHz electron paramagnetic resonance spectroscopy. *Chemical Physics Letters* 382, **2003**, 528–533.

Bernardi R, Finiguerra MG, Rossi AA, Palmieri S. Isolation and biochemical characterization of a basic myrosinase from ripe Crambe abyssinica seeds, highly specific for epi-progoitrin. *J. Agricultural Food Chem.* 51, **2003**, 2737-2744.

Finiguerra MG, Iori R, Palmieri S. Solubile and Total Myrosinase Activity in Defatted *Crambe abyssinica* Meal. *J. Agricultural Food Chem.* 49, **2001**, 840-845.

Ravasio N, Finiguerra MG, Gargano M. α-Pinene oxide isomerization promoted by mixed oxides. In *Supported Reagents and Catalysts in Chemistry*; B.K. Hodnett Ed.; Royal Society of Chemistry, **1998**, 231-232.

Ravasio N, Finiguerra MG, Gargano M. α-Pinene oxide isomerization promoted by mixed cogels. In *Catalysis of Organic Reactions*; F. Herkes Ed.; Marcel Dekker, **1998**, 513-517.

Biography

Michelina Finiguerra was born on 29 September, 1967 in Foggia, Italy. She earned her MSc degree in Chemistry in 1997 from the University of Bari *summa cum laude*. Her MSc graduation thesis was on the use of heterogeneous catalysts with and without copper, used in inorganic chemistry processes with low environmental impact.

After her degree, Michelina continued her collaboration with the University and Politecnico of Bari in the field of heterogeneous catalysis, and qualified to practice as a professional Chemist in 1998.

She then worked from 1999 to 2001 in the Biochemistry department at the Istituto Sperimentale per le Colture Industriali (ISCI, Institute for Research on Industrial Crops) in Bologna. There, she focused her research on glucosynolates, working on their isolation and on protein purification in plants belonging to the *Brassicaceae* family.

In 2002 Michelina started her PhD studies at Leiden University, the Netherlands, with a joint research between the MetProt group of Prof. Dr. G. W. Canters and the Physics group of Prof. Dr. E. J. J. Groenen, under the supervision of Prof. M. Ubbink and Dr. M. Huber. The results of her research are presented in this thesis.

In 2005 she moved to Italy, and in 2007 she got appointed as fulltime teacher of Chemistry in secondary schools. She currently holds her teaching position at a secondary school in Reggio Emilia, Italy.

Acknowledgements

Thanks to Irene and Giulia, who unconsciously give me so much strength. It is wonderful that you are here, that you are exactly as you are. Thank you for your love, for when you have been patient and for when your patience was exhausted, indicating me that it was too much. You are my light and my happiness. It is great growing with you. And, thanks to Davide, with whom I am sharing my life. Thanks for your Love. Your everyday support has been and is fundamental, "rejoicing in hope, patient in suffering". You are part of me.